A ship-derived climatology of oceanic precipitation, 1950–2019

Harrison Khanh TRAN

A Thesis submitted in partial fulfillment of

the requirements for the degree of

Master of Science

(Atmospheric and Oceanic Sciences)

at the

UNIVERSITY OF WISCONSIN-MADISON

May 2024

Thesis Declaration and Approval

I, Harrison Khanh TRAN, declare that this Thesis titled 'A ship-derived climatology of oceanic precipitation, 1950–2019' and the work presented in it are my own.

Harrison Khanh TRAN		
Author	Signature	Date

I hereby approve and recommend for acceptance this work in partial fulfillment of the requirements for the degree of Master of Science:

Grant W. Petty		
Committee Chair	Signature	Date

Daniel J. Vimont		
Faculty Member	Signature	Date

Hannah Zanowski		
Faculty Member	Signature	Date

Abstract

A ship-derived climatology of oceanic precipitation, 1950–2019

by Harrison Khanh TRAN

Shipboard observations of present weather (ww), reported voluntarily from vessels world-wide, comprise the only source of in-situ information regarding precipitation over much of the global ocean. While the current understanding of oceanic precipitation has largely arisen from remotely sensed precipitation retrievals in recent decades, ships continue to report ww and remain a key source of ground truth. Over 99 million non-automated shipboard ww reports made during the 70-year period from 1950 to 2019 are used to reconstruct relative frequencies and long-term trends in four classes of precipitation: i) drizzle, ii) moderate or heavy intensity non-drizzle, iii) non-drizzle associated with deep convection or thunderstorms, and iv) frozen-phase precipitation.

Following quality control of the shipboard weather data contained within the International Comprehensive Ocean-Atmosphere Data Set (ICOADS), a compositing procedure is used to aggregate ship reports and estimate the annual and seasonal frequencies of these phenomena on a global $1° \times 1°$ grid where sufficient data exists. An ordinary least squares regression is applied to these estimated frequencies to infer long-term trends, which are subjected to significance testing to evaluate the robustness of the ship observations.

The inferred frequencies of the precipitation classes using shipboard ww produces geographically coherent results consistent with previous findings using similar data, as well

as results derived from other instruments and techniques. Oceanic drizzle is closely linked to distributions of marine stratocumulus, occupying a larger share of precipitation over cool eastern boundary currents. The proportion of oceanic precipitation falling at heavier intensities appears to be related with the mean distribution of precipitable water. Significant differences in estimated frequencies are found in all four precipitation classes between the period with satellite-derived oceanic precipitation estimates (1979–2019) and the pre-satellite era (1950–1978).

These changes are reflected in the finding of statistically significant 70-year linear trends in the relative frequencies of the four surveyed precipitation classes. Many of these trends emerge in both annual and seasonal frequencies. Positive trends in the proportion of drizzle are observed throughout the tropics with declines in areas with abundant marine stratiform clouds. An increase in moderate and heavy intensity precipitation as a fraction of non-drizzling precipitation is observed across the subtropical North Pacific. Fractional increases in both heavier precipitation and deep convection or thunderstorms are observed over the Mediterranean Sea, Yellow Sea, and along the U.S. Atlantic coast. Negative trends in oceanic frozen precipitation within the mid-latitude Northern Hemisphere suggest a shrinking of the Arctic region receiving frozen precipitation. These ship-observed changes are placed in the context of climate change and compared to findings from other platforms and trends expected from climate models.

"The question of the rainfall is, perhaps, the most unsatisfactory with which to deal in ocean meteorology."

David Wilson Barker (1904)

Acknowledgements

Fully enumerating the many people who made this thesis and my journey here possible would certainly be an endless endeavour. *Journey* is an apt description, and this work serves as both a milestone following an over two-decade aggregation of twists and turns in life, as well as hopefully just one of many milestones in the years to come.

I would like to extend my heartfelt gratitude to my advisor, Grant Petty, for taking me up as a research assistant and introducing me to this wonderful project. Grant, it has been an honor working under your tutelage and mentorship. I know that the use of shipboard weather reports for oceanic climatology has been a bit of a passion project, being a former shipboard weather observer yourself, and hope that this research forms a key part of making your vision for this project a reality. I would like to thank my other committee members, Dan Vimont and Hannah Zanowski, for their comments and insight during our meetings, for their immensely helpful classes (many of those Jupyter notebooks were incorporated into this research), and of course, for reviewing this thesis.

Coming to the concrete behemoth that is the AOSS building would not be as worthwhile were it not for the vibrant professors, students, and researchers that altogether foster a steady drumbeat of learning and scientific exploration. Thanks to my office-mate, Quinn, for keeping the office lively and providing the wonderful reclining chairs that were greatly appreciated after a long day's work. I'd like to also thank those in and out of the department that I've come to know over my time here in Madison, particularly for our wonderful Tuesday Trivia team. I'd also like to give a special shoutout to the Moon (and of course, the Sun) for providing an ethereal experience with the total solar eclipse earlier this year, providing a reminder of the awe and wonderment offered in nature.

The University of Wisconsin-Madison is but one part of my journey, and I would like to extend an emphatic thanks to my many teachers and mentors throughout the years, from elementary school through college, for giving me the tools to not only learn or

vi

succeed academically, but to deeply appreciate life itself and to stay curious about the world. Thank you to all of my friends near and far who have had to put up with my excitement about meteorology over the years. I would like to specifically acknowledge the on-air meteorologists that I grew up with in Austin: Burton Fitzsimmons, Adam Krueger, Maureen McCann, Rich Segal, and Jim Spencer. Your calm, instructive, and informative voice during severe weather got me interested in meteorology. I don't think my 4-year-old self, afraid of lightning and thunder, would even come close to envisioning where I'd be today.

Finally, I want to thank my family for their unwavering support throughout the years, and for making this journey possible in the first place. Daniel – thank you for keeping a sense of practicality when it came to approaching life and life's work. Alan – I think it was your excitement about astronomy that got me interested in science as a little kid in the first place. Mom – thank you for all of your support, for keeping me on the ball when it came to knowing the weather forecast, and, of course, for your unparalleled cooking. Dad – I would not be here without your strength, wisdom, and unshakable commitment to present and future. Thank you.

Contents

List of Figures

Abbreviations

CDR	Climate Data Record
CCN	Cloud condenstation nuclei
COADS	Comprehensive Ocean-Atmosphere Data Set
ERSST	Extended Reconstructed SST
GCOS	Global Climate Observing System
GTS	Global Telecommunications System
GPCP	Global Precipitation Climatology Project
GPM	Global Precipitation Measurement Mission
IMMA	International Maritime Meteorological Archive
IMO	International Meteorological Organization
ICOADS	International Comprehensive Ocean-Atmosphere Data Set
IMERG	Integrated Multi-satellitE Retrievals for GPM
ITCZ	Inter-Tropical Convergence Zone
OWS	Ocean Weather Ship
PMM	Precipitation Measurement Mission
PMW	Passive microwave
SPCZ	South Pacific Convergence Zone
SST	Sea surface temperature
TRMM	Tropical Rainfall Measurement Mission
WMO	World Meteorological Organization
VOS	Voluntary Observing Ship

Symbols

AT	air temperature
i_X	station/weather indicator (WMO code table 1860)
PT	platform type
N	total cloud cover (WMO code table 2700)
ww	present weather (WMO code table 4677)
f	True fraction of occurrence
$\hat{f}$	Estimated fraction of occurrence
$\hat{\sigma}$	Estimated uncertainty of $\hat{f}$

Chapter 1

Introduction

1.1 Oceanic precipitation

1.1.1 Overview

The state of the hydrological cycle and perturbations in its associated fluxes engender a wide range of consequences for both human civilization and the natural environment, affecting food security, water resource management, and ecosystem health (Grimm et al., 2013, Huntington, 2010, Rast et al., 2014). The Global Climate Observing System (GCOS) has identified precipitation as one of 54 essential climate variables key to characterizing and understanding climate (Ballari et al., 2023). The various characteristics of precipitation, including its frequency, phase, intensity, and amounts, can be studied to elucidate climate trends and the physical processes resulting in precipitation (e.g. Chou

et al., 2012, Fowler and Hennessy, 1995, Shi and Liu, 2021). Observed trends in the characteristics of precipitation may highlight the effects of climate change on the global hydrologic cycle and help validate results from global climate models (Tapiador et al., 2017), increasing confidence in their projections and highlighting strengths or weaknesses. Although aggregate precipitation amounts and characteristics in climate models tend to align with observations, accurate modeling of precipitation variability and other finer details remains a challenge (e.g. Legates, 2014, Stephens et al., 2010). For example, while precipitation amount and precipitation frequency are interlinked (Reed, 1979), estimations and projections of both quantities across model depictions differ considerably. Satellite data suggest that global dynamical models tend to greatly overestimate the frequency of precipitation, depicting light rainfall too often, though accumulated precipitation totals tend to be in good agreement (Stephens et al., 2010).

A comprehensive understanding of the global hydrologic cycle cannot be achieved without an accurate understanding of precipitation over the ocean, which covers over 70% of the Earth's surface and receives around 77% of global precipitation (Marvel and Bonfils, 2013). Precipitation constitutes a larger component of the hydrologic cycle over the ocean compared to land given the vast oceanic extent and the relatively small contributions of other fluxes related to streams, groundwater, and transpiration (Levizzani and Cattani, 2019). Oceanic precipitation represents the movement of around $4.24 \times 10^5 \pm 10\%$ km^3 of water annually, representing the largest exchange of water between any of the ocean, land, or atmosphere outside of oceanic evaporation (Douville et al., 2021). Over the

ocean, changes to the hydrologic cycle directly impact oceanic salinity through the interplay between evaporation, precipitation, and to a lesser extent runoff (Yu et al., 2020). Changes to salinity, a major component of seawater density, drives changes to the global ocean circulation, highlighting a strong link between oceanic precipitation and the global ocean state. In addition to shedding light on the hydrologic cycle, global precipitation is fundamental to the global atmospheric energy budget, and the hydrologic cycle and energy cycle are closely intertwined. The occurrence of precipitation is associated with cloud formation, with oceanic evaporation serving as a significant source for the water vapor that eventually condenses and releases latent heat. Latent heat flux comprises a sizable component of the surface energy budget, with a global mean flux over three times that of surface sensible heat flux and roughly one-fifth of surface longwave emission. In turn, the distribution and magnitude of precipitation can be used as a proxy for determining latent heat flux (Stephens et al., 2012). Uncertainty in precipitation amounts, particularly over the ocean, thus propagates uncertainties to the rest of the global energy cycle.

Despite the significance of oceanic precipitation, the vastness of the global ocean makes observing oceanic precipitation a challenge. In-situ measurement of precipitation over most of the ocean is sparse to non-existent (Kidd et al., 2022), with available surface-based precipitation datasets relying on spatially disparate dedicated buoys, vessels, or observations on islands and atolls (Levizzani and Cattani, 2019). Data collected from rain gauges characterizes precipitation over just 25–30% of the Earth's surface and only about 4% of the ocean falls within 100 km of a rain gauge (Kidd et al., 2017a, New

et al., 2001). These sampled areas are predominantly coastal and would thus provide little information on precipitation over the open ocean.

Without the dense rain gauge networks available on land, our present understanding of oceanic precipitation characteristics arises from satellite retrievals, oceanographic measurements, climate models, and a sparse patchwork of surface-based observation platforms such as ships and buoys. Spaceborne radars, which represent the most sensitive and accurate remote sensing instruments for sampling precipitation over the ocean, suggest a global average oceanic precipitation rate of nearly 3 mm day^{-1} (Behrangi et al., 2014). The greatest annual oceanic precipitation amounts occur over the tropical ocean in association with the Inter-Tropical Convergence Zone (ITCZ) and the South Pacific Convergence Zone (SPCZ), where mean precipitation amounts exceed 5 mm day^{-1} (Adler et al., 2020). Precipitation amounts are generally lower over the subtropical latitudes and are higher in the common storm track regions of the mid-latitude ocean. Over the tropical oceans, precipitation amounts may be either positively or negatively correlated with sea surface temperature (SST) depending on which is the dominant influence between the enhancement of convection from warmer SST or the warming of SST from increased insolation (Trenberth, 2011). Oceanic precipitation frequency as inferred from satellite estimates also shares a similar distribution, with the greatest frequencies (precipitation exceeding 0.02 mm hr^{-1} over 25% of the time, hourly-resolved) occurring over tropical ocean and the most infrequent precipitation occurring over the subtropics, particularly on the eastern portions of ocean basins (Trenberth and Zhang, 2018).

1.1.2 Natural and anthropogenic influences and projections

Variability in global SST imprints strongly on regional precipitation trends as surface temperatures tend to be positively correlated with evaporation (Adler et al., 2017, Hoerling et al., 2010); the opposite is true in areas where the dominance of subsidence associates cloud-free periods with higher SST (Trenberth, 2011). Forcing from the El Niño–Southern Oscillation (ENSO) is associated with opposing monthly anomalies in precipitation quantity between the central/eastern tropical Pacific and the Indo-Pacific Warm Pool (Wang et al., 2016). Similar dipolar correlations are also observed between the equatorial Atlantic and western Indian oceans. Global mean precipitation amounts are positively correlated with ENSO, with a $9\%\,°C^{-1}$ relationship between precipitation amount and surface temperature inferred by satellite observations (Adler et al., 2017). Multidecadal variability in Atlantic and Pacific SST (e.g. Gu and Adler, 2012, Zhao et al., 2022) and the variance of the Indian Ocean Dipole (e.g. Harou et al., 2006) also appear linked to natural modulation of regional precipitation. Volcanic eruptions produce a more irregular negative forcing on global mean precipitation amounts (Adler et al., 2017), with a shallower but longer lasting response over ocean compared to land (Iles et al., 2013).

An increase in global mean surface temperature as a result of climate change stemming from anthropogenic increases in greenhouse gas emissions is expected to result in an increase in global mean precipitation amounts (Trenberth, 2011). This result directly follows from the increased water vapor-holding capacity of warmer air described by the Clausius-Clapeyron equation, though the corresponding increase in precipitation should

lag behind the increase in water vapor to satisfy the global energy budget (Allan et al., 2020). These anticipated changes are not globally uniform, with concurrent changes in the atmospheric circulation accelerating moisture transport and generally leading to wetter regions becoming wetter and drier regions becoming drier (e.g. Allan et al., 2020, Sarojini et al., 2016, Yu et al., 2020). Increased global temperatures are expected to increase the frequency of heavy precipitation relative to light precipitation (Chou et al., 2012), and the global frequency of rainfall at all rain rates may increase (Pendergrass and Hartmann, 2014). An increase in the frequency of the heaviest precipitation events has also been evident in observations and reproduced in modelling, and climate models project their continued increase (e.g. Donat et al., 2016, Fischer and Knutti, 2016, O'Gorman, 2015).

Warming temperatures should also result in an increased frequency of liquid relative to frozen precipitation, particularly towards the ends of an area's snow season and in areas with mean temperatures near the freezing line (Trenberth, 2011). The reduction of frozen precipitation manifests as a decrease in snowfall extremes, extent, and the snow-rain event ratio, which has been evident in both observations and model simulations (e.g. Kunkel et al., 2016, Mudryk et al., 2020, O'Gorman, 2014, Shi and Liu, 2021). In contrast, the anthropogenic influence on lightning occurrence and the sign of trends in lightning frequency remain unclear (e.g. Albercht et al., 2011, Finney et al., 2018, Price and Rind, 1994, Singh et al., 2017, Thornton et al., 2017), and historical trends in environmental parameters related to thunderstorm development are inconsistent between rawinsondes and model reanalyses (Taszarek et al., 2021).

An intensification of the global hydrologic cycle has been inferred from analyses of ocean salinity (e.g. Yu et al., 2020), glacial mass (e.g. Radić and Hock, 2013), and other hydrologic variables (Huntington, 2006). While satellite datasets previously suggested little to no significant overall long-term trend in global mean precipitation amount since the begninng of the credible satellite record in 1979 (Adler et al., 2017), a statistically significant but weakly positive trend has become apparent in recent years (Gu and Adler, 2023). Seasonally, this trend is stronger in austral summer than boreal summer. Over ocean, a weakly positive but not statistically significant trend of around 0.0080 mm day^{-1} per decade has been observed by satellites. However, the observed sensitivity of global precipitation to surface temperature changes is comparable to climate model outputs, and projections from those models suggest that the imprint of greenhouse gases on global precipitation will become increasingly apparent in the near future. Within the satellite record, interdecadal variability adds considerable noise to the long-term globally averaged signal. Long-term precipitation trends interlinked with trends in temperature and columnar water vapor are much more evident at regional scales. When masking out the influence of Pacific or Atlantic multidecadal variability, increasing trends have been observed over the core region of the ITCZ and SPCZ and the Indo-Pacific Warm Pool, as well as in the tropical Indian and Atlantic oceans. Decreasing trends in precipitation amount have been inferred primarily over the subtropics and on edges of the ITCZ (Adler et al., 2017). While not as clearly captured in the satellite record, the freshening of the high-latitude ocean in both hemispheres suggests a corresponding increase in high-latitude precipitation (Trenberth, 2011).

Model reanalyses reproduce trends similar to those observed in the satellite record (Gu and Adler, 2023). Regionally, renalyses depict a historical increase in precipitation amounts over the tropical ocean (Dore, 2005). Historical simulations from Phase 5 of the Coupled Model Intercomparison Project (CMIP5; Taylor et al., 2012) suggest an increase in annual precipitation over the Arctic as a result of anthropogenic forcing (Sarojini et al., 2012). Similar trends are also depicted over the high-latitude Southern Ocean, consistent with an observed freshening of the Southern Ocean. The modeled signal is clearer in the higher-latitudes than in the subtropics and tropics. RCP8.5 simulations from CMIP5 suggest an increase in mean precipitation near the oceanic equator and decreased precipitation over the subtropics, particularly over the eastern parts of oceanic basins, out to 2100 (Pendergrass et al., 2017). Seasonal precipitation variability is also modeled to change by similar sign over the aforementioned regions. Models in Phase 6 of the Coupled Model Intercomparison Project (CMIP6; Eyring et al., 2016) also show similar zonal patterns in total precipitation changes relative to pre-industrial baselines, with increases in annual precipitation amount over the Arctic, Southern Ocean, and along the equator, and decreases in annual precipitation amount generally over the eastern oceanic subtropics, with the exception of the northeastern Pacific. Annual snowfall amounts are also projected to decrease over the high-latitude oceans, though model averages depict slight increases over the Arctic and coastal Antarctic (Gutiérrez et al., 2021).

Anthropogenic releases of aerosols also impact precipitation, which can be viewed through the lens of their direct effect on the distributions of cloud condensation nuclei (CCN) (e.g. Rosenfeld et al., 2008) or through the indirect impacts on cloud formation arising

from the radiative effects of aerosols (e.g. Ming et al., 2010). However, the magnitude of these effects are not well-understood and remain a significant source of uncertainty for climate forcing projections, producing bifurcating outcomes in both theoretical and modeling results (Tao et al., 2012). In the microphysical framework, the increase in CCN concentrations leads to the formation of smaller cloud droplets as liquid water content (LWC) is nucleated over more CCN, potentially delaying the formation of larger, aggregating raindrops. This may lead to suppression of precipitation or favor increased cloud evaporation, undercutting the precipitation process entirely (e.g. Leung et al., 2023, Mann et al., 2014). However, observations suggest that this suppressive process holds for submicrometer CCN entrained into shallow clouds but has the opposite effect on deep convective clouds and for giant CCN (Rosenfeld et al., 2008). Aerosols may also enhance precipitation in moist environments and suppress precipitation in arid environments (Li et al., 2011). In the radiative framework, aerosols may either enhance precipitation by modifying the atmospheric energy balance to enable increased surface heating and cloud formation, or suppress precipitation by stabilizing the lower atmosphere (Fan et al., 2008, Ming et al., 2010). L'Ecuyer et al. (2009) found evidence that precipitation frequency and amount in maritime clouds was positively correlated with sea-salt concentration, but that this may be counteracted by an opposing impact from sulfates. Still, a global observational understanding of the relationship between aerosols and clouds remains difficult to achieve due to the challenges associated with satellite retrieval of CCN and ice nuclei concentrations (Rosenfeld et al., 2014).

1.2   Current oceanic precipitation datasets

The gap between in-situ oceanic observations and our understanding of oceanic precipitation characteristics has been primarily filled by indirect satellite-based precipitation measurements. Such estimates have been obtained using visible and infrared radiometers, passive microwave (PMW) sensors, and spaceborne radars, leveraging either the radiative characteristics of precipitation or the relationship between precipitation and cloud characteristics (Kidd and Levizzani, 2011, Levizzani and Cattani, 2019).

The earliest endeavours into estimating precipitation from satellites made use of the relationship between the reflectance of clouds at visible wavelengths or the temperatures of clouds derived from infrared wavelengths and precipitation, with bright and cold clouds being more likely producers of heavier precipitation (Kidd et al., 2022). These wavelengths were frequently observed by early polar and geostationary satellites at reasonably high resolutions, but struggled to identify non-convective precipitation and provided highly uncertain estimates (Arkin and Ardanuy, 1989, Martin and Scherer, 1973).

Wilheit et al. (1977) provided a theoretical basis for quantitatively estimating precipitation rates over the ocean at PMW wavelengths. The ocean radiates at those wavelengths at relatively consistent and low emissivity, but the received power from spaceborne PMW sensors is increased in scenes with rain droplets, allowing for the development of a more physically direct relationship between microwave brightness temperature and precipitation rate. This general principle has supported PMW-derived estimates, especially

following the launch of the Special Sensor Microwave/Imager (SSM/I) in 1987 which provided for the first time operational, continuously operating, and multichannel microwave imaging (Barrett et al., 1988). In 1997, the launch of the Precipitation Radar (PR) onboard the Tropical Rainfall Measurement Mission (TRMM) ushered in an era of active microwave, radar-based precipitation retrievals from space, which has since been continued with the launch of the Dual Precipitation Radar (DPR) as part of the Global Precipitation Measurement (GPM) mission in 2014 (Kidd et al., 2022). The launch of the CloudSat Cloud Profiling Radar (CPR; Stephens et al., 2002) mission in 2006 demonstrated the sensitivity of millimeter-wavelength radars to clouds and lighter precipitation (Battaglia et al., 2020). These radars offer the most direct assessment of precipitation from space and have served as calibration and validation standards for PMW retrievals (e.g. Kidd et al., 2017b, You et al., 2020).

Due to the differing spatiotemporal resolutions and coverage of Earth-observing satellites, construction of a long-term satellite-derived precipitation record requires the harmonization of precipitation estimates derived from the wide range of observed wavelengths. The Goddard profiling algorithm (GPROF; Kummerow et al., 2015) is one widely-used physically-based Bayesian scheme that can be applied to data from a wide array of PMW sensors to estimate surface precipitation, incorporating information about SST and total precipitable water over the ocean. Other techniques like the Integrated Multi-satellite Retrievals for the GPM Mission (IMERG; Tan et al., 2019) and the Climate Prediction center morphing method (CMORPH; Joyce et al., 2004) blend data from both infrared

and microwave wavelengths to achieve merged estimates of precipitation with relatively high resolutions.

Nonetheless, the satellite record of oceanic precipitation remains relatively short for climate applications. The longest satellite precipitation record, provided by the Global Precipitation Climatology Project (GPCP), covers only five decades from 1979 to the present (Adler et al., 2018). The satellite-only IMERG algorithm, now applied to both TRMM and GPM data, extends back only as far as 2000 as of version 6 (Tan et al., 2019). While some precipitation datasets incorporate more than the minimum 30 years of satellite observation recommended by GCOS for climate observation (Sun et al., 2018, Yang et al., 2013), the overall satellite record may not allow reliable differentiation between anthropogenic forcing and natural variability at decadal or multidecadal timescales.

One significant caveat in our current understanding of the global hydrologic cycle is the lack of closure present in current climate datasets (Dorigo et al., 2021). In other words, some water is unaccounted for when considering the estimated or observed values for fluxes included in the hydrologic cycle. Gutenstein et al. (2021) assessed that uncertainties in satellite-derived estimations of the difference between evaporation and precipitation (the freshwater flux, E–P) over the ocean were large compared to estimates, making improved assessment of E–P an important consideration in closing the water budget. The uncertainty in oceanic precipitation based on satellite and model-derived datasets is on the order of 5%, comparable to half of the global river discharge (Behrangi, 2021, Rodell et al., 2015).

Given the scarcity of observational data over the ocean, evaluation of satellite retrievals over the ocean has been limited. Pradhan et al. (2022) found that only 3 out of 101 peer review articles specifically examined the performance of IMERG over the ocean. Those studies have shown both underestimations or overestimations of precipitation by the algorithm (e.g. Khan and Maggioni, 2019, Prakash et al., 2017). Adler et al. (2017) posited undersampling of intense tropical precipitation as a likely source of oceanic underestimation in GPCP. The present, satellite-based view of oceanic precipitation, derived almost entirely from infrared and PMW observations, calibrated in part by spaceborne radar, are susceptible to large changes arising from algorithm modifications and calibration adjustments (Liu, 2016). In contrast, satellite retrievals over land, particularly over areas with a high density of gauges, permit effective calibration of satellite estimates not possible over the global ocean. Petty (1997) identified an inability to accurately capture showery warm-rain oceanic precipitation among ten microwave-based precipitation algorithms. Both PMW and spaceborne radars also face difficulties in detecting the light and shallow precipitation characteristic of higher latitudes (Tapiador et al., 2017). This includes the lack of selectivity in PMW sensors between drizzle and cloud droplets. Satellite-based precipitation datasets tend to be constrained to 60°S-60°N due to algorithmic or observational limitations. Moreover, PMW and infrared-based precipitation estimates rely on brightness temperatures arising from bulk radiative properties, blurring the distinction between cloud properties, hydrometeors leaving the cloud base, and precipitation at the ocean surface. For instance, virga may appear indistinguishable from rainfall, leading to erroneous quantitative precipitation retrievals (Wang et al., 2018). Spaceborne radars

may also face similar challenges identifying precipitation reaching the surface (Tan et al., 2018).

The short data record of satellite-derived oceanic precipitation and the influence of non-climatic factors on oceanic precipitation estimates suggests the need for an independent dataset to both validate satellite results and potentially provide a longer climate data record (CDR) for oceanic precipitation. A longer data record would improve understanding of climate change and contextualize our current satellite-based view (Smith, 2013). Reconstructions of oceanic precipitation may be achieved through correlations with other observed fields (e.g. Smith, 2013) or from model reanalyses (Sun et al., 2018). Nonetheless, these alternate datasets do not represent directly observed, open ocean precipitation. Furthermore, intercomparisons between these disparate data sources show disagreement at regional and seasonal scales, especially within the high-latitudes (Behrangi et al., 2016).

1.3 Shipboard weather observations

1.3.1 Overivew

The importance of oceanic weather conditions to maritime interests fostered a need for sailors to systematically document oceanic weather (Woodruff et al., 1987). Shipboard observations have served as a crucial component to understanding global climate, providing insight to the global atmospheric circulation as early as the 17th century (Webster, 2004). For much of the historical record and over much of the ocean, weather reports

from ships serve as the only significant form of in-situ observation of precipitation, particularly prior to 1970 (JCOMM, 2011). Despite their prevalence and unique role, ship observations have not been integrated into many of the precipitation datasets commonly used today. None of the 20 observation-based precipitation products surveyed by Sun et al. (2018) incorporate shipboard weather reports, relying instead on satellite retrievals; their gauge-based product counterparts are limited to land. Reanalysis products such as ERA5 (Hersbach et al., 2020) also do not incorporate such observations (ECMWF, 2023). Shipboard precipitation observations represent an independent and long-term data record that can support validation of satellite-derived measurements or shed an in-situ perspective on oceanic precipitation well before the advent of satellites or newer observational technologies such as Passive Aquatic Listeners (e.g. Li et al., 2023).

More broadly, surface marine observations obtained from ships may be useful in building long-term CDRs (Kent et al., 2019). The combination of high-resolution satellite data and the long record of ship observations may prove insightful in assessing the changing characteristics of oceanic precipitation, particularly throughout the 20th century (Groisman and Legates, 1995). Ship observations may also help identify some weaknesses and biases inherent in satellite precipitation estimation algorithms (Petty, 1997).

Shipboard observations of precipitation are almost entirely qualitative, describing their occurrence and characteristics without reference to their quantitative amounts. Directly measuring precipitation via shipboard rain gauge is difficult due to possible contamination of the data by sea spray, the movement of the rain gauge induced by the ship or the sea

state, and perturbation of the local winds by the ship or instrument (WMO, 1962). Gauges of different sizes also capture rainfall differently in windy conditions (Elliott and Reed, 1973). Although better-optimized shipboard rain gauges are now available (e.g. Hasse et al., 1998, Klepp, 2015) and recommendations for reducing their uncertainty have been developed (e.g. Yuter and Parker, 2001), their use remains highly limited. The use of alternate devices to quantitatively measure precipitation, such as the disdrometer used for the OceanRAIN dataset (Klepp et al., 2018), have also seen limited use.

1.3.2 History and current practice

The earliest maritime documentation of present weather was largely descriptive, cataloging atmospheric conditions as the observer saw fit. The maritime logbooks of the British Royal Navy, Hudson's Bay Company, and East India Company in the 18th and 19th centuries—one of the most expansive records of maritime conditions from the era—reported the prevailing weather conditions among other meteorological parameters (Wheeler and Wilkinson, 2005). Though less known than his eponymous wind scale, Francis Beaufort, an admiral in the British Royal Navy, developed a coded system of letters for characterizing weather conditions; his system included 26 types of weather phenomena, including some classifications of precipitation, in its 1807 version (Wheeler and Wilkinson, 2005). Beaufort's classifications drew from commonly used terms for weather conditions in British maritime logbooks of the era. His scheme was widely adopted and was also borrowed by the United States Weather Bureau in the first edition of *Instructions to Marine Meteorological Observers of the U.S. Weather Bureau* in 1906 (Page,

1906). The 1853 International Maritime Conference in Brussels sought to systematize and standardize the collection and documentation of meteorological and oceanographic data over the global ocean (Houvenaghel, 1990). A standardized tabulation of data encapsulating observed conditions was developed at the conference, including one column dedicated to describing precipitation. Recognizing the difficulty of directly measuring precipitation amounts at sea, the conference utilized a temporal estimate of precipitation through which rain, snow, hail, or fog could be recorded in terms of the length of time in which they were observed (Maury, 1854). Eighteen countries ultimately agreed to participate in the maritime reporting effort envisaged by the conference (Rigby, 1965). A numeric shorthand for indicating weather conditions became necessary as the practice of transmitting weather observations through telegraphy became prevalent in the late-19th century. Numeric schemes for documenting weather conditions were developed and revised by the International Meteorological Organization (IMO) over the first half of the 20th century (Foken and Rülke, 2021). The 1929 IMO meeting in Copenhagen adopted a universal code for reporting observations and stipulated that participating nations select ships to regularly document and relay observations at synoptic times (Calvert, 1930). A numeric code for present weather with values from 00–99 was introduced to U.S.-recruited observers beginning with the sixth edition of *Instructions to the Marine Meteorological Observers of the U. S. Weather Bureau*, borrowing from the conventions established by the IMO (United States Weather Bureau, 1938). The phenomenon associated with each value was generally similar in ordering and format to what would eventually become the World Meteorological Organization's (WMO) code table for present weather in the

WMO's 1971 *Manual of Codes.* By 1950, the present weather codes prescribed by the IMO largely resembled the modern WMO code table, which serves as the current standard for reporting present weather conditions (Smith et al., 2016, United States Weather Bureau, 1950).

The majority of shipboard observations available today arise from Voluntary Observing Ships (VOS). Crews of VOS fleets, which include commercial and research vessels, are trained, recruited, and managed by National Meteorological and Hydrological Services (NHMSs) (Kent et al., 2010). These ships record and transmit meteorological observations within an international framework established by the WMO and managed by the Joint WMO-IOC Commission for Oceanography and Marine Meteorology (JCOMM) (Vettor and Soares, 2014). The combination of VOS and its predecessors form the longest in-situ record of weather observation over the ocean (Kent et al., 2006), and these observations have formed the backbone of atlases of marine climate (Kent et al., 1993). Observations are typically taken at the standard synoptic times of 00:00, 06:00, 12:00, and 18:00 UTC, but additional observations at intermediate times are encouraged (JCOMM, 2021). The observations from ships today provide useful information for a wide array of both scientific and mercantile applications (Smith et al., 2019).

There are no currently available spatiotemporal gridded datasets consolidating global shipboard precipitation observations. Datasets of precipitation derived from quantitative shipboard observations such as OceanRAIN, though exhibiting high temporal resolution, are limited to along-track measurements from dedicated vessels (Klepp et al., 2018). The

International Comprehensive Ocean-Atmosphere Dataset (ICOADS) is the most comprehensive freely-available collection of surface marine observations. With Release 3.0 of ICOADS, the dataset includes over 455 million individual marine observations between 1662–2014 (Freeman et al., 2016). The dataset stores uniformly-represented observational data across numerous meteorological parameters. The breadth of data provided by shipboard observations in ICOADS has been used to provide robust reconstructions or validation of historical sea surface temperatures (e.g. Minobe and Maeda, 2005, Woodruff et al., 2008), global heat flux (e.g. Berry, 2005, Berry and Kent, 2011), cloud cover (e.g. Bedacht et al., 2007, Hahn and Warren, 1999, Hahn et al., 1992), marine fog (e.g. Danielson et al., 2020, Dorman et al., 2019, Li et al., 2016), sea-level pressure (e.g. Ansell et al., 2006), or regional climate characteristics (e.g. Clark et al., 1996, García-Herrera et al., 2018). Synoptic shipboard observations have also been used to elucidate diurnal and semidiurnal variability (Dai, 2001a).

Among the parameters included in ICOADS is present weather (ww), which borrows its conventions from the WMO Manual on Codes (Freeman et al., 2016, Smith et al., 2016). The WMO defines ww (code table 4677) in the synoptic code as the "present weather reported from a manned weather station" (WMO, 2019). ww is reported as a two-digit value encapsulating the qualitative characteristics of precipitation, with values 00–49 indicating no precipitation and values 50–99 indicating the present occurrence of a variety of precipitation classes (WMO, 2019). The precipitation classes are generally organized in decades, with 50–59 describing drizzle, 60–69 describing rain, 70–79

describing non-showery precipitation, and 80–99 describing showers or thunderstorm activity. Values 20–29 indicate precipitation within the preceding hour but not at the time of observation. While the descriptions associated with the precipitation classes provide some sense of precipitation intensity, there are no quantitative thresholds associated with the intensity descriptors, which include qualitative terms like "slight" or "moderate or heavy" (WMO, 2019). Present weather is routinely reported but occurs less frequently than some other meteorological parameters, including temperature (Cayan and Reverdin, 1994, Fuchs et al., 2001). Nonetheless, the record of ww in ICOADS contains over 99 million present weather observations from crewed vessels from 1950–2019. The WMO synoptic code and ICOADS also include the previous weather codes W_1 and W_2 (code table 4561), which characterize the preceding predominant weather conditions at a manually operated station. Each single-digit value associated with these parameters describes broader phenomena than those described by ww (Smith et al., 2016). About 61.1% of ICOADS reports between 1950–2019 report ww, compared to only about 0.03% providing a quantitative precipitation amount (RRR) during the same period.

1.3.3   Previous uses of shipboard present weather for precipitation analysis

Present weather reports from ships have been previously used to infer oceanic precipitation characteristics or reconstruct precipitation distributions, using the state of the

weather as a proxy for precipitation occurrence and frequency. These analyses of ship-board data provided for the first time a picture of oceanic precipitation that was previously only inferred by spatially extrapolating coastal or insular observations over the ocean (Jacobs, 1968), forming the primary means of constructing oceanic precipitation climatologies before the advent of satellite precipitation retrievals (Adler et al., 2017). In lieu of reliable or robust quantitative measurements of oceanic precipitation, quantification of precipitation amount using shipboard present weather reports has been primarily informed by land-based stations which can both report present weather and directly measure precipitation amounts. Other methods have also attempted to incorporate other meteorological shipboard measurements (e.g. Berry, 2005, Tsonis, 2002).

The earliest use of ship observations to infer oceanic precipitation distributions date as far back as the early 19th century using observations from merchant vessels (Park et al., 2017). Early analyses using the modern standardized coded system for weather reporting constructed precipitation climatologies using observations from Ocean Weather Ships (OWS), which operated at designated locations and documented present weather regularly year-round (Austin and Geotis, 1980). Tucker (1961) used ww reports from OWSs to construct a 1953–1957 climatology of precipitation amounts over the North Atlantic. To quantify the present weather reports, nominal values were assigned based on presumed relationships between the phenomena described by precipitating present weather reports ($ww \geq 50$) and light, moderate, or heavy continuous rainfall. Empirical coefficients of 1.85 mm hr^{-1}, 5.66 mm hr^{-1}, and 8.13 mm hr^{-1} were obtained for light, moderate, and heavy continuous rainfall, respectively, based on 12 land stations in Britain.

Monthly coefficients were also developed to calibrate estimated monthly precipitation totals. This novel technique was subsequently adapted to estimate annual and seasonal oceanic precipitation using other regions and sets of ships (e.g. Elliott and Reed (1973) using lightships off the U.S. Pacific Northwest coast, and Reed and Elliott (1973) using OWSs across the North Pacific).

Reed and Elliott (1977) assessed that the nominal precipitation coefficients obtained by Tucker (1961), extracted solely from land-based stations in Britain, were reliable poleward of 40° latitude and possibly sufficient poleward of 25° latitude but greatly underestimated tropical rainfall. Two primary methods were developed to sidestep or augment the limited regional utility of the Tucker (1961) coefficients. Dorman and Bourke (1978) developed a modification to the coefficients by regressing the residual between observed precipitation amounts and Tucker's method on observed air temperature annually, seasonally, and monthly at coastal stations. Their results empirically suggested a correction to the coefficients that scaled quadratically with temperature, with precipitation totals exceeding those derived using the Tucker (1961) methodology by as much as a factor of 5 where the annual mean temperature was around 30°C. Oceanic precipitation climatologies constructed with these modified coefficients identified for the first time mid-latitude precipitation maxima associated with the Gulf Stream and Kuroshio western boundary currents. These modified coefficients were applied by Dorman and Bourke (1979) to ship observations over the Pacific between 30°S–60°N on a 2° × 5° grid and by Dorman and Bourke (1978) to ship observations over the Atlantic between 30°S–70°N on a 2° × 5° grid. Goroch et al. (1984) applied the temperature adjustment method to commercial and U.S.

Navy *ww* reports to develop maps of rain rate covering the Indian, North Atlantic, and North Pacific oceans.

Reed (1979) proposed an alternate method of using overall precipitation frequency to quantify oceanic precipitation amounts based on observations from 12 oceanic weather ships in the Northern Hemisphere without intensity delineations or the use of individual *ww* values. This methodology was applied by Reed and Elliott (1979) to precipitation frequencies drawn from U.S. Navy marine climatic atlases, deriving distributions of quantitative precipitation totals throughout much of the North Pacific and North Atlantic. A global climatology of oceanic precipitation was obtained by Elliott and Reed (1984) using the same technique. The temperature-weighted methodology developed by Dorman and Bourke (1978) and the frequency-based methodology developed by Reed (1979) produced disparate results, with the former method tending to produce greater precipitation totals (Dorman, 1980, Dorman and Bourke, 1981). The temperature-weighted methodology also resulted in a spurious decrease in precipitation in spring (da Silva et al., 1994). The lack of robust quantitative oceanic precipitation data prior to the advent of satellite estimation precluded determination of the relative accuracy of either method (Reed, 1980), though a later analysis by Berry (2005) suggested temperature calibration overcorrected at low latitudes and undercorrected at high latitudes when evaluated against GPCP. Despite the inherent uncertainty in extrapolating quantitative precipitation information from the occurrence of shipboard *ww* reports, the general contours of the methodology first utilized by Tucker (1961) formed the basis of oceanic precipitation maps published

in the USSR and the United States (Sharova, 1990). Sharova (1990) produced global estimates of precipitation amounts using a blend of old and new methodologies, combining the frequency of precipitation reported by ships with intensities derived from extrapolating coastal and insular precipitation amounts out to sea. To reconcile differences in the temperature-based methodology (Dorman and Bourke, 1979, 1981) and frequency-based methodologies Jaeger (1983), Legates and Willmott (1990) assumed that their differences were highly correlated with air temperature and developed a multiple linear regression for each month converting frequency-based quantitative precipitation estimates to temperature-based estimates to construct a global precipitation climatology.

The use of qualitative ship observations to infer oceanic precipitation amounts appears to have declined after the 1980s, concurrent with the increasing prevalence of satellite PMW-based estimates of oceanic precipitation. With increasingly accurate satellite-based techniques filling large spatiotemporal gaps in the understanding of oceanic precipitation, the need for ww-based quantifications of amounts diminished, particularly as the developed methodologies for generating amounts from ww reports remained disparate. Instead, subsequent precipitation studies using shipboard present weather focused primarily on the frequencies and character of various precipitation types. Cayan and Reverdin (1994) broadly considered the occurrence of all shipboard precipitation ($ww \geq 50$) to examine correlations between precipitation frequency and mean sea-level pressure over the ocean. Petty (1995) developed a classification system for the ww values based on their associated phase, intensity, and character, with combinations of those categorizations resulting in 22 classes of precipitation. These categories were used to infer seasonal distributions

of their occurrence across the global ocean. Dai (2001a) combined shipboard present weather observations to derive global seasonal distributions for the occurrence of precipitation associated with drizzle, non-drizzle, showers, non-showers, and thunderstorms between 1995–1997, adopting the Petty (1995) ww classifications. A similar analysis by Dai (2001b) inferred diurnal variabilities from shipboard present weather data. Tsonis (2002) attempted an empirical orthogonal function (EOF)-based reconstruction of oceanic precipitation to improve quantitative precipitation estimates derived from shipboard ww but did not obtain reliable results. Shi and Liu (2021) used ww data from ICOADS between 1978–2019 aggregated into $5° \times 5°$ boxes to infer trends in the occurrence of precipitation, snowfall, and the snow–precipitation event ratio. Their analysis observed a decline in the average snow event to precipitation event ratio over the ocean, including positive trends in precipitation occurrence over the tropical Atlantic, negative trends in precipitation occurrence over the western and northern Pacific, and negative trends in snow occurrence between 30°N–60°N. Due to constraints imposed on the minimum amount of data, their aggregated trends primarily arose from the Northern Hemisphere. Shipboard ww reports have also been used to assess the temperature characteristics of the rain–snow transition and the conditional likelihood of frozen precipitation (Liu, 2008, Sims and Liu, 2015). In addition to constructing precipitation climatologies, shipboard ww data have also been used as a source of validation for other quantitative precipitation estimation techniques, including satellite-based retrievals (e.g. Ellis et al., 2009, Garand, 1989, Petty, 1997).

1.3.4   Ship data limitations

There are several possible weaknesses in a dataset relying on qualitative manual observations from mobile platforms like ships. Although the identification of broad precipitation types may be understood by weather observers, the characterization of present weather is ultimately subjective. In particular, differentiation between qualitative precipitation intensities and the continuous, intermittent, or showery nature of precipitation may be inconsistent between observations and subject to the observer's experience, biases, or local practices. The most recent update to the WMO *Manual on Codes*, published in 2019, provides no specific guidance in determining the intensity of precipitation (WMO, 2019). The Manual on Codes does, however, provide instructions on when to indicate a thunderstorm in the *ww* code. The WMO's *Guide to Meteorological Instruments and Methods of Observation* includes descriptions of precipitation and visual differences between precipitation intensities and characteristics tailored for shipboard observers (WMO, 2021). While such guidance may constrain the range of phenomena conceivably classified by a particular *ww* value, their mostly qualitative nature intrinsically leaves room for inconsistent reporting. Instructions from the United States Weather Bureau and the National Oceanic Atmospheric Administration (NOAA) have historically provided some recommendations for determining precipitation intensity, such as the reduction in visibility caused by snow or the ability for the observer to resolve individual rain droplets (e.g. National Weather Service, 1971, Office of the Federal Coordinator for Meteorological Services and Supporting Research, National Oceanic and Atmospheiric Administration,

2019, United States Weather Bureau, 1959). Despite the delineations in visibility used to determine snowfall intensity, the influence of the time-of-day and characteristics of the hydrometeors complicates the relationship between snowfall intensity and visibility (Rasmussen et al., 1999). Nonetheless, these recommendations represent only one country's recommended practices and do not eliminate the subjectivity of present weather reporting. Additionally, changes in recording practices over time may introduce non-climatic variability for specific present weather classifications, though distributions and trends concerning broader categorizations of present weather conditions are likely to be more robust.

Ship observations do not represent a spatially or temporally uniform dataset. As ships tend to cluster around shipping lanes, areas between shipping lanes are often much less sampled (Berry and Kent, 2011), as detailed in Section 2.2.1. The areas most sampled by ships globally include the northwestern Pacific, northern Atlantic, and North Sea where the sampling density exceeds 5 observations per 100 km^2 per year. The availability of ship observations has also varied throughout the 20th and 21st centuries. Observations from VOS, which constitute a majority of manual ship observations, have declined since about 1984–85, when the VOS fleet included around 7,700 ships (Vettor and Soares, 2014).

Unlike land-based stations and fixed marine observation platforms, ships are prone to seek calmer conditions when possible. Extreme events may be entirely unsampled (Berry and Kent, 2011). Thus, the meteorological data provided by shipboard observations may be subject to this "fair-weather bias." This tendency may impact wind observations (e.g.

Gulev et al., 2003), wave heights (e.g. Grigorieva et al., 2020), and estimates of sensible heat flux (e.g. Gulev et al., 2007), though it is uncertain whether or not such a bias significantly and systematically impacts global shipboard observations (Kent et al., 2012, Kent and Taylor, 1995). Estimates of precipitation using shipboard observations alone may underestimate the magnitude or frequency of oceanic precipitation (Willmott and Legates, 1991), though Béranger et al. (2006) assessed that a shipboard-based oceanic precipitation climatology developed at the Center for Climatic Research (CCR) indicated higher precipitation values in the equatorial Pacific compared to other datasets. Ships also tend to slow down but remain on course during episodes of inclement weather (Gulev et al., 2007, Kent and Taylor, 1995). A "foul-weather bias" may also arise from the data as ships may overreport inclement conditions if they are traversing slowly through them (Warren et al., 2015) or if observers report significant weather and disregard non-significant weather disproportionately (Petty, 1995). The tendency for ships to report more during the day compared to night also introduces another possible bias in shipboard present weather data (Warren et al., 2015). However, analysis of these potential biases using cloud cover comparisons between transient ships and stationary weather ships by Warren et al. (1988) suggested that these biases were generally small.

Despite the quality issues inherent in shipboard present weather observations, Ellis et al. (2009) found good concordance between ICOADS-based precipitation frequency and CloudSat precipitation frequency between 2006–2007 across the global ocean.

1.4   Research objectives

This thesis represents a step in a broader research effort to infer long-term climatological information on oceanic precipitation from shipboard present weather reports, with the ultimate goal of inferring quantitative precipitation amounts from the historical ship record calibrated using modern satellite-derived estimates. The lengthy, globally-spanning, and uniquely in-situ record of shipboard ww reports provides an opportunity to explore key questions about oceanic precipitation that this research effort seeks to address, including:

- Can the shipboard ww record be used to reconstruct physically-sensible historical data on oceanic precipitation?

- Are modern satellite-based precipitation retrievals over the ocean consistent with in-situ observations?

- How has oceanic precipitation changed since 1950?

- Where have changes to oceanic precipitation been most evident?

In Petty and Tran (2023), long-term trends in the overall fractional time precipitating in the period 1950–2019 were identified using the shipboard ww record, finding significant positive trends in precipitation frequency within the subtropics and tropics and negative trends at higher latitudes. This study extends the findings of Petty and Tran (2023) and employs similar techniques to explore selected subtypes of precipitation, providing a closer look at the changing character of oceanic precipitation. These ship-inferred

characteristics—independent of precipitation estimates from other platforms—are used to identify long-term trends in oceanic precipitation incorporating data predating modern instrumentation.

Chapter 2 characterizes the data and details the methods used in reconstructing ship-derived precipitation frequencies, including quality control of ship-based data and the derivation of frequencies and trends. Chapter 3 presents the frequencies and trends ascertained from shipboard present weather reports. Chapter 4 places these findings in the context of climate change, reconciling ship observations with our current understanding of the behavior of oceanic precipitation and highlighting areas where the ship-inferred data is discordant with other datasets. Chapter 5 summarizes this research and suggests avenues for future investigation.

Chapter 2

Data and Methods

2.1 Data sources

This analysis of shipboard present weather observations relies primarily on individual

observations from the International Comprehensive Ocean-Atmosphere Dataset. Gridded

SST data from the Extended Reconstructed SST and Kaplan Extended SST datasets are

also used to shed light on the relationships between SST and oceanic precipitation. The

use of two SST datasets with different data sources, methodologies, and resolutions is

used to better increase confidence in the validity of the precipitation-SST relationships.

2.1.1 International Comprehensive Ocean-Atmosphere Dataset (ICOADS)

ICOADS began as the Comprehensive Ocean-Atmosphere Dataset (COADS), emerging from a collaborative effort launched between the National Oceanic and Atmospheric Administration (NOAA) and the National Center for Atmospheric Research (NCAR) in 1981 (Woodruff et al., 1987). The first datasets collated in COADS were primarily provided by the National Climatic Data Center (NCDC) and the first release of COADS included observations from 1854–1979. The project was renamed the International Comprehensive Ocean-Atmosphere Dataset in 2002 in reflection of the increasing international cooperation and the archive's growing number of multinational data sources (Diaz et al., 2002) The current iteration of the ICOADS database is composed of Release 3.0, covering observations from 1662–2014 (ICOADS R3.0 Freeman et al., 2016), and Release 3.0.2, a preliminary, near-real time archive of marine observations from 2015–present from Global Telecommunications System (GTS) sources (ICOADS R3.0.2 Liu et al., 2022). The compendium of datasets constituting of ICOADS is actively evolving and may incorporate newly recovered or digitized datasets in the future (e.g. Teleti et al., 2023).

This analysis is based on ICOADS data from 1950–2019, drawing upon both ICOADS components and spanning 70 years of shipboard observational records. This period was chosen to seek more global consistency in observations without the possible effects on shipping due to major naval conflicts and with greater global coordination following

World War 2 and the formation of the WMO. The International Maritime Meteorological Archive (IMMA) file format encoding the conventions and definitions for values in ICOADS are described by Smith et al. (2016). ICOADS Release 3.0 and 3.0.2 are freely available from NCAR at `https://rda.ucar.edu/datasets/ds548.0/`. Several metadata and meteorological parameters are extracted from the dataset, including present weather (ww), dry-bulb air temperature (AT), and total cloudiness (N), among others. Present weather is encoded with a two-digit value associated with a characteristic weather condition. The present weather parameter is used as the primary determinant for the occurrence of precipitation, as all ww values exceeding 50 indicate ongoing precipitation at the time of reporting and take precedence over other ongoing phenomena. To begin with as many observations as reasonably available from the outset, the data was retrieved with "enhanced" filtering applied, which has relaxed constraints for data inclusion compared to the "standard"-filtered dataset.

ICOADS monthly summary products are also available for some observational parameters. Present weather is not included in these products, though its inclusion in future releases of ICOADS has been discussed (Joint WMO-IOC Commission for Oceanography and Marine Meteorology, 2011).

2.1.2   Extended Reconstructed SST (ERSST)

The United States National Oceanic and Atmospheric Administration (NOAA)'s Extended Reconstructed SST, version 5 (ERSSTv5) dataset provides monthly estimates of SST on a global $2° \times 2°$ latitude-longitude grid spanning the period from January 1854

to the present (Huang et al., 2017). The ERSSTv5 reconstruction uses SST observations from ICOADS R3.0, GTS reports, and Argo floats, with the data adjusted in part using sea ice concentrations from the Hadley Centre Sea Ice and Sea Surface Temperature dataset, version 2 (HadISST2; Titchner and Rayner, 2014) and the Hadley Centre Nighttime Marine Air Temperature, version 2 (HadNMAT2; Kent et al., 2013).

2.1.3 Kaplan Extended SST

The Kaplan Extended SST V2 dataset maintained by the UK Met Office provides monthly estimates of SST on a global $5° \times 5°$ latitude-longitude grid spanning the period from January 1856 to the present (Kaplan SST; Kaplan et al., 1998). Kaplan SST uses ship and satellite-derived observations subjected to optimal smoothing, Kalman filtering, and optimal interpolation. The underlying data for Kaplan SST are based on an adjustment of gridded SST from the ship-based Meteorological Office Historical Sea Surface Temperature dataset (Parker et al., 1994) for the period 1856–1991 and multiplatform-based optimally interpolated SST dataset described by Reynolds and Smith (1994).

2.2 ICOADS filtering

There are numerous maritime platforms that record meteorological information, including various automated platforms that have become increasingly prevalent in recent decades. However, shipboard present weather observations provide the most global coverage of in-situ precipitation available today (Kent et al., 2010). Characterization of present weather has also been subject to automation (e.g. Landolt et al., 2019, Merenti-Välimäki et al.,

2001). The quality controls used in this analysis were used in Petty and Tran (2023), except where noted. In order to minimize heterogeneities introduced by incorporating different platforms—particularly temporal heterogeneities produced by newer observing technologies throughout the period of record—the analysis presented here is limited to manual observations of present weather taken onboard ships. This excludes buoys, floats, or other automated platforms. To tailor the analysis to ships, ICOADS observations with platform types (PT) of either 0 (U.S. Navy, "deck" log, or unknown; 37.4 million observations), 1 (merchant ship or foreign military; 4.3 million observations), or 5 (ship; 121.3 million observations) were used. The inclusion of $PT = 0$ and $PT = 1$ as part of the ship record follows the recommendation from Smith et al. (2016) to treat such observations as equivalent to $PT = 5$ due to their poor documentation. Observations from dedicated ocean station vessels ($PT = 2$ or 3) and lightships ($PT = 4$), despite having human observers, were excluded to ensure a more spatially homogeneous dataset; such ships make a large majority of their observations in proximity to select locations for a limited number of years. Observations with missing PT, indicating unknown platform type, were also excluded from the analysis.

Before 1982, a "/" value for ww the synoptic code indicated that the present weather observation was unavailable (Hahn et al., 1992). A WMO rule change came into effect on 1 January 1982 that permitted a ww value of "/" if there was no significant present weather observed by a human observer (Dai, 2001a, Hahn et al., 1992, Petty, 1995). This rule change implied that a wet-bias would be observed if only extant ww reports were considered in the early 1980s (da Silva et al., 1994). A new station/weather indicator

i_X was added to the synoptic code to clarify whether the omission of ww was due to insignificant weather or the lack of data availability. While ship reports quickly adopted the practice of omitting ww given insignificant weather, usage of i_X was not reliably consistent until 1985 (Hahn et al., 1992). Previous efforts to address this discrepancy have typically used reporting of cloud cover N (encoded in oktas) as a proxy for valid observations. da Silva et al. (1994) and Petty (1995) both utilized the assumption that an accompanying mandatory report of total cloud cover N implied that ww was either available or intentionally omitted. Dai (2001a) assumed $ww = 3$ ("clouds generally forming or developing") in cases where ww and i_X were missing and accompanied by $N \leq 7$. This analysis borrows the conjecture from Petty (1995), in that the presence of non-missing N in a report was evidence that a human observer had made a sky and present-weather observation, with an accompanying missing ww presumed to suggest non-significant phenomena and thus no precipitation. The same ad hoc scheme was applied to this analysis. All observations with either ww or N were thus kept in cases where i_X was missing. Where i_X was available, only ship observations with $i_X \leq 3$ were kept; these values explicitly indicate manned observations. Between 1950–2019, within the selected platform types, 37.0 million observations were explicitly manual ($i_X \leq 3$), 10.5 million observations were explicitly automated ($i_X > 3$), and 115.5 million observations did not include an i_X value.

Although small in comparison to the overall dataset, 11,724 crewed ship observations of ww report snow accompanying air temperatures greater than 10°C, accounting for about 1.1% of all snow observations. Using ICOADS data between January 1950 through May

2007, Sims and Liu (2015) suggested that the globally-averaged conditional probability of oceanic snowfall was 50% with an accompanying air temperature of 1.9°C, as well as determining a 5.0°C temperature range between the 90% and 10% conditional probabilities. The conditional probability of oceanic snowfall falls below 5% at around 5°C and diminishes to near 0% at around 10°C. Additionally, 2,090 ship observations of ww report frozen precipitation over the tropical ocean between 10°N–10°S, though many of these observations are not accompanied by air temperature measurements. CloudSat retrievals suggest that the conditional mean snowfall rate over the ocean between 30°N–30°S is approximately 0% (Liu, 2008). Shipboard frozen precipitation reports in anomalously hot or tropical conditions are thus likely erroneous. To eliminate these reports, the entire ICOADS dataset was filtered to only include ship observations with an accompanying report of AT, and observations of frozen precipitation with $AT > 10\,°C$ were discarded.

This analysis also excluded all observations originating from the Inter-American Tropical Tuna Commission (IATTC), which are indicated in ICOADS with a deck number (DCK) of 667. COADS observations matching this criteria introduced large temporal and spatial inhomogeneities to the underlying dataset. These observations were initially introduced to COADS to improve coverage of SST and cloudiness fields within the eastern tropical Pacific (Wolter, 1997, Woodruff et al., 1993). This data was quality-controlled and provided by the IATTC and was first added to COADS Release 1a under pseudonymous IDs (Woodruff et al., 1998, Worley, 1992). Woodruff et al. (1993) attributed a bias towards weaker winds within the IATTC data to fair weather bias, and excluded IATTC data from published enhanced statistics concerning winds for COADS Release

1a. IATTC data continues to be selectively excluded from COADS Monthly Summary Group products due to these biases. The excluded IATTC observations consist of around 1.148 million observations between 1971–1997 (Smith et al., 2016).

The analysis also excluded observations from the Russian Marine Meteorological Data Set (MORMET), which are indicated with $DCK = 732$ and consist of roughly 7.5 million marine observations between 1888–1995, with a higher volume of reports between 1950–1990 (Smith et al., 2016). Their inclusion introduced large spatial and temporal inhomogeneities in the analysis, particularly over the eastern Pacific. Observations from deck 732 have been previously excluded from other analyses using ICOADS (e.g. Kennedy et al., 2011, Minobe and Maeda, 2005).

2.2.1 Dataset characteristics

Taken together, the final, filtered ICOADS dataset used for this analysis includes 99.7 million ship observations, representing an average of around a thousand ship observations globally every six hours for 70 years. The annual number of ship observations were highest between the 1960s and 1990s, with a maximum annual count of 2.4 million in 1967 (Figure 2.1). No year in the period features less than 500,000 ship observations. The meridional distribution of reports has remained relatively consistent throughout the 70-year period and with ship observations taken in the mid-latitudes of the Northern Hemisphere persistently accounting for the majority of observations in a year (Figure 2.2). Reports are primarily clustered around major shipping lanes (Figure 2.4), with better coverage across the mid-latitudes of the Northern Hemisphere and more sparse observations over

the Arctic, Southern, and southeastern Pacific Oceans. Each season is approximately equally represented in the counts of global reports (Figure 2.3), though reports in the higher latitudes are heavily concentrated in the summertime (Figure 2.5).
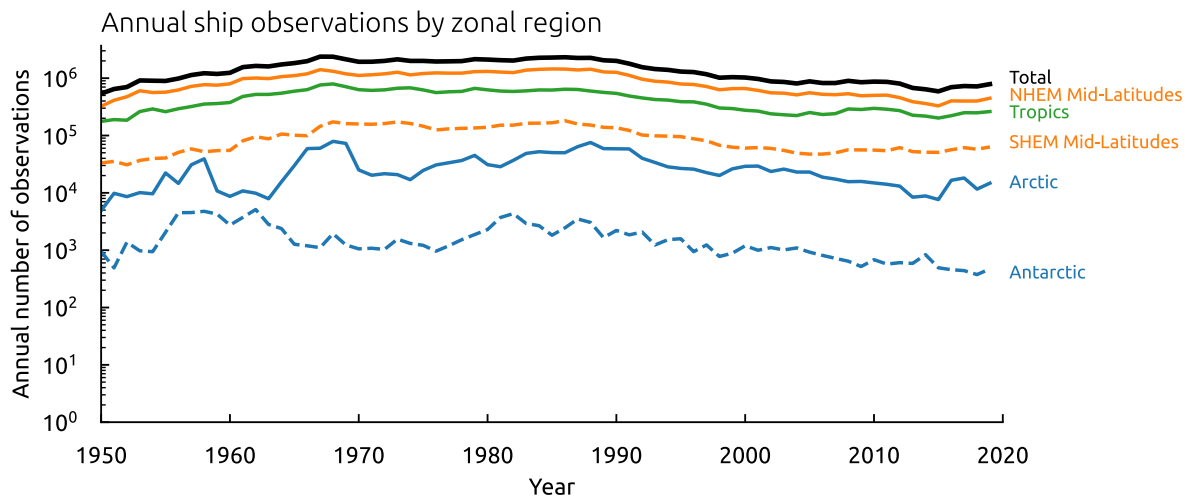
FIGURE 2.1: Annual counts of ship observations used in this analysis aggreggated by latitudinal region. The Arctic and Antarctic regions are areas poleward of 66.56° latitude in the Northern (NHEM) and Southern (SHEM) hemispheres, respectively, while the tropics cover the region between the Tropics of Cancer and Capricorn. The mid-latitudes cover the region between the tropics and polar regions in either hemisphere.
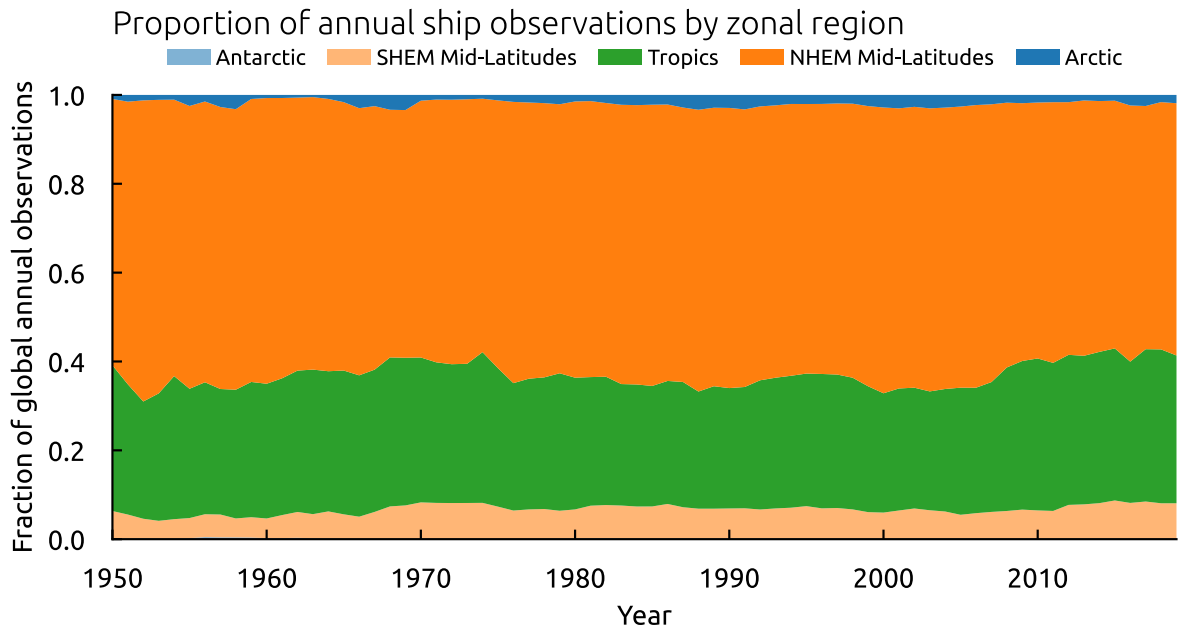
FIGURE 2.2: Percentage of global annual observations within each of the latitude bands described in Figure 2.1.
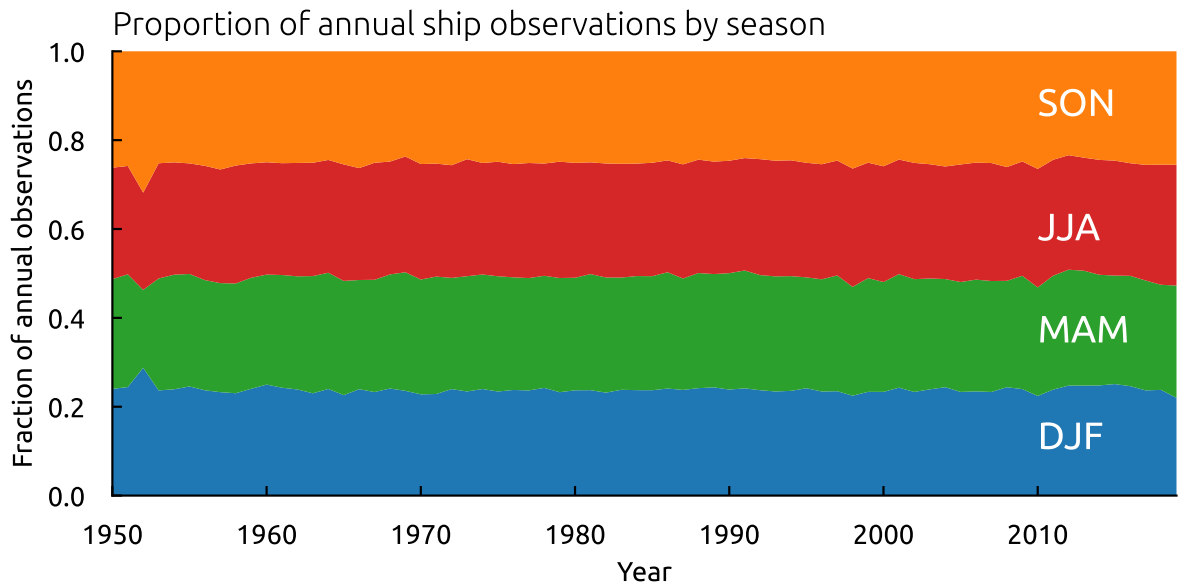
FIGURE 2.3: Annual percentage of global observations occurring within each season.

FIGURE 2.4: Mean count of annual ship observations per $1° \times 1°$ area.
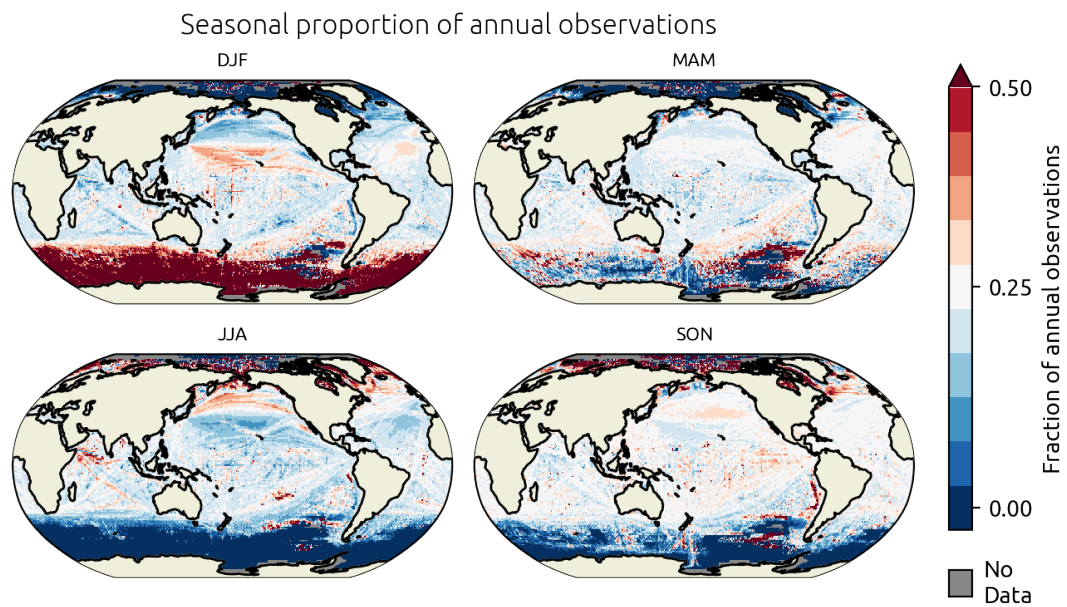
FIGURE 2.5: Fraction of shipboard observations occurring in each season per $1° \times 1°$ area.

TABLE 2.1: Selected groupings of precipitation used in this analysis and their associated ww values. Refer to Table 1 in Petty (1995) for standardized interpretations of individual ww codes.

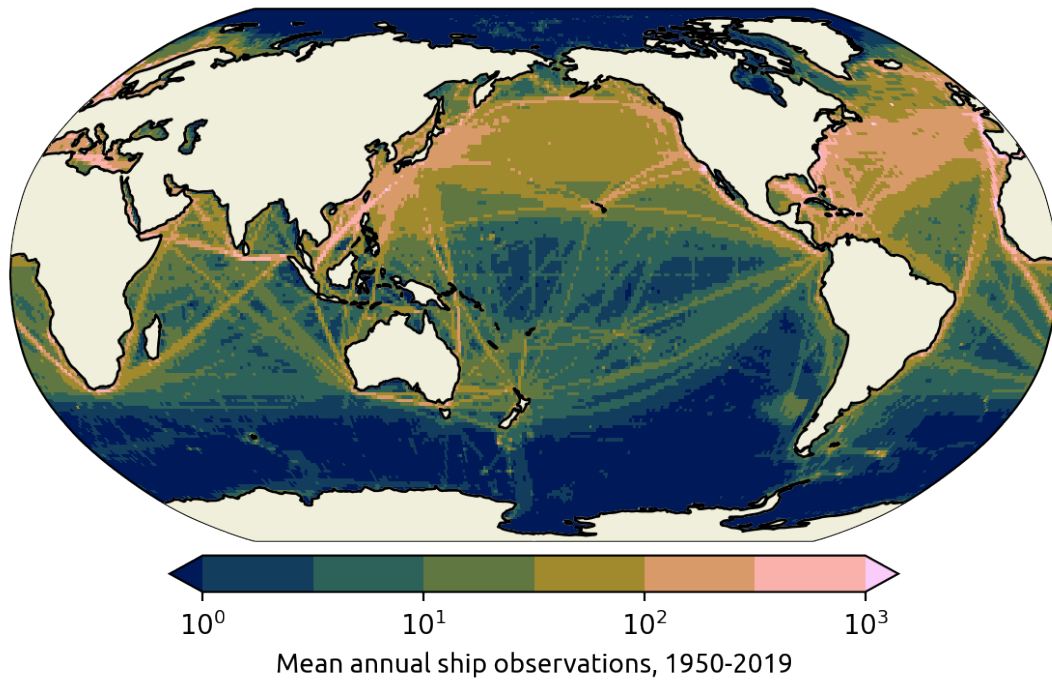| Precipitation category	ww values
All precipitation	$ww \geq 50$
Drizzle	50, 51, 52, 53, 54, 55, 57, 65, 77, 78
Moderate/heavy non-drizzle	59, 62, 63, 64, 65, 67, 69, 72, 73, 74, 75, 81, 82, 84, 86, 88, 90, 94, 95, 96, 97, 98, 99
Deep convection and thunderstorms	82, 89, 90, 91, 92, 93, 94, 95, 96, 97, 98, 99
Frozen-phase	70, 71, 72, 73, 74, 75, 76, 77, 78, 85, 86

2.2.2 Selected precipitation groupings

This analysis focuses on four categories of precipitation described in Petty (1995): 1) drizzle-intensity precipitation, 2) moderate- and heavy-intensity non-drizzling precipitation, 3) precipitation accompanying thunder and deep convection, and 4) frozen-phase precipitation. The ww values associated with each category are described in Table 2.1.

For shipboard observers, the WMO recommends precipitation be classified as drizzle when consisting of "fairly uniform precipitation of very fine drops of water very close to one another that fall from a cloud" (WMO, 2021). The intensities of non-drizzling liquid precipitation are distinguished by visual accumulation on the ship deck, the sound of the rainfall, and whether individual raindrops can be discerned. For frozen precipitation, the WMO recommends distinguishing intensities by their effect on visibility.

2.3 Frequency estimation

The shipboard observations used in this analysis describe conditions at the ship solely at the time and place of observation, providing spatiotemporally limited information. Thus, ship reports must be aggregated in both time and space to provide climatologically informative precipitation estimates. The use of the categorical ww from ICOADS precludes the use of techniques tailored to estimating amounts and errors associated with quantitative shipboard measurements (e.g. Kent and Berry, 2005, Morrissey and Greene, 2008, Vettor and Soares, 2021). Instead, a composited Bayesian approach is applied to gridded and aggregated ship observations to infer estimates of the frequency of precipitation. In this analysis, "frequency" refers to the fractional time precipitating.

For a selected temporal subset of total observations, and within any one grid cell, there are n_total valid ship observations in the selected time period. Among these are $n \leq n_\text{total}$ ship observations reporting a desired subset of ww observations, and of these, $m \leq n$ report a narrower subset of ww observations. The simple ratio m/n provides one estimator for the frequency of m conditioned on n. For example, given $n = 50$ observations of rain and $m = 10$ observations of drizzling rain, the frequency of occurrence for drizzle given rainy conditions within the target area may be approximated by $m/n = 0.2$. Past estimates of precipitation frequencies using ship observations have been largely computed in this manner (e.g. Dai, 2001a).

However, this method of frequency estimation can produce unrealistic depictions of precipitation distributions, particularly when the underlying physical phenomena is rare or if the spatiotemporal subset is not well sampled by ships, such that m may be quite small, if not 0. This is especially true over the open ocean far from major shipping lanes and for relatively infrequent phenomena such as mixed-phase precipitation. In these circumstances, the sample probability of occurrence may undesirably be 0% within a grid cell. Alternatively, Bayesian estimates for f may be more effective in reconstructing f for poorly sampled events (Basu et al., 1996). In this analysis, the estimation of f is derived from determining the probability of randomly observing the target phenomenon m times out of n observations, assuming f is equiprobable between $[0, 1]$. This choice of a uniform distribution for f as a non-informative Bayesian prior corresponds to a Beta distribution with $\alpha = 0$ and $\beta = 1$. The resulting Bayesian probability estimator for f, $\hat{f}$ and the corresponding estimator for the error σ, $\hat{\sigma}$ is thus given by

$$\hat{f} = \frac{m+1}{n+2} \tag{2.1}$$

$$\hat{\sigma} = \left[\frac{(m+1)(n-m+1)}{(n+3)(n+2)^2} \right]^{1/2} \tag{2.2}$$

Equation 2.1 is a suitable approximation for $\hat{f}$ when m and or f are small and converges towards m/n for large m and n. When $n \lesssim 5$ and $m = 0$, the uncertainty is considered too large to be useful, and $\hat{f}$ is treated as indeterminate. Further details of the derivation for Equation 2.1 can be found in Appendix A.

Ship observations were initially tabulated on a $1° \times 1°$ global grid, excluding lakes and landmasses using the Python `global-land-mask` module. To generate maps of overall frequencies and trends, $\hat{f}$ and $\hat{\sigma}$ were computed at varying spatial resolution by mapping ship reports to global grids with square $1°$, $3°$, $5°$, $7°$, $9°$, $11°$, and rectangular $13°$ x $26°$ cells. The values were initially computed for the coarsest spatial resolution and progressively replaced with the results obtained at finer resolutions at each $1°$ gridbox so long as the finer sampling did not considerably increase the relative uncertainty given by $\hat{\sigma}/\hat{f}$. The result of this procedure is a smoothed $1° \times 1°$ grid of estimated frequencies for the precipitation groupings of interest. This procedure was independently computed for each precipitation grouping and each seasonal period. This composited $\hat{f}$ reflects an aggregation of observations over a broader surrounding area for data-sparse regions and finer resolution in data-rich regions such as shipping lanes and coastal areas.

70-year mean frequencies were not computed for grid cells where more than 5 years of aggregate ship observations were missing or where $\hat{\sigma}/\hat{f} \geq 0.4$. As this parameter varies depending on the number of relevant ship observations m, the data coverage differs between ww groupings even if they share the same n. A two-tailed Student's t-test was applied to the mean frequencies to gauge the significance of differences between 1950–1978 (the period predating the GPCP, the longest satellite precipitation record) and 1979–2019 (the period spanned by the GPCP and other satellite-based datasets) at the 95% confidence level.

2.4   SST correlation

To produce correlation maps between the $1° \times 1°$ resolution gridded shipboard data and coarser $2° \times 2°$ and $5° \times 5°$ resolutions of ERSSTv5 and Kaplan SST, respectively, the ship data were first upscaled to match the gridded SST dataset resolutions using the conservative method (Jones, 1999) implemented via the Python `xesmf` package (Zhuang et al., 2023). To assess the correlation between the two datasets, each dataset was detrended by subtracting the ordinary least-squares regression (OLR) for the period 1950–2019 before computing the Pearson correlation coefficient r between the yearly relative precipitation frequencies and the yearly mean Kaplan SST anomaly. A two-tailed Student's t-test was applied to the correlation data to evaluate significance relative to the null hypothesis of $r = 0$ at the 95% confidence level. Though the length of either the SST or ship observation data at each gridbox $S = 70$ years, a reduced effective independent sample size $S' = S(1 - \rho)/(1 + \rho)$, where ρ is the lag-1 autocorrelation, was used for the significance test (Box et al., 2015).

2.5   Trend estimation

Temporal trends in frequency were computed using the composited frequency grids. At each gridpoint, OLR was performed to identify decadal trends. The significance of the linear trend was tested using a two-tailed Student's t test against the null hypothesis of zero trend evaluated at the 95% significance level using the same effective sample size procedure as for SST correlation. The results of the OLR trend analysis did not differ

considerably from a weighted least squares regression of the same data weighted by $\hat{\sigma}$.

As with frequencies, 70-year trends were not computed for grid cells where more than 5

years of aggregate ship observations were missing or where $\hat{\sigma}/\hat{f} \geq 0.4$.

Chapter 3

Results

3.1 Drizzle

Shipboard drizzle-intensity ww observations are most prevalent in the subtropics and in the eastern halves of oceanic basins annually and in all seasons (Figure 3.1). In particular, the relative frequency of drizzle as a fraction of all precipitation peaks during the summer in either the Northern and Southern hemispheres. Where sufficient data are available, the zonal mean annual drizzle fraction reaches peaks of 0.39 ± 0.09 in the Southern Hemisphere and 0.33 ± 0.01 in the Northern Hemisphere, with both peaks occurring near 47° latitude (Figure 3.4a). The relative proportion of drizzle is reduced over the tropics, with mean annual fractions near 0.15 typical of the region. Drizzle accounts for a majority of annual shipboard precipitation reports along the Atlantic coast of southern Africa and along the equatorial Pacific coast of South America, and

accounts for a majority of shipboard precipitation reports during JJA for much of the northern Pacific (Figure 3.4c). Annually, the proportion of precipitation reports with drizzle is generally positively correlated with SST over the western Pacific and negatively correlated over the Eastern Pacific (Figure 3.2), with the strongest negative correlations over the equatorial East Pacific, where $r < 0.5$. This bifurcation in correlation is more meridionally oriented in the Atlantic, with positive correlations over the mid- to higher-latitude North Atlantic and negative correlations over the equatorial and tropical South Atlantic, particularly near Africa. Over the Indian Ocean, the observed drizzle fraction shows generally weaker negative correlations ($r < -0.3$).

The ship-based drizzle record indicates a greater preponderance of drizzle over most regions during the period spanned by satellite-based precipitation datasets compared to the pre-satellite era (Figure 3.3c), with statistically significant positive differences prevalent over the Indian Ocean, western Pacific, and central Atlantic. Meridional mean increases in the drizzle fraction are greatest over the Indian Ocean (Figure 3.3d). The ship record suggests that slight but nonetheless statistically significant decreases in the prevalence of drizzle over the mid-latitude northern Pacific during the satellite era compared to the pre-satellite era, reflected by a decrease in the zonal mean drizzle fraction between roughly 40–60°N by around 2–4 percentage points (Figure 3.4c).

Mean fraction of precipitation with drizzle intensity (1950-2019)
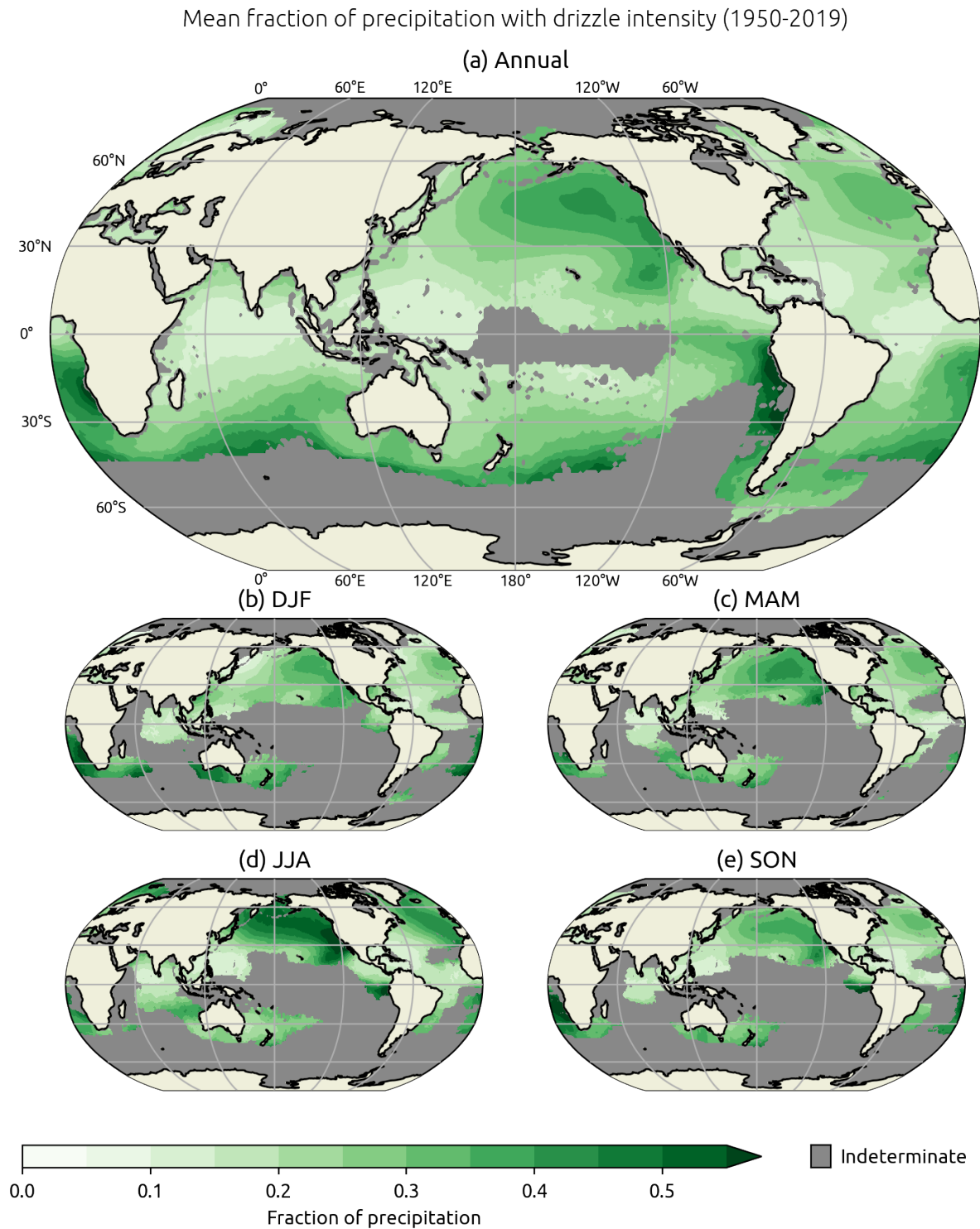
FIGURE 3.1: Mean (a) annual and (b-e) seasonal fractions of precipitation events occurring with drizzle intensity. Gray shading denotes areas with more than 5 years of missing values or excess uncertainty after the compositing procedure is performed. Gray shading denotes areas with more than 5 years of missing values or excess uncertainty after the compositing procedure is performed.

Correlation between SST and annual fraction of precipitation reports with drizzle
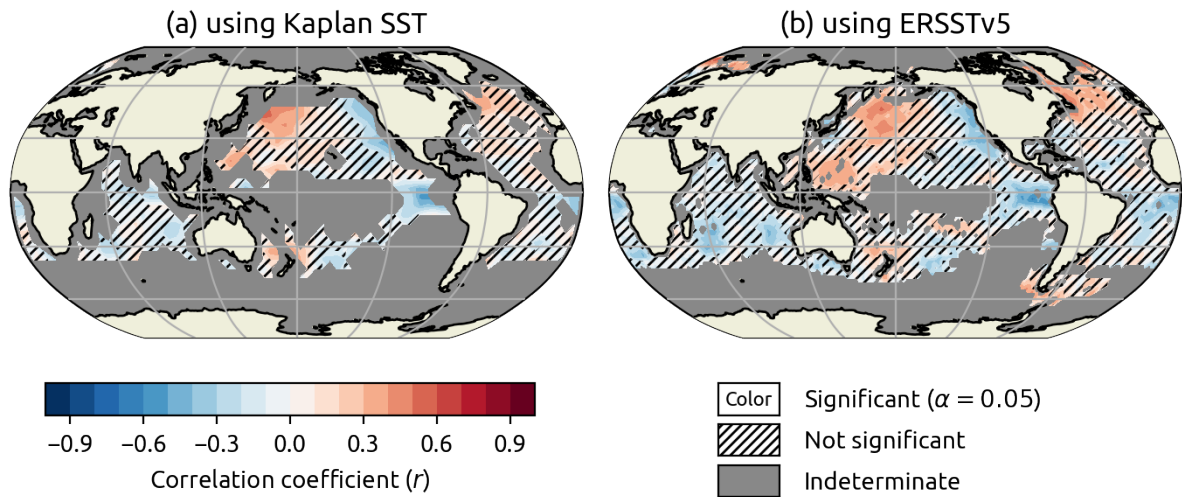
FIGURE 3.2: Correlation coefficient between the detrended annual fraction of precipitation events occurring with drizzle intensity, regardless of phase, with detrended SSTs using (a) Kaplan SST and (b) ERSSTv5. Hatching indicates areas with statistically significant trends at the 95% confidence level. Correlations were only computed for areas with sufficiently low uncertainty.

FIGURE 3.3: The mean annual fraction of precipitation events occurring with drizzle intensity, regardless of phase, during (a) 1950–1978, the period preceding satellite-derived precipitation estimates, and (b) 1979–2019, the period overlapping with satellite-derived precipitation estimates. (c) shows the difference between (b) and (a), with hatching indicating statistically significant differences in means between the two periods at the 95% confidence level. Means are only computed for areas with sufficiently low uncertainty.

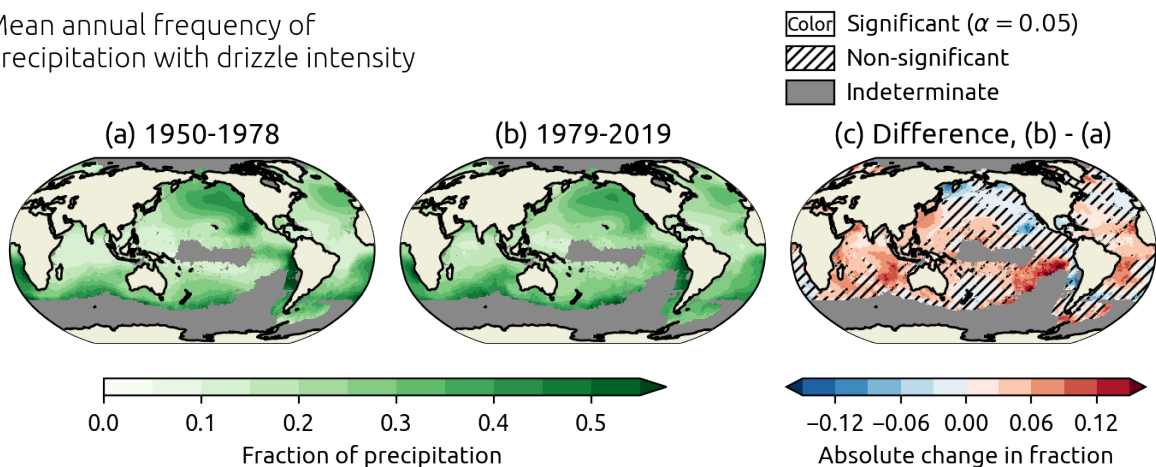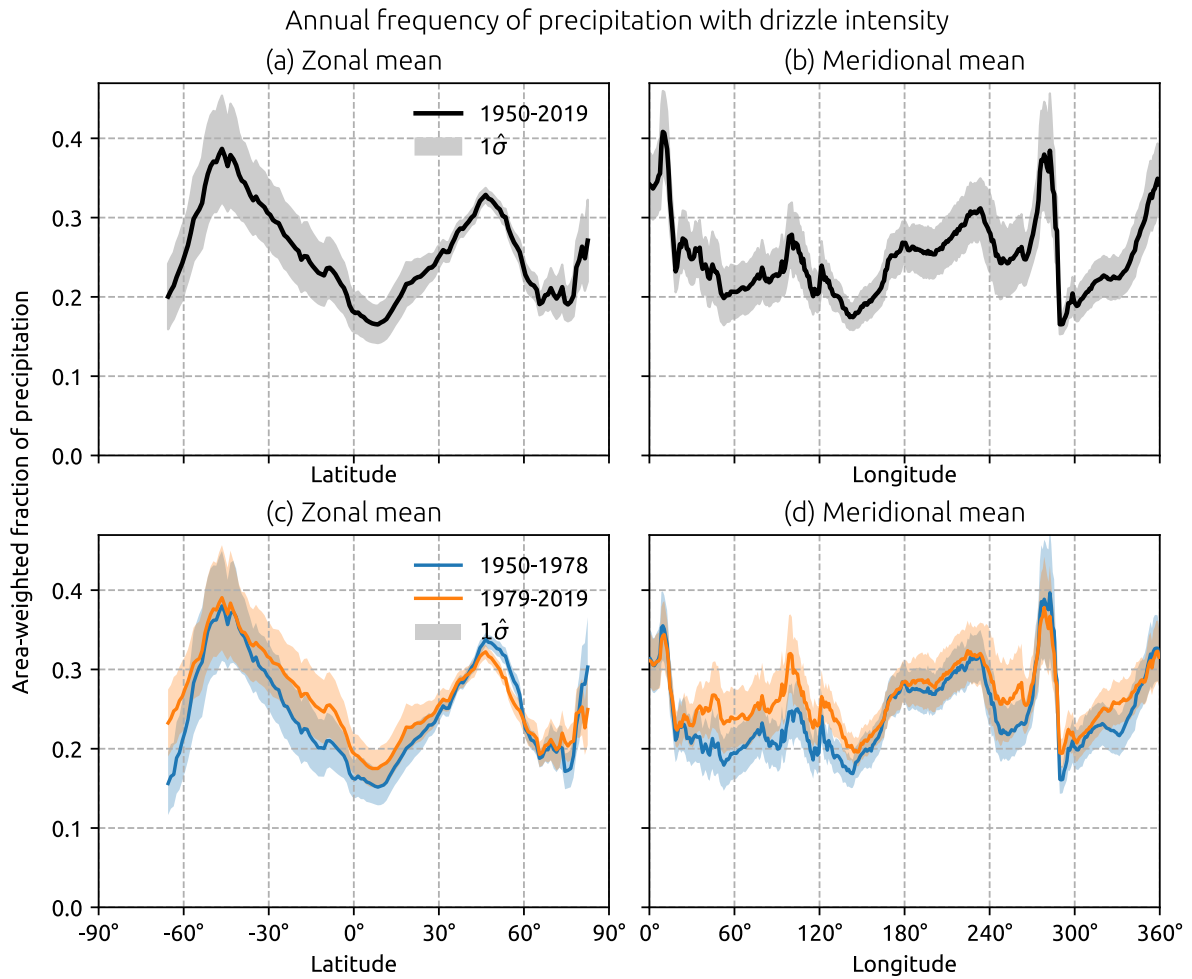FIGURE 3.4: The zonal (a, c) and meridional (b, d) mean annual fraction of precipitation events occurring with drizzle intensity, regardless of phase, during 1950–2019 (a, b) and for the periods 1950–1978 and 1979–2019 (c, d). The estimated mean zonal and meridional uncertainty $\pm\hat{\sigma}$ is shaded for each timeseries. Means are only computed over areas with sufficiently low uncertainty.

Over the 70-year period from 1950 through 2019, statistically significant positive trends in the drizzle fraction have been observed throughout the tropics of both hemispheres annually and seasonally, with positive fractional trends of up to 15% per decade in the equatorial Indian Ocean, and the tropical South Atlantic (Figure 3.5). These trends represent absolute increases between about 1–4 percentage points per decade. Where statistically significant, the 70-year trend is positive in virtually all areas equatorward of $25°$ outside of a small portion of the eastern North Pacific.

Weakly negative but statistically significant negative trends have been observed the mid-latitude North Pacific and in limited portions of the eastern subtropical North Pacific and eastern mid-latitude Atlantic, with fractional decreases mostly less than 4% per decade. The decrease in the annual fraction over the mid-latitude North Pacific and North Atlantic has been largely driven by negative trends during JJA. For many areas, the positive trend in drizzle fraction has been marked by a gradual increase in fraction over the 70-year period. Much of the high positive tendency calculated for the tropical Atlantic east of Brazil may be due to uncharacteristically large drizzle fractions observed in JJA 2016 and DJF 2018 (Figure 3.6b). However, a slight positive trend is still apparent for the region's annual fraction outside of those years across the 70-year period. Shipboard observations capture a possible signal of multidecadal variability in the drizzle fraction over the Tropical Indian Ocean (Figure 3.6d) and East China Sea (Figure 3.6e), with broad peaks in the annual and seasonal drizzle fractions occurring around 1970, 2000, and 2015.

Relative trend of precipitation with drizzle intensity (1950-2019)

(a) Annual

(b) DJF   (c) MAM

(d) JJA   (e) SON

Relative trend of fraction [% per decade]

Significant ($\alpha = 0.05$)

Non-significant

Indeterminate

FIGURE 3.5: 70-year relative linear trend in the (a) annual and (b) seasonal fraction of precipitation events occurring with drizzle intensity, regardless of phase. Hatching indicates areas with statistically significant trends at the 95% confidence level. Gray shading denotes areas with more than 5 years of missing values or excess uncertainty after the compositing procedure is performed.

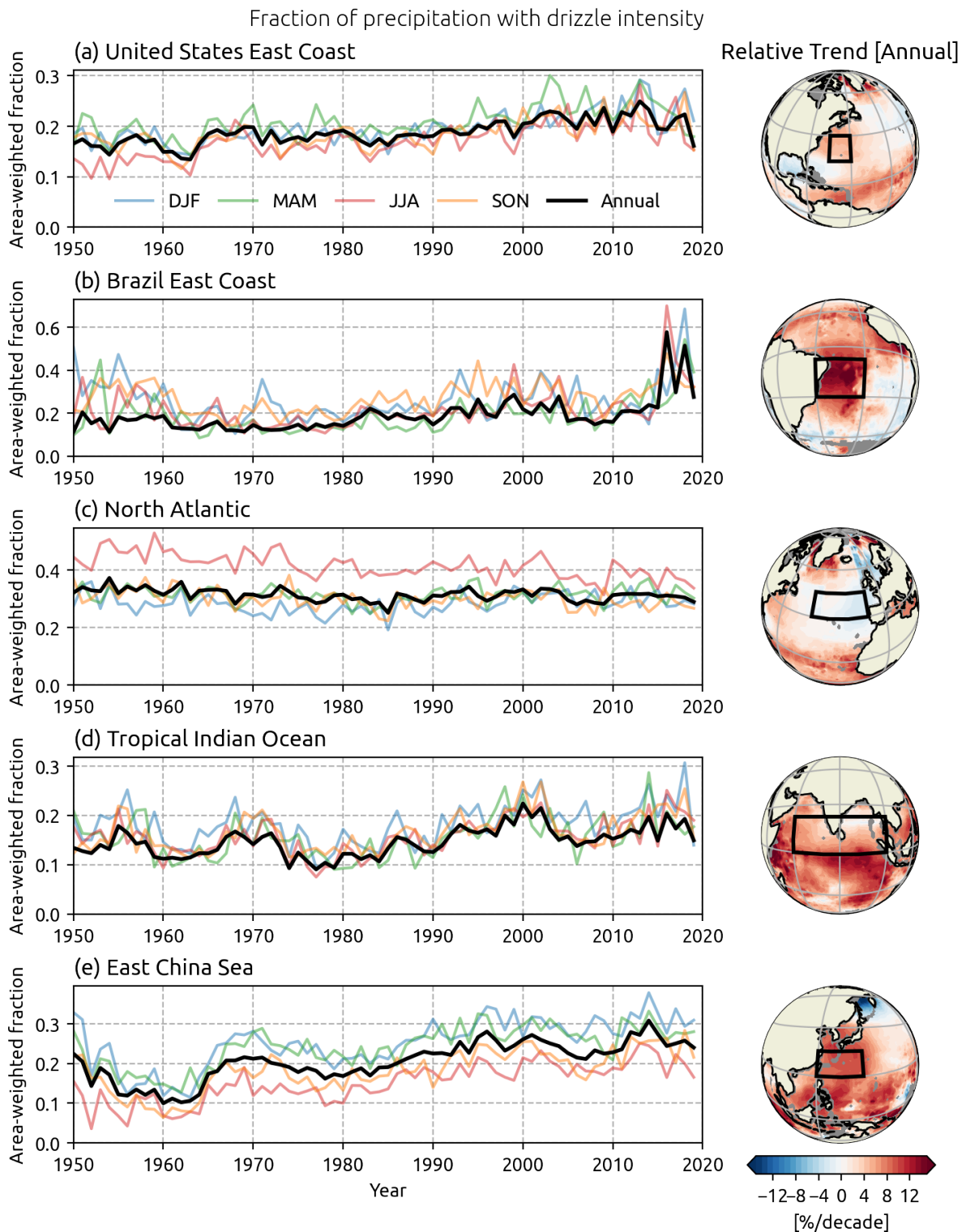Fraction of precipitation with drizzle intensity

FIGURE 3.6: Regionally-aggregated and area-weighted year-to-year annual and seasonal fractions precipitation events occurring with drizzle intensity (left) for the selected region outlined by the rectangular region (right). Gray shading denotes areas with more than 5 years of missing values or excess uncertainty after the compositing procedure is performed.

3.2   Moderate or heavy intensity non-drizzle

Precipitation reported as having either "moderate" or "heavy" intensity accounts for a larger share of non-drizzling shipboard ww reports over the tropics and higher latitudes seasonally and annually compared to the subtropics, with the highest annual values observed over the tropical Indian Ocean, equatorial Central Pacific, and near the Maritime Continent (Figure 3.7a). The annual zonal mean fraction reaches a maximum just north of the equator, peaking at 0.46 ± 0.04 near 4.5°N (Figure 3.10a). The subtropical northeastern Pacific and subtropical southern Atlantic are regional minima in the annual fraction, with moderate and heavy intensity precipitation accounting for as low as 20% of non-drizzling precipitation reports. Over the mid-latitude North Pacific and North Atlantic, this proportion of moderate and heavy intensity non-drizzle is greatest during DJF and SON and reaches a minimum in JJA (Figure 3.7b-e). The Yellow Sea and East China Sea are also a regional minimum for this precipitation class, though this distinction is most evident in DJF (Figure 3.10b).

The annual zonal mean relative fraction of moderate or heavy intensity non-drizzle reaches minima of 0.38 ± 0.05 near 25°S and 0.37 ± 0.02 near 26°N (Figure 3.10a). Over the mid-latitude Northern Hemisphere, where data coverage is more widespread compared to the Southern Hemisphere, a broad zonal minimum is captured between 20–50°N, with the fraction increasing poleward. Shipboard ww reports suggest possible differences in the relationship between SST and the annual preponderance of moderate or heavy intensity precipitation between the Northern Hemisphere and Southern Hemisphere (Figure 3.8).

The fraction is generally negatively correlated over much of the Northern Hemisphere, outside of parts of the eastern subtropical Pacific and the eastern subtropical Atlantic. In contrast, positive correlations prevail over much of the Southern Hemisphere, though in most part these correlations are not statistically significant.

Shipboard reports of moderate or heavy non-drizzle have accounted for a larger share of non-drizzling precipitation during the satellite era than the pre-satellite era over parts of the tropical and subtropical North Pacific and the western North Atlantic (Figure 3.9). These changes are marked by a shrinking of the regional minimum over the subtropical northeastern Pacific and an expansion and increase in the fraction straddling Central America and off the East Coast of the United States. Shipboard fractions are also significantly higher during the satellite era over the Mediterranean Sea and along the Pacific coast of Asia. These increases are reflected by an increase in the zonal mean fraction across the Northern Hemisphere, particularly between the equator and 50°N (Figure 3.10c) .The zonal minimum in the Northern Hemisphere is shifted northward relative to the pre-satellite era, occurring near 50°N. A decrease in the satellite era relative to the pre-satellite era was observed throughout the Indian Ocean and over the eastern Atlantic, but this difference was not statistically significant.

Mean fraction of non-drizzle precipitation with moderate / heavy intensity (1950-2019)

(a) Annual

(b) DJF

(c) MAM

(d) JJA

(e) SON

FIGURE 3.7: As in Figure 3.1, but for moderate/heavy intensity precipitation as a fraction of non-drizzle precipitation.

Correlation between SST and annual fraction of
non-drizzle precipitation with moderate / heavy intensity

(a) using Kaplan SST

(b) using ERSSTv5

−0.9 −0.6 −0.3 0.0 0.3 0.6 0.9
Correlation coefficient (r)

Color Significant ($\alpha = 0.05$)

Not significant

Indeterminate

FIGURE 3.8: As in Figure 3.2, but for moderate/heavy intensity precipitation as a
fraction of non-drizzle precipitation.

Mean annual frequency of non-drizzle precipitation
with moderate / heavy intensity

Color Significant ($\alpha = 0.05$)

Non-significant

Indeterminate

(a) 1950-1978

(b) 1979-2019

(c) Difference, (b) - (a)

0.20 0.25 0.30 0.35 0.40 0.45 0.50 0.55
Fraction of non-drizzle precipitation

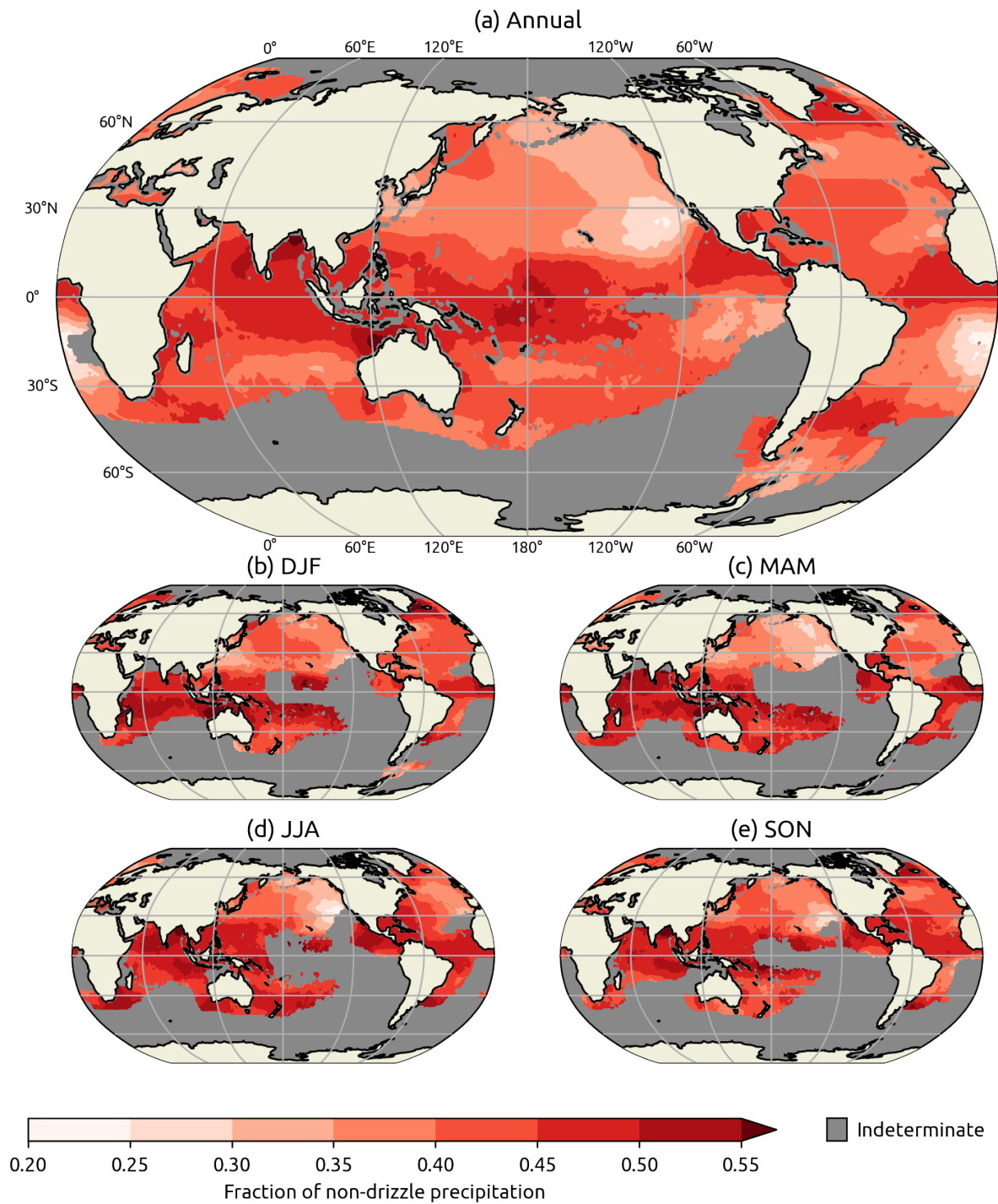−0.12 −0.06 0.00 0.06 0.12
Absolute change in fraction

FIGURE 3.9: As in Figure 3.3, but for moderate/heavy intensity precipitation as a
fraction of non-drizzle precipitation.

FIGURE 3.10: As in Figure 3.4, but for moderate/heavy intensity precipitation as a fraction of non-drizzle precipitation.

The clearest 70-year trends in the fraction of non-drizzle precipitation with moderate or heavy intensity are over the subtropical North Pacific, Mediterranean Sea, Yellow Sea, where statistically significant and positive trends have been observed annually and seasonally with relative magnitudes on the order of 5–10% per decade (Figure 3.11). The mean zonal trend peaks annually and seasonally between 20–35°N, with a mean relative increase of around 3–4% per decade. The pattern of trends is not zonally symmetric about the equator, with the positive trends in the subtropical Northern Hemisphere contrasted by weakly negative trends in the tropical Southern Hemisphere.

A belt of positive trends in the subtropical Pacific is only present in the North Pacific between 15–30°N, with a lack of clear trend in the subtropical South Pacific. Over the central and eastern North Pacific, a sharp increase in the share of non-drizzle intensity occurring at higher intensities was reported by ships during the latter half of the 1960s, particularly along the Pacific coast of Northern America (Figure 3.12b, c). Since 1970, this fraction has held relatively steady for these areas. For the Mediterranean and Yellow seas, the positive 70-year trends observed reflect a more gradual increase throughout the period (Figure 3.12a, d). Globally, the area covered by statistically significant decreasing trends in the proportion moderate or heavy intensity precipitation is generally smaller and lower in magnitude than positive-trending regions.

Relative trend of non-drizzle precipitation with moderate / heavy intensity (1950-2019)

FIGURE 3.11: As in Figure 3.5, but for moderate/heavy intensity precipitation as a fraction of non-drizzle precipitation.
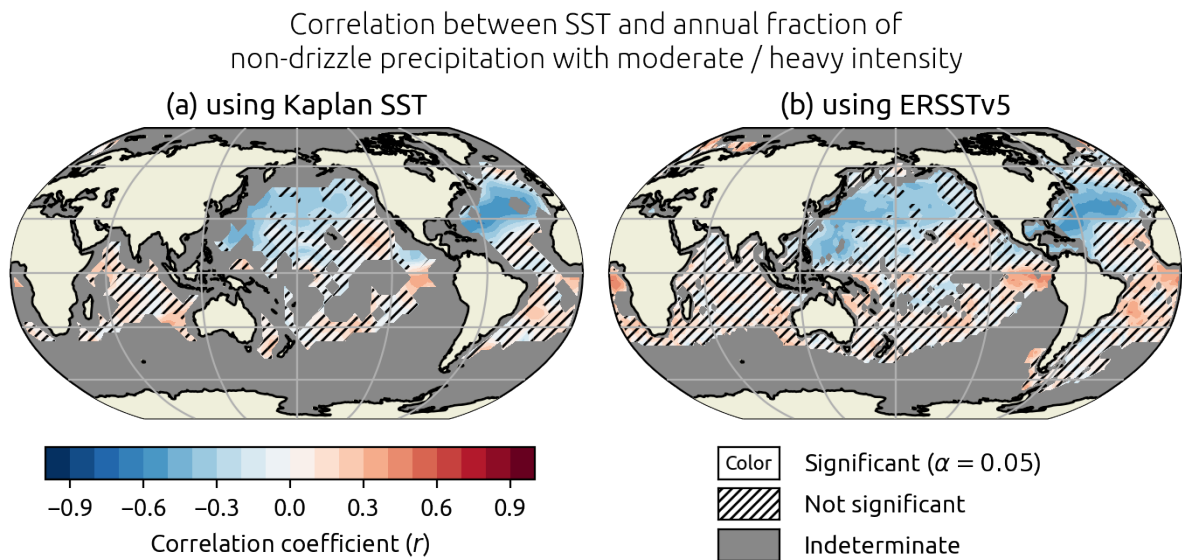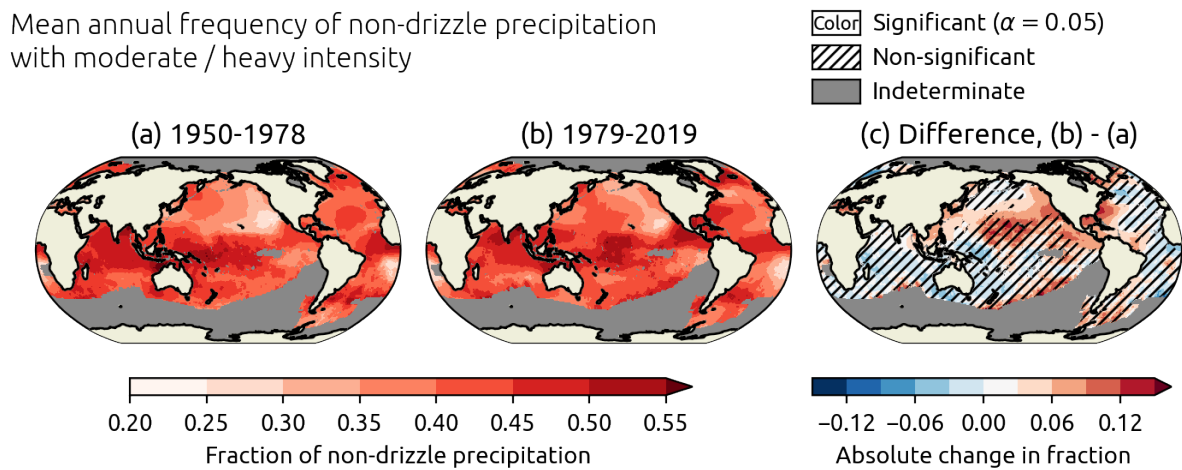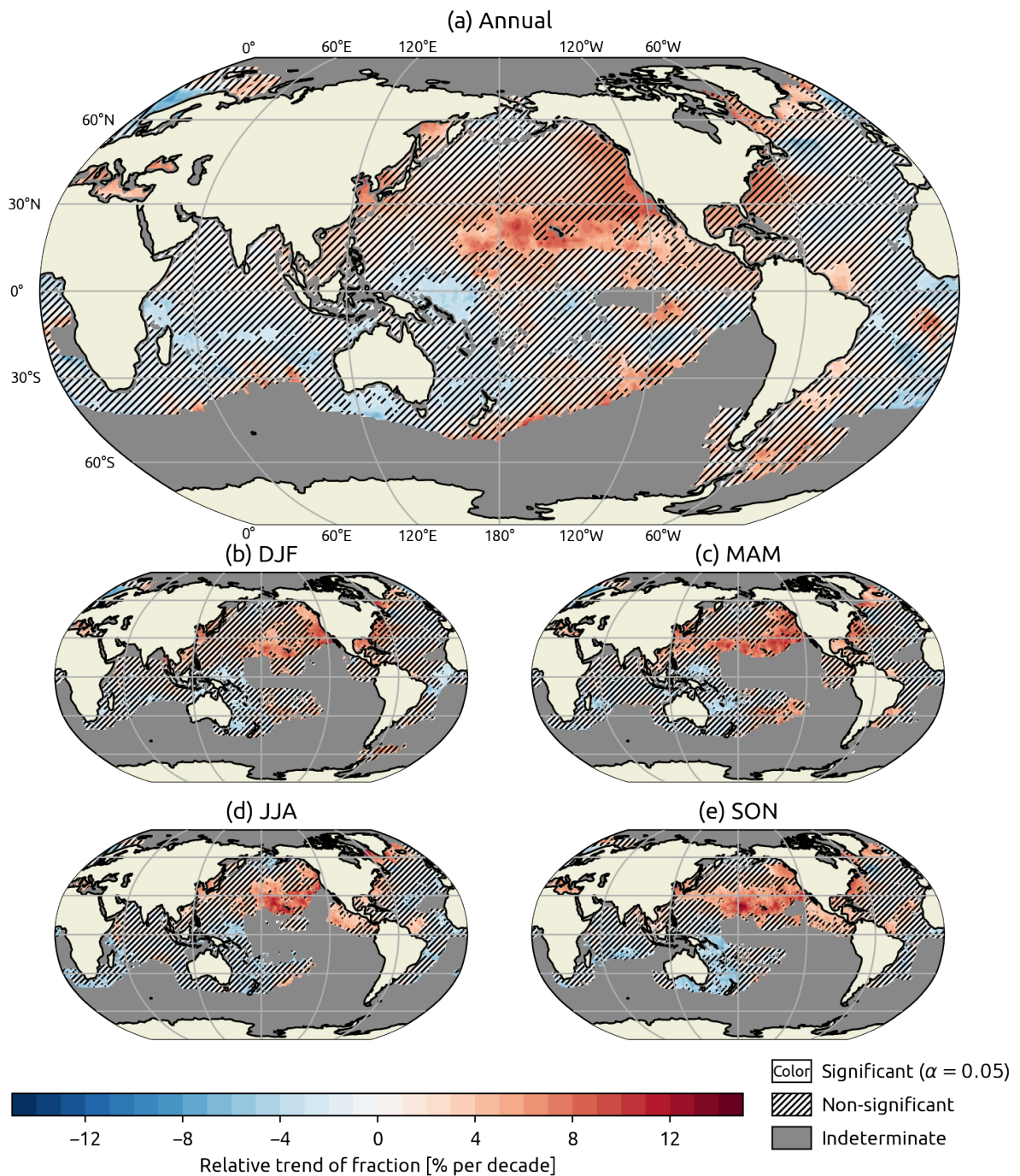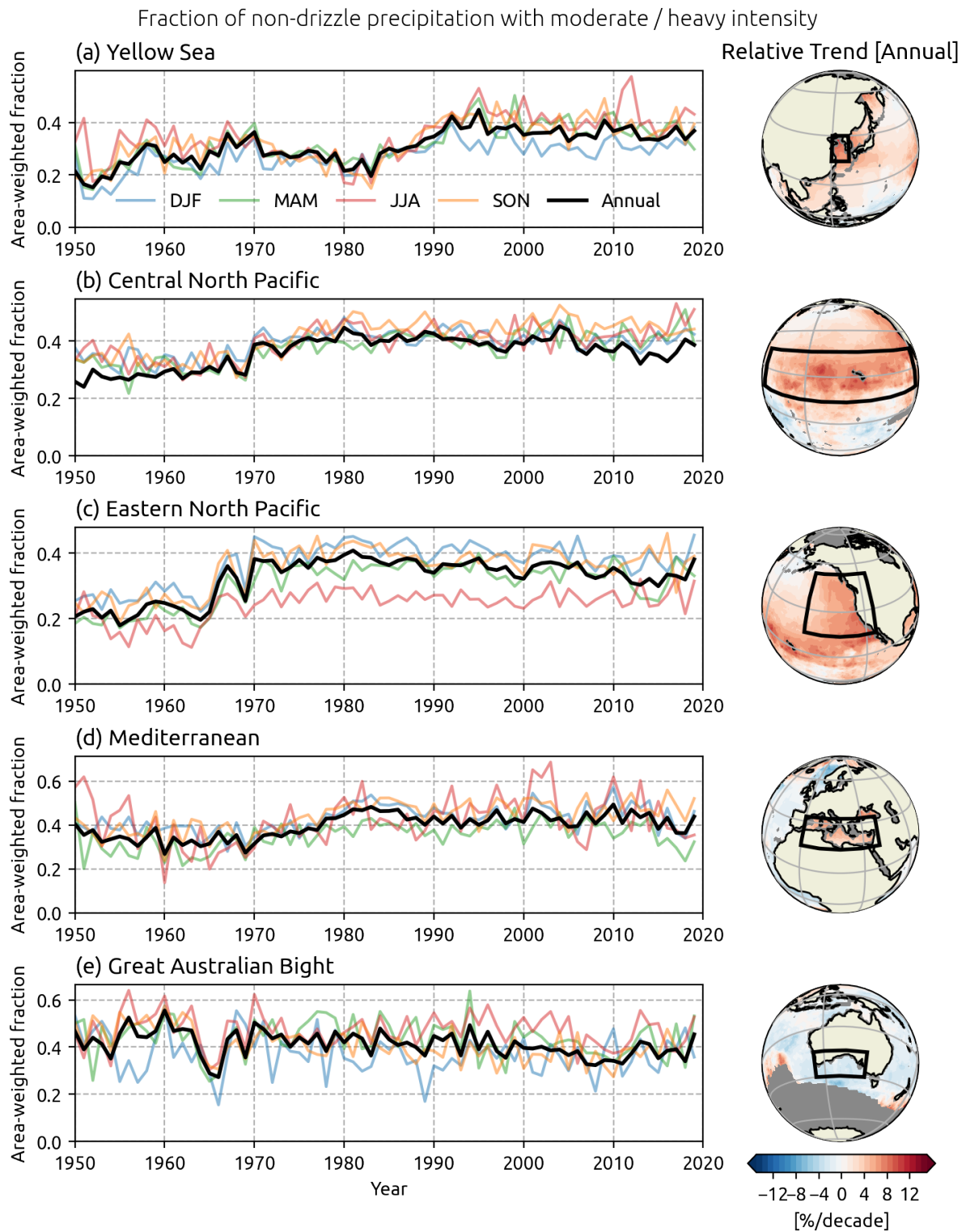
FIGURE 3.12: As in Figure 3.6, but for moderate/heavy intensity precipitation as a fraction of non-drizzle precipitation.

3.3 Deep convection and thunderstorms

Shipboard observations of deep convection and thunderstorms are most prevalent annually over the equatorial Atlantic off Africa, over the western Atlantic and along the Pacific coast of Central America, and in the Mediterranean (Figure 3.13a). In these areas, the annual fraction of non-drizzle precipitation associated with deep convection or thunderstorms reaches as high as about 0.16. The relative occurrence of deep convection and thunderstorms in the western Atlantic is highest in JJA (Figure 3.13c), while a maximum is observed in the Mediterranean in SON (Figure 3.13e). During these seasons, the mean fraction exceeds 0.2 in parts of these areas. A seasonal maximum in this relative fraction also occurs over the equatorial Indian Ocean during MAM (Figure 3.13c). Statistically significant negative correlations between annual non-drizzling deep convection/thunderstorm activity and SST have been observed over the subtropical Atlantic (Figure 3.14), with a local minimum in correlation over the Sargasso Sea ($r \approx -0.6$). A positive relationship is apparent along the Pacific coast of Mexico and Central America using the higher-resolution ERSSTv5 data, with correlation coefficients as high as 0.5.

For most areas with sufficiently low uncertainty, the observed difference in the relative frequency of oceanic deep convection and thunderstorms between the satellite and pre-satellite era is not statistically significant (Figure 3.15c). However, positive statistically significant differences are observed over the western Atlantic and Mediterranean, where

the relative fraction is 3–6% higher during the satellite era. Statistically significant negative differences are also observed throughout the open North Atlantic and eastern equatorial Atlantic.

FIGURE 3.13: As in Figure 3.1, but for the fraction of non-drizzle precipitation associated with deep convection or thunderstorms.
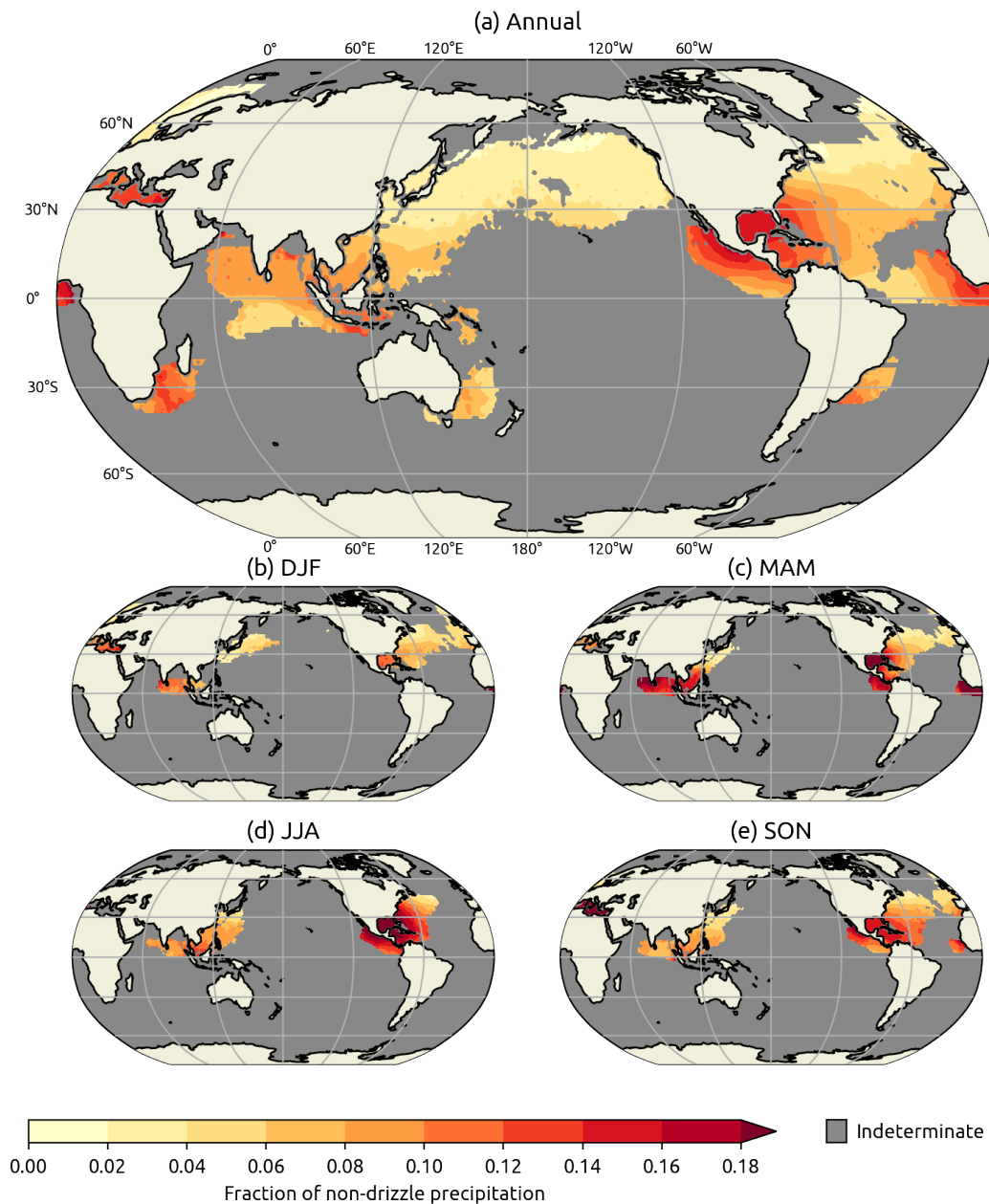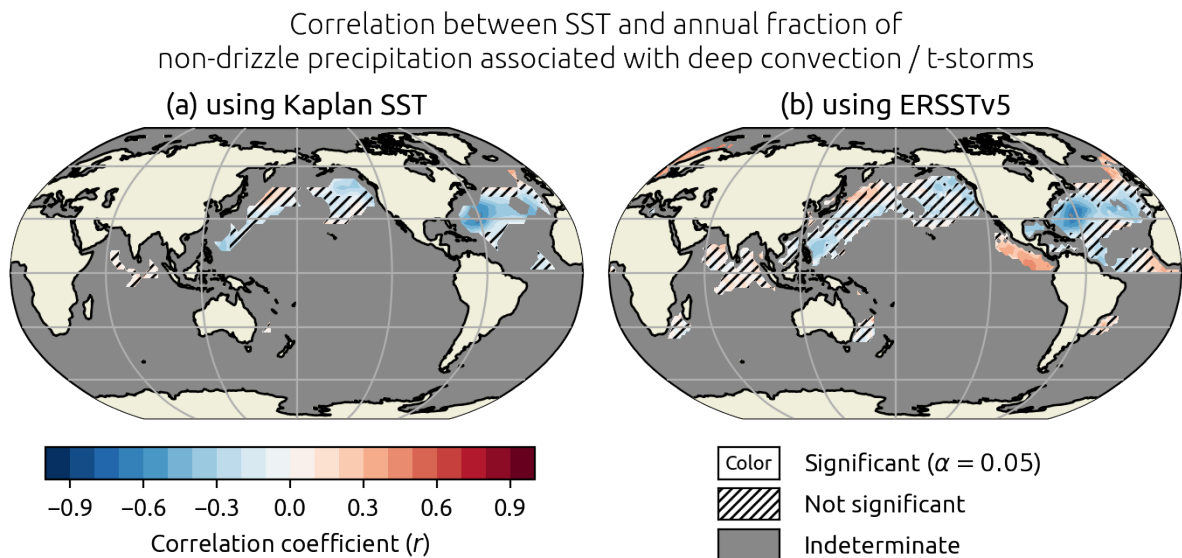
FIGURE 3.14: As in Figure 3.2, but for the fraction of non-drizzle precipitation associated with deep convection or thunderstorms.
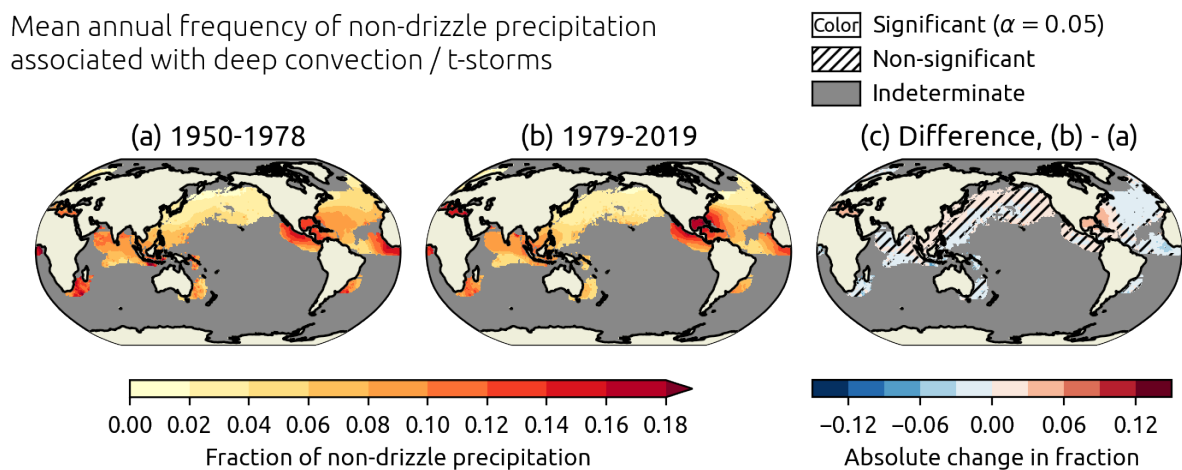
FIGURE 3.15: As in Figure 3.3, but for the fraction of non-drizzle precipitation associated with deep convection or thunderstorms.
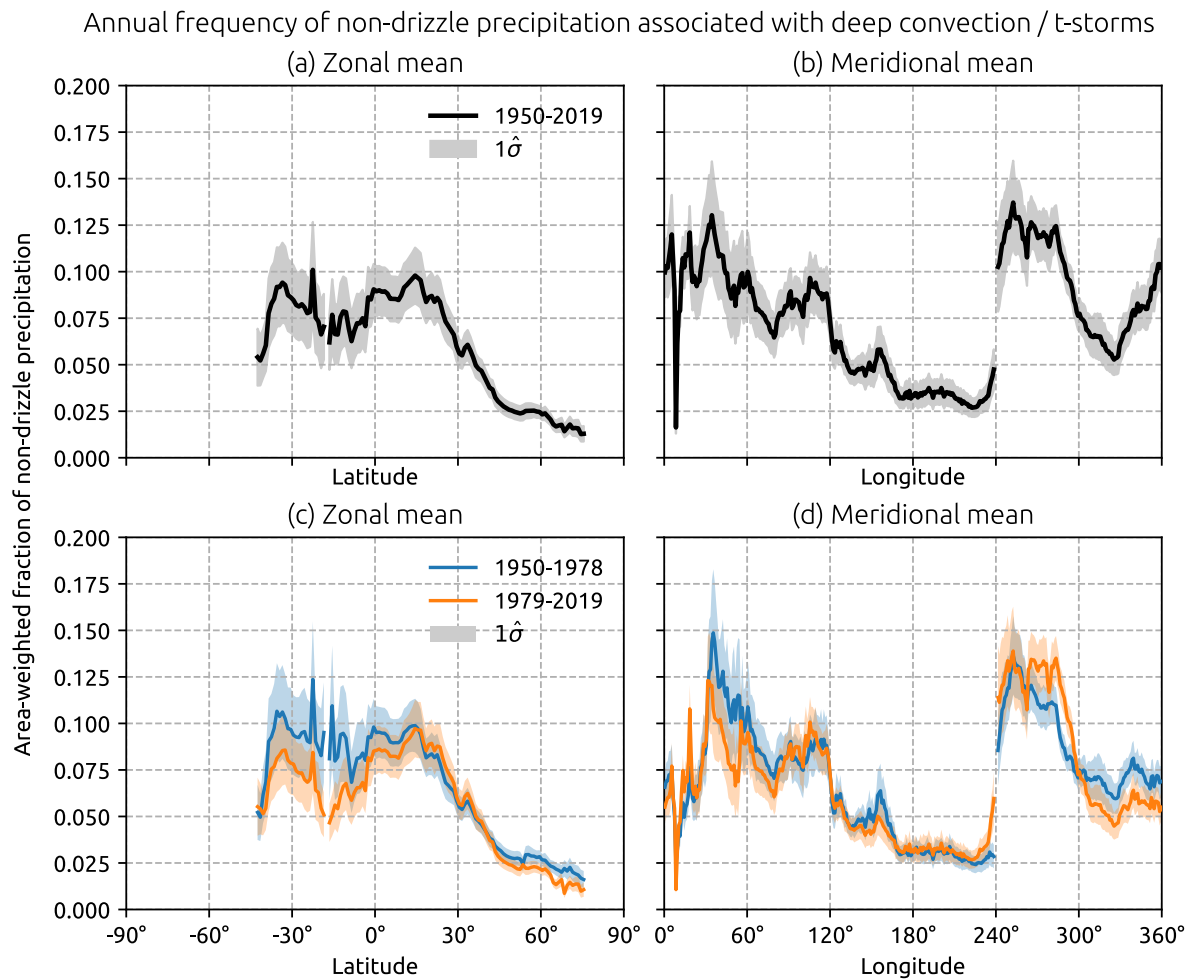
FIGURE 3.16: As in Figure 3.4, but for the fraction of non-drizzle precipitation associated with deep convection or thunderstorms.

Due to the relatively infrequent occurrence of deep convection and thunderstorms in ww reports, small changes in the proportion of these events are reflected by large relative trends. A prominent statistically significant and decreasing trend in the annual proportion of deep convection and thunderstorm ww reports has been observed by ships over the open mid-latitude North Atlantic and eastern equatorial Atlantic, with some relative trends in excess of 15% per decade, equivalent to a decrease in the absolute fraction of about 1% per decade (Figure 3.17). The decrease in the annual fraction over the North Atlantic has been more marked since 1970, with seasonal decreases most evident in DJF (Figure 3.18d). In contrast, relative trends have been more steady for the North Atlantic during JJA and SON. Statistically significant decreases have also been observed in the annual fraction along the equatorial Indian Ocean and the Arabian Sea, with relative trends of around 4–8% per decade. Statistically significant increases on the order of 5–15% per decade across annual and seasonal fractions have been observed over the East China Sea, Mediterranean Sea, Yellow Sea, and the western North Atlantic, equivalent to a 1–2% percentage point increase in the fraction per decade. Statistically significant positive trends have also been observed during MAM and SON along the Pacific coast of Japan. The trend over the Mediterranean and Yellow seas reflects a more gradual increase since 1950 (Figure 3.18b, c), compared to a larger change occurring in the latter half of the 1960s in the western Atlantic (Figure 3.18a).

FIGURE 3.17: As in Figure 3.5, but for the fraction of non-drizzle precipitation associated with deep convection or thunderstorms.

Fraction of non-drizzle precipitation associated with deep convection / t-storms
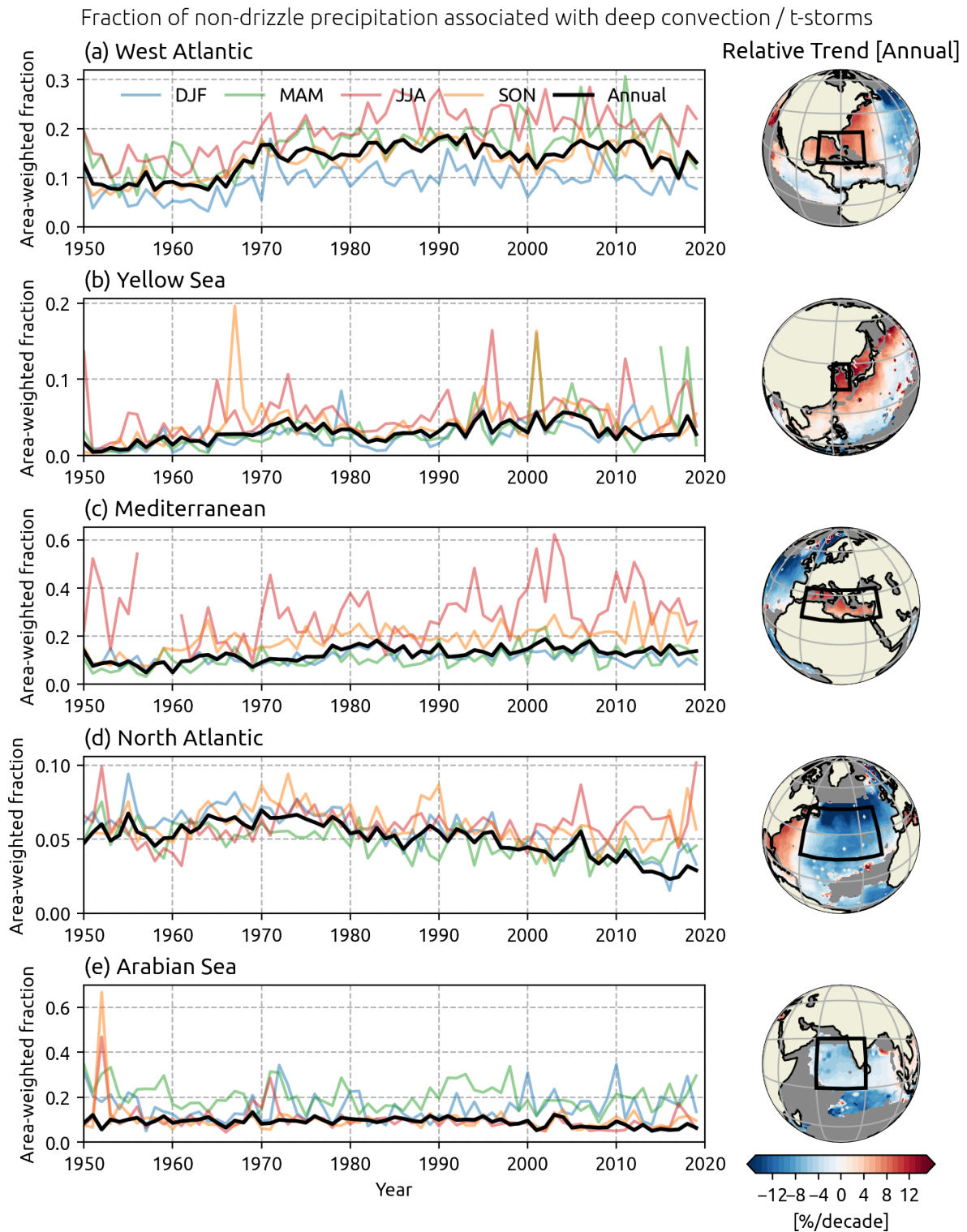
FIGURE 3.18: As in Figure 3.6, but for the fraction of non-drizzle precipitation associated with deep convection or thunderstorms.

## 3.4   Frozen precipitation

Oceanic frozen precipitation as reported by ships is predominant during wintertime over the Southern Ocean and over the higher latitudes of the Northern Hemisphere (Figure 3.19a). In the North Atlantic and North Pacific, frozen precipitation frequencies are highest over the western continental margins, such as over the Sea of Okhotsk and Labrador Sea. The annual zonal mean fraction of frozen precipitation reaches peaks of 0.91 ± 0.06 near 76°S and 0.54 ± 0.04 near 79°S (Figure 3.22), though these latitudes are not as well sampled by ships. Over the Northern Hemisphere, the frozen precipitation fraction is negatively correlated with SST across all sufficiently sampled areas (Figure 3.20), meeting statistical significance over nearly the entire region. This correlation is less apparent in the Southern Ocean.

Mean annual frozen precipitation fractions show positive statistically significant differences over the northwestern Pacific and over the central North Atlantic east of Newfoundland during the satellite era relative to the pre-satellite era, with statistically significant increases of 3–12 percentage points (Figure 3.21c). Ship observations during the satellite era also show a statistically significant reduction in frozen precipitation fraction over the Norwegian Sea and northeastern Pacific relative to the pre-satellite era, with a decrease by as much as 10 percentage points in the former.

Mean fraction of precipitation with frozen phase (1950-2019)

(a) Annual

(b) DJF   (c) MAM

(d) JJA   (e) SON

Fraction of precipitation

Indeterminate

FIGURE 3.19: As in Figure 3.1, but for the fraction of precipitation with frozen phase. Additionally, areas with mean annual or seasonal composite fractions < 1% are treated as indeterminate.

Correlation between SST and annual fraction of precipitation reports with frozen phase
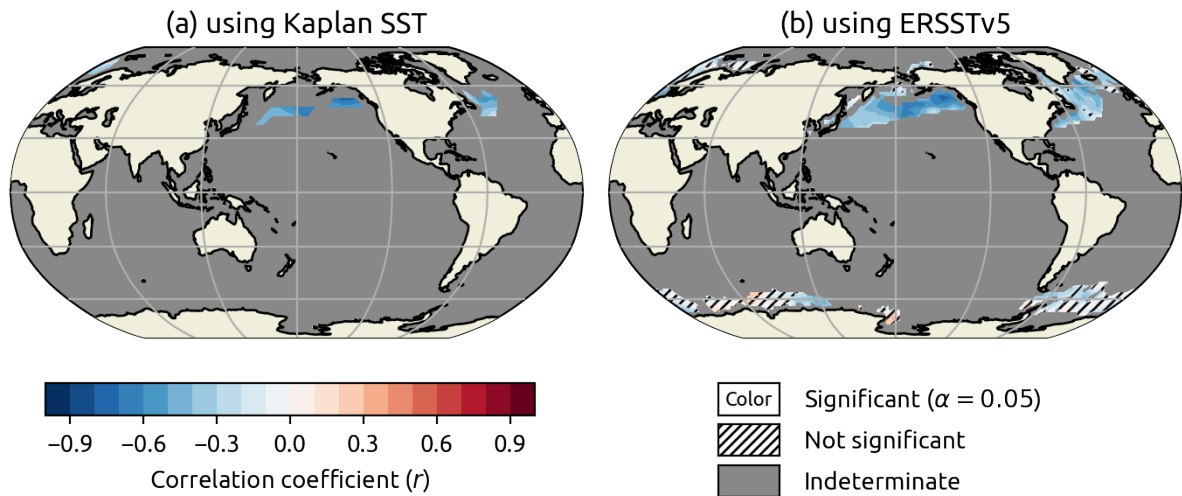
FIGURE 3.20: As in Figure 3.2, but for the fraction of precipitation with frozen phase. Additionally, areas with mean annual or seasonal composite fractions $< 1\%$ are treated as indeterminate.
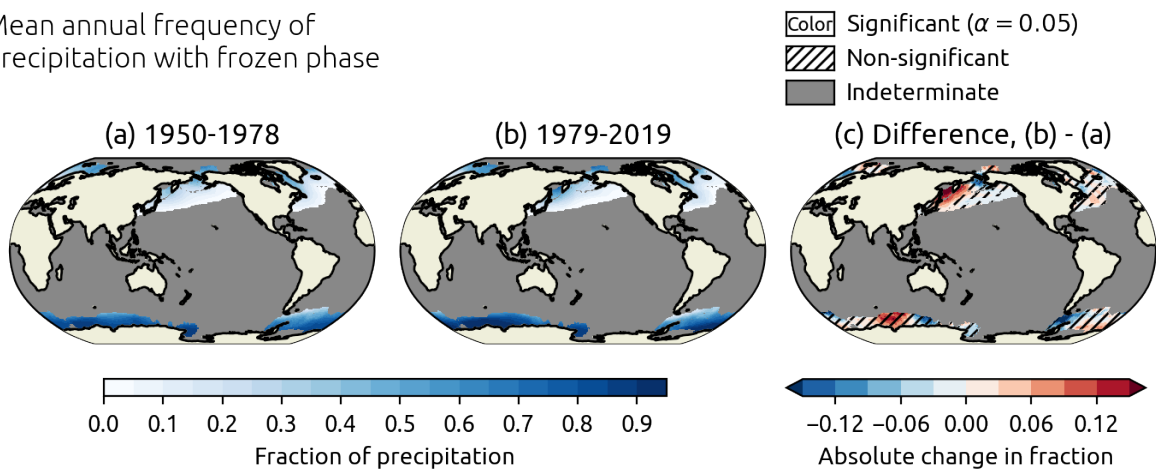
FIGURE 3.21: As in Figure 3.3, but for the fraction of precipitation with frozen phase. Additionally, areas with mean annual or seasonal composite fractions $< 1\%$ are treated as indeterminate.
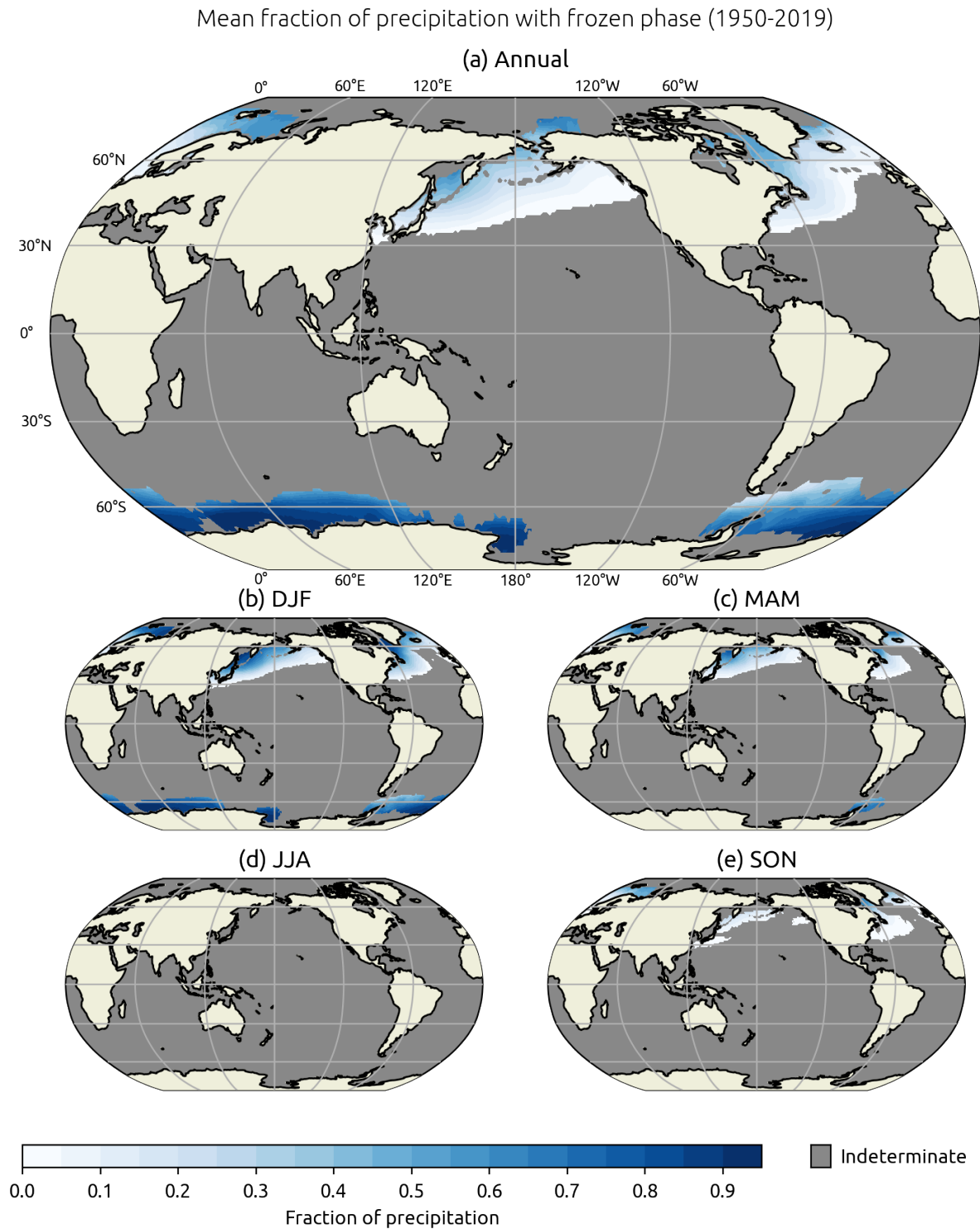
Annual frequency of precipitation with frozen phase
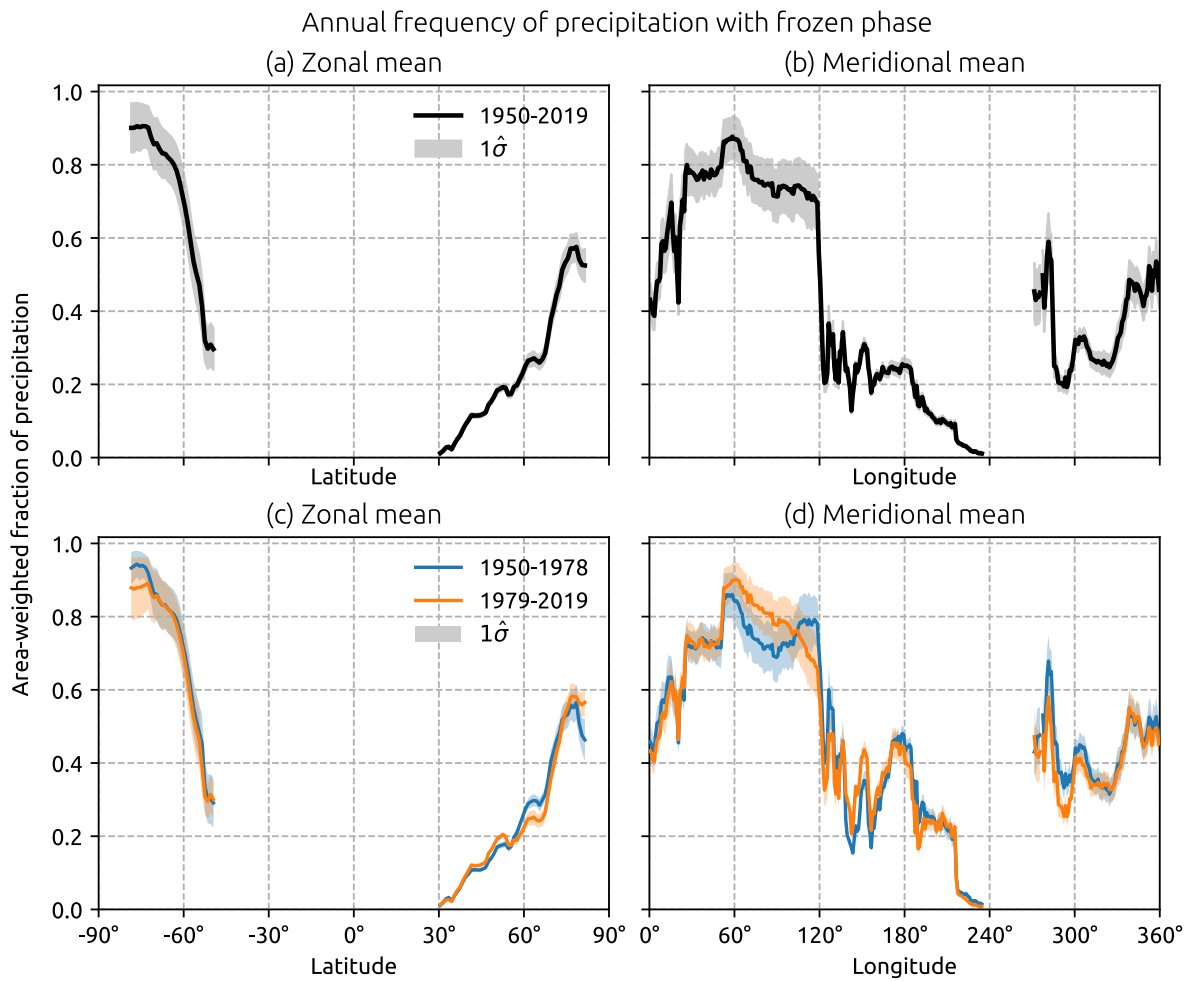
FIGURE 3.22: As in Figure 3.4, but for the fraction of precipitation with frozen phase. Areas with mean annual or seasonal composite fractions < 1% are omitted from aggregation.

Decreasing trends in the fraction of annual precipitation reports with frozen phase have been observed along the equatorward edges of the areas in the North Pacific and North Atlantic receiving frozen precipitation (henceforth the North Pacific Transition Zone and North Atlantic Transition Zone, respectively), most prominently over the former (Figure 3.23). These trends represent decreases in the absolute proportion of frozen precipitation of around 0–1% per decade. Decreasing trends have been most evident since about 1980 in both the transition zones of the North Atlantic and North Pacific (Figure 3.24c, d). Decreasing relative trends with similar magnitudes have also been observed over the Norwegian Sea. An area of statistically significant positive trends both annually and during the DJF and MAM has been observed over the central North Atlantic east of Newfoundland, with relative trends exceeding 10% per decade, representing a 1–2% percentage point increase per decade in the frozen precipitation fraction. While the transition zone between frozen and liquid precipitation is not as well-sampled in the Southern Hemisphere, a prominent and statistically significant decrease in the annual frozen precipitation fraction has been observed in and near the Drake Passage where the fraction is lower than other observed areas of the Southern Ocean. The relative decrease is steeper than 10% per decade, with decreases in the absolute fraction by as much as 6% percentage points per decade. Trends elsewhere in the Southern Ocean, mostly reflective of trends during DJF, are lower in magnitude but show statistically significant increases over the Cooperation Sea south of the Indian Ocean and significant decreases in the adjoining seas.

Relative trend of precipitation with frozen phase (1950-2019)

(a) Annual

(b) DJF

(c) MAM

(d) JJA

(e) SON

Color Significant ($\alpha = 0.05$)

Non-significant

Indeterminate

Relative trend of fraction [% per decade]
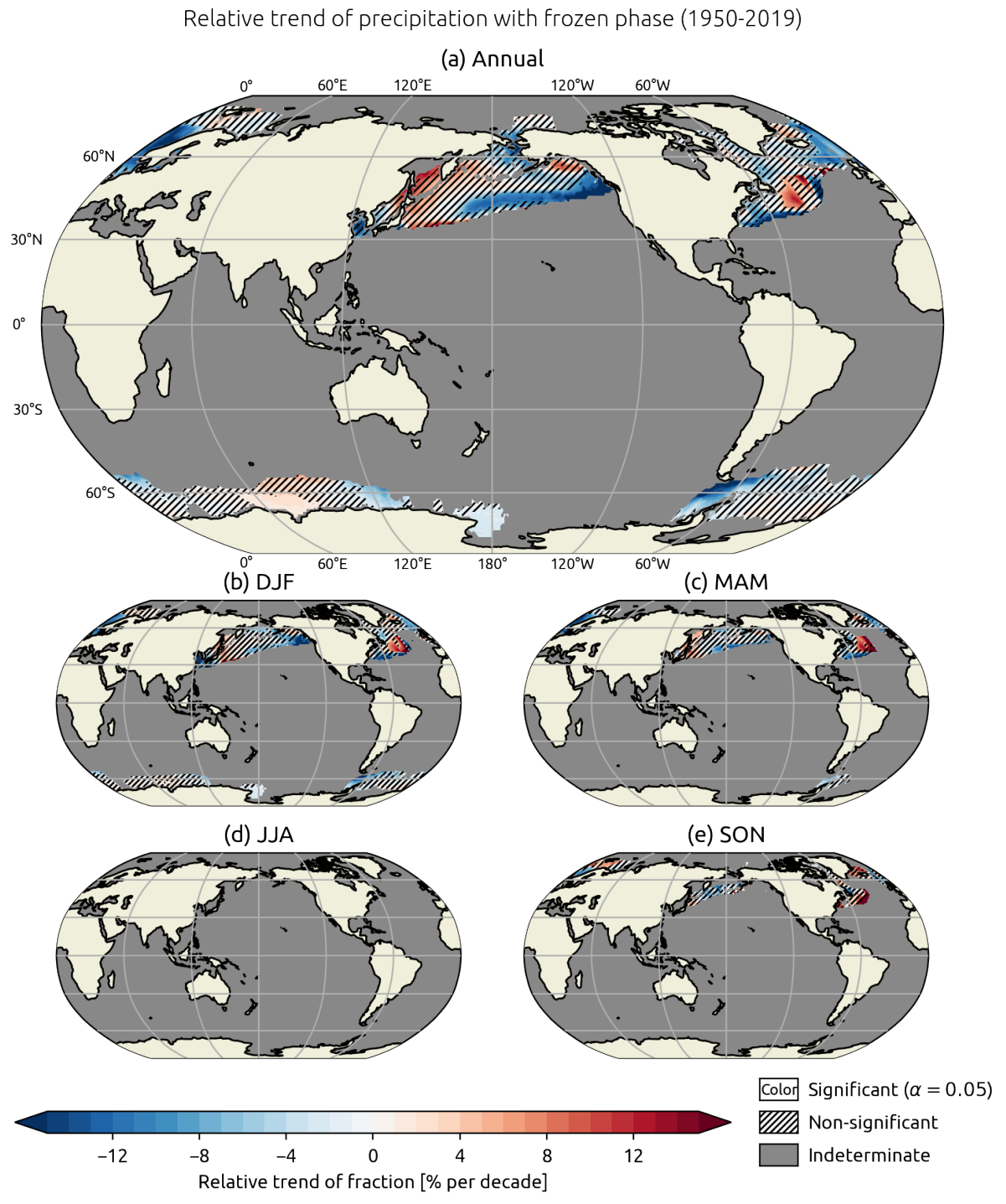
FIGURE 3.23: As in Figure 3.5, but for the fraction of precipitation with frozen phase. Trends are not displayed for areas with mean annual or seasonal composite fractions $< 1\%$.

FIGURE 3.24: As in Figure 3.6, but for the fraction of precipitation with frozen phase. Trends are not displayed for areas with mean annual or seasonal composite fractions < 1%.

Chapter 4

Discussion

Despite the inherent difficulties with using shipboard ww reports as discussed in Section 1.3.4, the methodology employed in Chapter 2 yields geographically coherent and consistent results for the estimated frequencies of precipitation even when mapping often widely-spaced observations to a relatively high-resolution $1° \times 1°$ grid. The frequencies and trends computed along the major shipping lanes evident in Figure 2.4, where sampling may be 1–2 orders of magnitude more frequent than over the surrounding ocean, do not contrast strongly with more data-sparse regions.

The composite frequency results obtained for the four precipitation classes align well with the distributions and magnitudes obtained for the same classes in Petty (1995). The general distributions of drizzle and snow as a proportion of precipitation occurrence are also consistent with the oceanic distribution of similar classes in Dai (2001a), though the

calculated frequencies are potentially higher in this analysis in part due to the choice of $\hat{f}$ used.

4.1 Drizzle

Drizzle is commonly observed in marine boundary layer stratocumulus clouds (Ghate and Cadeddu, 2019, Stevens et al., 2003, vanZanten et al., 2005). The increased preponderance of drizzle over the subtropical and mid-latitude Pacific and Atlantic observed by ships, particularly over the eastern halves of those basins, matches well with the distribution of these clouds (Muhlbauer et al., 2014). While these clouds develop over much of the global ocean, they are most common across broad areas of the North Pacific north of 35°N and North Atlantic north of 40°N, with more localized concentrations of frequent marine stratocumulus over the eastern continental margins of the subtropical North Pacific, subtropical South Pacific, and subtropical South Atlantic (Klein and Hartmann, 1993). The increased prevalence of drizzle in these marine stratocumulus hotspots during JJA is also consistent with the increased prevalence of stratiform boundary layer clouds observed during JJA. For these areas, the negative correlation observed between the fraction of precipitation falling as drizzle and SST is consistent with the negative correlation observed between the coverage of marine stratocumulus and SST, arising due to the favored development of marine stratocumulus in conditions where the combination of cooler waters and subsidence over the free atmosphere maximizes the temperature inversion within the boundary layer (Hanson, 1991). While these results are consistent with low-level stratiform clouds being a principal driver of drizzle occurrence when prevalent,

different mechanisms may influence the occurrence of drizzle more strongly where drizzle fraction and SST are positively correlated, as is the case over the mid-latitude North Atlantic and western Pacific.

The often consistent trends observed in both the seasonal and annual fractions of drizzle suggest that long-term forcing on drizzle behavior may be robust to seasonal variability, especially in the tropics. The areas where marine stratiform clouds are commonplace are some of the only areas where statistically significant trends in the fraction of precipitation with drizzle have been observed over the 70-year period of study. Consequently, decreases in the drizzle fraction have primarily occurred over areas with higher rates of drizzle occurrence. This trend may imply long-term changes in the coverage or occurrence of marine stratiform clouds in these areas or a decline in the efficiency of drizzle production in such clouds.

Warming SST due to climate change could result in a reduction in low-level stratiform cloud cover by locally weakening the boundary layer inversion, resulting in increased lower-tropospheric stability and an increased concentration of moisture within the boundary layer (McCoy et al., 2017, Wood and Bretherton, 2006). While climate models exhibiting this relationship produce decreased low-level cloud cover in climate projections (e.g. Qu et al., 2015), the observed trends in low-level cloud amount are not consistent with a decrease in low cloud cover cover stratocumuli-rich regions, instead showing long-term increases in low-level cloud amount across much of the subtropics (Liu et al., 2023, Marchand, 2013, Seethala et al., 2015). Similarly, the observed trends in low cloud cover

do not correspond well with the broad increase in drizzle observed throughout the tropics or the variations in the magnitude of the trends, suggesting that changes in the frequency of occurrence of stratiform clouds per se are not sufficient to explain global patterns in ship-observed trends in oceanic drizzle since 1950.

Alternatively, the long-term trends in the occurrence in drizzle may stem from long-term trends in drizzle production efficiency. Elevated anthropogenic aerosol production can suppress drizzle production via the second indirect effect of aerosols (Albrecht, 1989, Lohmann and Feichter, 2005), decreasing the mean radii of cloud condensation nuclei (CCN) distributions (Ferek et al., 2000, Fu and Dan, 2014) or decreasing cloud droplet sizes via the increase in overall CCN concentrations (Mann et al., 2014). In particular, the microphysical properties of marine stratiform clouds are heavily influenced by local aerosol characteristics (Christensen et al., 2020). The suppression of drizzle may increase cloud lifetimes and thereby increase low-level cloud fields, potentially explaining some cases, such as the subtropical eastern Pacific, where long-term declining trends in drizzle have occurred concurrently with increasing trends in low cloud cover. While studies have demonstrated a suppression of drizzle along ship tracks (e.g Ferek et al., 2000, Lu et al., 2007b), the lack of clustering of trends around ship tracks suggests that these effects may be too localized or short-lived for ships to be the primary mechanism for the observed trends. An analysis of trends in aerosol optical depth (AOD) during the period 2001–2014 using the Moderate Resolution Imaging Spectroradiometer (MODIS) and Multi-angle Imaging Spectroradiometer (MISR) sensors noted a marked region of statistically significant increases in annual and seasonal AOD around the Arabian Peninsula and

Indian subcontinent. During the same period, the ship-observed trend in drizzle fraction was negative in these areas, concordant with drizzle suppression. However, the satellite-observed trends in AOD elsewhere are less consistent with trends in drizzle during the same period, and it is unclear whether the long-term increase in tropical drizzle fraction is associated with a long-term trend in aerosols over the tropics.

Drizzle efficiency may be complicated by the contrasting relationship between cloud depth and drizzle production. Thicker stratiform clouds may exhibit higher likelihoods of generating drizzling precipitation, with greater virga depth (Yamaguchi et al., 2017) and drizzle production (Yang et al., 2018). The suppressive effect of aerosols on drizzle is also more pronounced for thinner clouds (L'Ecuyer et al., 2009, Terai et al., 2012), making cloud thicknesses susceptible to entrainment (Chen et al., 2011). Thus, while cloud coverage and thicknesses may be sustained longer by a reduction in drizzle, thicker clouds may be more prolific producers of drizzle. Recent intensification of the Walker circulation within the Pacific (L'Heureux et al., 2013) may provide one mechanism by which cloud thicknesses increase in the western Pacific and decrease in the eastern Pacific, potentially leading to a pattern of greater increasing trends in drizzle fraction observed over the western Pacific compared to the eastern Pacific. However, this pattern is not distinct in the ship-based data and such trends in cloud thickness have not been clearly observed in satellite observations (Lelli et al., 2014), nor has analogous behavior been observed in other oceanic basins.

Beyond aerosols, an increase in vertical wind shear may alter turbulent kinetic energy

production and entrainment, enhancing drizzle production in marine stratocumuli and reducing their cloud fraction and depth (Jeong et al., 2023, Wu et al., 2017). Taken together, there may be multiple competing influences on drizzle production, without a clear dominant mechanism leading to the prominent increase in drizzle frequency observed throughout the global tropics.

The regional multidecadal variation in the drizzle fraction observed over parts of the Indian Ocean and western Pacific (Figure 3.6d, e), with similarly-timed peaks in the fraction, suggest a possible, low-frequency and large-scale mode affecting drizzle behavior over these regions. A low-frequency variability in the thermocline depth of the eastern Indian Ocean was identified by Ummenhofer et al. (2017) with similar periodicity to the observed variability in drizzle frequency. This mode was shown to strongly modulate the behavior of the Indian Ocean Dipole (IOD; Saji et al., 1999), the dominant mode of variability for monthly-resolved SST in the tropical Indian Ocean. The low-frequency mode be linked to the Pacific decadal oscillation (PDO; Mantua and Hare, 2002), which can influence regional precipitation (e.g. Krishnan and Sugi, 2003, Wang et al., 2014, Wei et al., 2021). Thus, the observed multidecadal variation in drizzle may be a byproduct of these basin-scale modes.

4.2   Moderate/heavy intensity non-drizzle

The annual and seasonal distributions of the proportion of non-drizzling oceanic precipitation occurring at moderate or heavy intensities is nearly an inversion of the distribution

of drizzle, with the most prevalent heavier precipitation occurring within the tropics and minima located near areas with abundant low-level marine stratiform clouds discussed in Section 4.1. Within the lower latitudes, more prevalent occurrence of heavier precipitation is consistent with areas with higher precipitable water (Zveryaev and Chu, 2003), consistent with the close relationship between precipitable water and daily extreme precipitation over the tropics (Kim et al., 2022). The negative relationship between the proportion of SST and heavier precipitation as observed by ships in the northern subtropics and western North Pacific are consistent with areas where the atmosphere is a stronger control on ocean conditions than vice versa (Trenberth and Shea, 2005, Xue et al., 2022). A negative correlation between monthly mean surface temperature and precipitation amount is more fully realized in the Northern Hemisphere than Southern Hemisphere, perhaps leading to the contrasting correlation between heavier precipitation and SST in the shipboard observations.

The most prominent signature in moderate/heavy intensity precipitation trends—the increase in the prevalence of heavier precipitation over the subtropical Central Pacific— may be a reflection of the observed widening of the Hadley cell due to climate change (Hu et al., 2010). Expansion of the Hadley cell is associated with a widening of the moist tropical belt (Seidel et al., 2007) and the shifting and expansion of the subtropical dry zone poleward, with these effects potentially more prominent over ocean (Schmidt and Grise, 2017). These changes may result in decreased descent along the expanding tropical belt, leading to an increased likelihood of heavier precipitation. However, the distribution of trends does not align with the large-scale pattern of trends expected of

Hadley cell expansion. While, the belt of statistically significant increases over the central Pacific is closely aligned with the latitudes where both historically observed and modeled precipitation are most positively correlated with the width of the Hadley cell, though a corresponding decreasing trend in the preponderance of heavier precipitation has not been clearly observed within the mid-latitudes. These observed changes, present in all seasons, also differ from the expansion of the subtropical dry zone depicted in climate projections (e.g. Lu et al., 2007a, Scheff and Frierson, 2012). While distributions of precipitation intensity are expected to shift towards precipitation extremes globally, a globally-spanning increase is not clearly apparent in the 70-year ship record. However, in some areas, such as the Mediterranean Sea (e.g. Norrant and Douguédroit, 2005, Tramblay and Somot, 2018), Yellow Sea (e.g. Wang et al., 2017), and the Pacific coast of the continental United States (e.g. Jiang et al., 2016), the increases in heavier precipitation observed by ships corresponds with increases in the occurrence of extreme precipitation observed on nearby land-based stations and is consistent with climate simulations.

4.3   Deep convection and thunderstorms

The ship-observed distribution of deep convection and thunderstorms is broadly consistent with the distribution of lightning occurrence as detected by radio lightning sensors (Kaplan and Lau, 2021), with the global maximum over the western Atlantic and eastern Pacific captured well in both datasets. As with the inferred relationship between SST and the preponderance of heavier precipitation, the observed negative correlation between

oceanic deep convection and SST is consistent with areas where atmospheric forcing tends to drive oceanic conditions.

Datasets of lightning occurrence, mainly limited to the 21st century, have not suggested clear trends in global thunderstorm activity (e.g. Kaplan and Lau, 2022, Williams et al., 2019). An assessment of the ERA5 global reanalysis by Taszarek et al. (2021) suggested statistically significant increases in the 95th percentile of convective available potential energy (CAPE) over the Mediterranean Sea, western Atlantic, and along the coast of China, with broad and significant decreases throughout the tropics during 1979–2019. However, no comparable signal is identified over the oceanic mid-latitudes where ships have observed decreases in the relative occurrence of deep convection and thunderstorms.

4.4   Frozen precipitation

Given the strong correlation observed between the fraction of precipitation occurrences with frozen phase and SST over the subpolar Northern Hemisphere, the decrease in the prevalence of frozen precipitation in the North Atlantic and North Pacific transition zones suggests a poleward retreat of the Arctic region receiving frozen precipitation, in agreement with an increase in near surface temperatures (Trenberth, 2011). These trends are consistent with a reduction in the snow event to precipitation event ratio observed over this region by Shi and Liu (2021) and a decline in annual snowfall amounts over sub-Arctic land areas as depicted in climate models (Krasting et al., 2013). The sensitivity of frozen precipitation to SST may be reflected at shorter timescales; for instance, an

increase in frozen phase precipitation occurrence over the North Atlantic in 2015 was coincident with a short-lived "blob" of anomalously cold SST that first emerged in 2014 (Maroon et al., 2021). Declines in snow cover and snow depth in Norway (e.g. Dyrrdal et al., 2012, Rizzi et al., 2017), particularly over coastal areas, may stem from climate trends similarly reflected by the statistically significant decrease in frozen precipitation events observed over the Norwegian Sea. Seasonal increases in snowfall are modeled in climate projections over land areas roughly north of the 20th century $-10\ ^\circ$C isotherm and have been observed over land, but have not been reflected in the long-term ship observations.

While ship observations did not suggest statistically significant trends in the prevalence of frozen precipitation near Japan, the tentative signal of increasing trends in northern Japan and declining trends farther south was observed over land during the period spanning 1961–2012 (Takahashi, 2020). Over the subpolar North Atlantic, the region with a statistically significant increase in the proportion of frozen precipitation east of Newfoundland observed by ships is located near a "warming hole" (Drijfhout et al., 2012, Li et al., 2021) where SSTs have declined during the last century, consistent with the close relationship inferred between frozen precipitation frequency and SST. This warming hole may produce downstream effects on precipitation over the Norwegian Sea, including declines in wintertime convective precipitation and snow-rain ratio (Iversen et al., 2023). Ship-observed declines in heavier precipitation and frozen precipitation during the wintertime over the Norwegian Sea may be reflective of these anticipated trends.

Over the Southern Ocean, ship reports are largely limited to austral summer, thus leaving the annual periods with the bulk of Antarctic precipitation unsampled (Wang et al., 2020). The observed decrease in the proportion of frozen phase precipitation during DJF near the Drake Passage and positive trends over the southern Indian Ocean may be in concordance with long-term trends with the same sign in sea ice concentration (Parkinson and Cavalieri, 2012), though the paucity of observations and the direct effect of sea ice on navigability of the polar ocean increases the uncertainty of ship-observed trends in frozen precipitation over the region.

Chapter 5

Conclusions and Future Research

By compositing reports of present weather reported voluntarily by ships globally and deriving estimated fractions of occurrence, global maps of various precipitation phenomena can be reconstructed. This analysis demonstrates that aggregating spatiotemporally discrete shipboard observations over an extended period of record in this manner can produce geographically coherent and sensible results, shedding light on oceanic precipitation behavior.

This ship-based reconstruction of oceanic precipitation in the 70-year period spanning 1950–2019 suggests that there are statistically significant differences in oceanic precipitation between the period included in satellite-derived datasets (1979–2019) and the period preceding (1950–1978), with statistically significant 70-year trends evident in the relative frequencies of all four precipitation classes examined in this study. A significant increase

in the occurrence of drizzle as a proportion of precipitation events has been observed throughout the tropics, with less prominent decreases occurring in areas with abundant stratiform cloud cover. A prominent belt of statistically significant increases in the proportion of non-drizzling precipitation events falling at moderate or heavy intensity has been observed over the subtropical central Pacific. However, this trend is most prominent before the satellite era. Positive trends in relative occurrence of heavier precipitation, deep convection, and thunderstorms have also been observed in the Mediterranean Sea, Yellow Sea, and along the United States East Coast, with declines in deep convection and thunderstorms observed over the open North Atlantic. Ship reports also suggest a gradual retreat of the oceanic polar region of the Northern Hemisphere receiving frozen precipitation, with decreases in the fraction of precipitation events falling with frozen phase noted along the mid-latitude transition zone consistent with global warming.

The trends inferred from in this analysis suggest numerous possible avenues of inquiry examining the physical mechanisms producing those trends. For example, despite a multitude of thermodynamic and microphysical influences on drizzle assessed in previous studies, it is unclear why a prominent increase in tropical drizzle has been observed since 1950. Future studies using shipboard ww reports may examine the climatology and trends of other classes of precipitation delineated by the ww code, such as showery precipitation or freezing precipitation like ice pellets and freezing rain. As marine observations are often accompanied by numerous other meteorological parameters, a further exploration of the relationship between precipitation or various classes of precipitation and other

physical variables such as air temperature, dew point temperature, wind, or even diurnal variability may provide additional insights into the behavior of oceanic precipitation.

The comprehensive wealth of information extracted from global shipboard ww reports, including the results presented here and in studies dating back to the 1960s, point to shipboard ww being a promising source for climatological data over the open ocean and worthy of continued investigation. Critically, such reports constitute the only in-situ observation of weather conditions for much of the ocean, filling a key niche for independent validation of satellite-based precipitation retrievals, model simulations, and other proxy-based estimates of oceanic precipitation. While satellite-based methods have largely supplanted shipboard observations in mapping oceanic precipitation, the qualitative aspects of the ww code can be leveraged to shed insight in the character of that precipitation. As more sophisticated methods for determining properties of oceanic precipitation emerge, the uniquely in-situ role of ship observations and other marine platforms and their extensive period of record should remain a key part in our evolving understanding of global climate.

As noted in Section 1.4, this thesis summarizes one phase of an overarching research effort to reconstruct a ship-based oceanic precipitation climatology. The next phase of this research will involve using the modern satellite PMW-based precipitation record to infer precipitation amounts from the composited ship data, potentially providing an in-situ look at the distribution of, and trends in, oceanic precipitation amount extending back to 1950.

Appendix A

Fraction estimation

If an event E has a true frequency f of occurring, then if the event is sampled m times out of n trials, the sample proportion $\hat{p} = m/n \approx f$ as m/n is an unbiased maximum likelihood estimator for f. However, if the event is poorly sampled (n small) or rare (f small), it is possible that $m = 0$ and thus $m/n = 0$. This can distort relative trends as variation between $m = 0$ and $m \neq 0$ produce unrealistic infinite or $\pm 100\%$ relative change.

Rather than approaching the problem of frequency estimation in the frame of what frequency f would most likely produce $\hat{p}$, we can instead find the expected value $\hat{f}$ of f given m and n. For any $f \neq 0$, the probability of m taking any value in $[0, n]$ (equivalently, $\hat{p}$ taking any value in $[0, 1]$) is non-zero. In this approach, $\hat{p} = 0$ may arise from any $f \in [0, 1]$.

The probability p of collecting m observations of E over n independent trials conditioned on E being associated with frequency f is given by the binomial distribution such that

$$p(m|f) = \binom{n}{m} f^m (1-f)^{n-m} \tag{A.1}$$

We then conservatively begin with the non-informative prior that f arises from a standard uniform distribution with $0 \leq f \leq 1$ such that

$$\int_0^1 p(f)\, \mathrm{d}f = 1 \tag{A.2}$$

Using Bayes' Theorem, the probability of the true frequency being f conditioned on observing the event m times, assuming a standard uniform distribution for f, is given by

$$p(f|m) = \frac{p(m|f)p(f)}{p(m)} \tag{A.3}$$

$$= \frac{\binom{n}{m} f^m (1-f)^{n-m} p(f)}{\int_0^1 \binom{n}{m} f^m (1-f)^{n-m} p(f)\, \mathrm{d}f} \tag{A.4}$$

$$= \frac{f^m (1-f)^{n-m} p(f)}{\int_0^1 f^m (1-f)^{n-m} p(f)\, \mathrm{d}f} \tag{A.5}$$

Given m, the value of f that maximizes $p(f|m)$ may be interpreted as the *most likely* value for f. The *expected value* $\hat{f}$ of f, given m, is given by the integrated total of all conditional probabilities $p(f|m)$ scaled by f, such that

$$\hat{f} = \int_0^1 f p(f|m)\, \mathrm{d}f \tag{A.6}$$

Which, by substituting Equation A.5, yields

$$\frac{\int_0^1 f^{m+1}(1-f)^{n-m}p(f)\,\mathrm{d}f}{\int_0^1 f^m(1-f)^{n-m}p(f)\,\mathrm{d}f} \tag{A.7}$$

A closed-form solution can be derived using the relationship between Beta integrals and

Gamma functions:

$$
\begin{aligned}
\hat{f} &= \frac{\int_0^1 f^{m+1}(1-f)^{(n-m)}\,\mathrm{d}f}{\int_0^1 f^M(1-f)^{(N-M)}\,\mathrm{d}f} && \text{Equation A.7}\\[2mm]
&= \frac{\mathrm{B}(m+2,n-m+1)}{\mathrm{B}(m+1,n-m+1)} && \text{Substitute with Beta functions}\\[2mm]
&= \frac{\Gamma(m+2)\Gamma(n-m+1)\Gamma(n+2)}{\Gamma(n+3)\Gamma(m+1)\Gamma(n-m+1)} && \text{Substitute with Gamma functions}\\[2mm]
&= \frac{\Gamma(m+2)\Gamma(n+2)}{\Gamma(n+3)\Gamma(m+1)} && \text{Cancel like terms}\\[2mm]
&= \frac{(m+1)!(n+1)!}{(n+2)!(m)!} && \text{Use factorial representation}\\[2mm]
&= \boxed{\frac{m+1}{n+2}}
\end{aligned}
$$

This expression for $\hat{f}$ converges to m/n for large n, and $\hat{f} \approx m/n$ if $m \approx N/2$. Larger

deviations between $\hat{f}$ and m/n occur for small n, but $|\hat{f} - m/n|$ is never larger than 0.34.

Bibliography

Adler, R., M. Sapiano, G. Huffman, J.-J. Wang, G. Gu, D. Bolvin, L. Chiu, U. Schneider, A. Becker, E. Nelkin, P. Xie, R. Ferraro, and D.-B. Shin, 2018: The Global Precipitation Climatology Project (GPCP) Monthly Analysis (New Version 2.3) and a Review of 2017 Global Precipitation. *Atmosphere*, **9**, 138, doi:10.3390/atmos9040138.

Adler, R. F., G. Gu, G. J. Huffman, M. R. P. Sapiano, and J.-J. Wang, 2020: GPCP and the Global Characteristics of Precipitation. *Advances in Global Change Research*, Springer International Publishing, 677–697.

Adler, R. F., G. Gu, M. Sapiano, J.-J. Wang, and G. J. Huffman, 2017: Global Precipitation: Means, Variations and Trends During the Satellite Era (1979–2014). *Surveys in Geophysics*, **38**, 679–699, doi:10.1007/s10712-017-9416-4.

Albercht, R. I., S. J. Goodman, W. A. Petersen, D. E. Buechler, E. C. Bruning, R. J. Blakeslee, and H. J. Christian, 2011: The 13 years of TRMM Lightning Imaging Sensor: From individual flash characteristics to decadal tendencies. *XIV ICAE: International Conference on Atmospheric Electricity*, number M11-0203.

URL https://ntrs.nasa.gov/api/citations/20110015779/downloads/20110015779.pdf

Albrecht, B. A., 1989: Aerosols, Cloud Microphysics, and Fractional Cloudiness. *Science*, **245**, 1227–1230, doi:10.1126/science.245.4923.1227.

Allan, R. P., M. Barlow, M. P. Byrne, A. Cherchi, H. Douville, H. J. Fowler, T. Y. Gan, A. G. Pendergrass, D. Rosenfeld, A. L. S. Swann, L. J. Wilcox, and O. Zolina, 2020: Advances in understanding large-scale responses of the water cycle to climate change. *Annals of the New York Academy of Sciences*, **1472**, 49–75, doi:10.1111/nyas.14337.

Ansell, T. J., P. D. Jones, R. J. Allan, D. Lister, D. E. Parker, M. Brunet, A. Moberg, J. Jacobeit, P. Brohan, N. A. Rayner, E. Aguilar, H. Alexandersson, M. Barriendos, T. Brandsma, N. J. Cox, P. M. Della-Marta, A. Drebs, D. Founda, F. Gerstengarbe, K. Hickey, T. Jónsson, J. Luterbacher, Ø. Nordli, H. Oesterle, M. Petrakis, A. Philipp, M. J. Rodwell, O. Saladie, J. Sigro, V. Slonosky, L. Srnec, V. Swail, A. M. García-Suárez, H. Tuomenvirta, X. Wang, H. Wanner, P. Werner, D. Wheeler, and E. Xoplaki, 2006: Daily Mean Sea Level Pressure Reconstructions for the European–North Atlantic Region for the Period 1850–2003. *Journal of Climate*, **19**, 2717–2742, doi:10.1175/jcli3775.1.

Arkin, P. A. and P. E. Ardanuy, 1989: Estimating Climatic-Scale Precipitation from Space: A Review. *Journal of Climate*, **2**, 1229–1238, doi:10.1175/1520-0442(1989)002<1229:ECSPFS>2.0.CO;2.

Austin, P. M. and S. G. Geotis, 1980: Precipitation Measurements over the Ocean. *Air-Sea Interaction*, Springer US, 523–541.

Ballari, D., L. M. Vilches-Blázquez, M. L. Orellana-Samaniego, F. Salgado-Castillo, A. E. Ochoa-Sánchez, V. Graw, N. Turini, and J. Bendix, 2023: Satellite Earth Observation for Essential Climate Variables Supporting Sustainable Development Goals: A Review on Applications. *Remote Sensing*, **15**, 2716, doi:10.3390/rs15112716.

Barrett, E. C., C. Kidd, and J. O. Bailey, 1988: A new instrument with rainfall monitoring potential. *International Journal of Remote Sensing*, **9**, 1943–1950, doi:10.1080/01431168808954993.

Basu, A. P., D. W. Gaylor, and J. J. Chen, 1996: Estimating the Probability of Occurrence of Tumor for a Rare Cancer with Zero Occurrence in a Sample. *Regulatory Toxicology and Pharmacology*, **23**, 139–144, doi:10.1006/rtph.1996.0035.

Battaglia, A., P. Kollias, R. Dhillon, R. Roy, S. Tanelli, K. Lamer, M. Grecu, M. Lebsock, D. Watters, K. Mroz, G. Heymsfield, L. Li, and K. Furukawa, 2020: Spaceborne Cloud and Precipitation Radars: Status, Challenges, and Ways Forward. *Reviews of Geophysics*, **58**, doi:10.1029/2019rg000686.

Bedacht, E., S. K. Gulev, and A. Macke, 2007: Intercomparison of global cloud cover fields over oceans from the VOS observations and NCEP/NCAR reanalysis. *International Journal of Climatology*, **27**, 1707–1719, doi:10.1002/joc.1490.

Behrangi, A., 2021: Emerging techniques for precipitation assessment and consistency studies. *The Joint IPWG/GEWEX Precipitation Assessment*, World Climate Research Programme, 108–115.

Behrangi, A., M. Christensen, M. Richardson, M. Lebsock, G. Stephens, G. J. Huffman, D. Bolvin, R. F. Adler, A. Gardner, B. Lambrigtsen, and E. Fetzer, 2016: Status of high-latitude precipitation estimates from observations and reanalyses. *Journal of Geophysical Research: Atmospheres*, **121**, 4468–4486, doi:10.1002/2015jd024546.

Behrangi, A., G. Stephens, R. F. Adler, G. J. Huffman, B. Lambrigtsen, and M. Lebsock, 2014: An Update on the Oceanic Precipitation Rate and Its Zonal Distribution in Light of Advanced Observations from Space. *Journal of Climate*, **27**, 3957–3965, doi:10.1175/jcli-d-13-00679.1.

Béranger, K., B. Barnier, S. Gulev, and M. Crépon, 2006: Comparing 20 years of precipitation estimates from different sources over the world ocean. *Ocean Dynamics*, **56**, 104–138, doi:10.1007/s10236-006-0065-2.

Berry, D. I., 2005: Improving Rainfall Estimates from Voluntary Observing Ships. Online. URL `https://icoads.noaa.gov/marcdat2/P_David_Berry.pdf`

Berry, D. I. and E. C. Kent, 2011: Air-Sea fluxes from ICOADS: the construction of a new gridded dataset with uncertainty estimates. *International Journal of Climatology*, **31**, 987–1001, doi:10.1002/joc.2059.

Box, G. E. P., G. M. Jenkins, and G. C. Reinsel, 2015: *Time Series Analysis: Forecasting and Control*. Wiley series in probability and statistics, John Wiley & Sons, Hoboken, N.J., fourth edition, includes bibliographical references (p. 685-699) and index. - Description based on print version record.

Calvert, E. B., 1930: The International Convention for Safety of Life at Sea, London, 1929. *Monthly Weather Review*, **58**, 156–159, doi:10.1175/1520-0493(1930)58<156:ticfso>2.0.co;2.

Cayan, D. R. and G. Reverdin, 1994: Monthly Precipitation and Evaporation Variability Estimated over the North Atlantic and North Pacific. *The Atlantic Climate Change Program: Proceedings From the Principal Investigators Meeting*, A.-M. Wilburn, ed., National Oceanic and Atmospheric Adminstration/Geophysical Fluid Dynamics Laboratory, 28–32.

Chen, Y.-C., L. Xue, Z. J. Lebo, H. Wang, R. M. Rasmussen, and J. H. Seinfeld, 2011: A comprehensive numerical study of aerosol-cloud-precipitation interactions in marine stratocumulus. *Atmospheric Chemistry and Physics*, **11**, 9749–9769, doi:10.5194/acp-11-9749-2011.

Chou, C., C.-A. Chen, P.-H. Tan, and K. T. Chen, 2012: Mechanisms for Global Warming Impacts on Precipitation Frequency and Intensity. *Journal of Climate*, **25**, 3291–3306, doi:10.1175/jcli-d-11-00239.1.

Christensen, M. W., W. K. Jones, and P. Stier, 2020: Aerosols enhance cloud lifetime and brightness along the stratus-to-cumulus transition. *Proceedings of the National Academy of Sciences*, **117**, 17591–17598, doi:10.1073/pnas.1921231117.

Clark, M. P., M. C. Serreze, and R. G. Barry, 1996: Characteristics of Arctic Ocean climate based on COADS data, 1980-1993. *Geophysical Research Letters*, **23**, 1953–1956, doi:10.1029/96gl01807.

da Silva, A. M., C. C. Young, and S. Levitus, 1994: Atlas of surface marine data 1994, volume 1: Algorithms and procedures. Technical Report 6, National Environmental Satellite, Data, and Information Service; National Oceanographic Data Center Ocean Climate Laboratory.
URL https://repository.library.noaa.gov/view/noaa/49337

Dai, A., 2001a: Global Precipitation and Thunderstorm Frequencies. Part I: Seasonal and Interannual Variations. *Journal of Climate*, **14**, 1092–1111, doi:10.1175/1520-0442(2001)014<1092:gpatfp>2.0.co;2.

— 2001b: Global Precipitation and Thunderstorm Frequencies. Part II: Diurnal Variations. *Journal of Climate*, **14**, 1112–1128, doi:10.1175/1520-0442(2001)014<1112:gpatfp>2.0.co;2.

Danielson, R. E., M. Zhang, and W. A. Perrie, 2020: Possible impacts of climate change on fog in the Arctic and subpolar North Atlantic. *Advances in Statistical Climatology, Meteorology and Oceanography*, **6**, 31–43, doi:10.5194/ascmo-6-31-2020.

Diaz, H., C. Folland, T. Manabe, D. Parker, R. Reynolds, and S. Woodruff, 2002: Workshop on Advances in the Use of Historical Marine Climate Data. *Bulletin of the World Meteorological Organization*, **51**, 377–380.

URL `https://icoads.noaa.gov/advances/clivarexchanges.pdf`

Donat, M. G., A. L. Lowry, L. V. Alexander, P. A. O'Gorman, and N. Maher, 2016: More extreme precipitation in the world's dry and wet regions. *Nature Climate Change*, **6**, 508–513, doi:10.1038/nclimate2941.

Dore, M. H. I., 2005: Climate change and changes in global precipitation patterns: What do we know? *Environment International*, **31**, 1167–1181, doi:10.1016/j.envint.2005.03.004.

Dorigo, W., S. Dietrich, F. Aires, L. Brocca, S. Carter, J.-F. Cretaux, D. Dunkerley, H. Enomoto, R. Forsberg, A. Güntner, M. I. Hegglin, R. Hollmann, D. F. Hurst, J. A. Johannessen, C. Kummerow, T. Lee, K. Luojus, U. Looser, D. G. Miralles, V. Pellet, T. Recknagel, C. R. Vargas, U. Schneider, P. Schoeneich, M. Schröder, N. Tapper, V. Vuglinsky, W. Wagner, L. Yu, L. Zappa, M. Zemp, and V. Aich, 2021: Closing the Water Cycle from Observations across Scales: Where Do We Stand? *Bulletin of the American Meteorological Society*, **102**, E1897–E1935, doi:10.1175/bams-d-19-0316.1.

Dorman, C. E., 1980: Comments on "The Relationship Between the Amount and Frequency of Precipitation Over the Ocean". *Journal of Applied Meteorology*, **19**, 1131–1133, doi:10.1175/1520-0450(1980)019<1131:corbta>2.0.co;2.

Dorman, C. E. and R. H. Bourke, 1978: A temperature correction for Tucker's ocean rainfall estimates. *Quarterly Journal of the Royal Meteorological Society*, **104**, 765–773, doi:10.1002/qj.49710444117.

— 1979: Precipitation over the Pacific Ocean, 30°S to 60°N. *Monthly Weather Review*, **107**, 896–910, doi:10.1175/1520-0493(1979)107<0896:potpot>2.0.co;2.

— 1981: Precipitation over the Atlantic Ocean, 30°S to 70°N. *Monthly Weather Review*, **109**, 554–563, doi:10.1175/1520-0493(1981)109<0554:potaot>2.0.co;2.

Dorman, C. E., J. Mejia, D. Koračin, and D. McEvoy, 2019: World marine fog analysis based on 58-years of ship observations. *International Journal of Climatology*, **40**, 145–168, doi:10.1002/joc.6200.

Douville, H., K. Raghavan, J. Renwick, R. P. Allan, P. A. Arias, M. Barlow, R. Cerezo-Mota, A. Cherchi, T. Y. Gan, J. Gergis, D. Jiang, A. Khan, W. P. Mba, D. Rosenfeld, J. Tierney, and O. Zolina, 2021: Water Cycle Changes. *Climate Change 2021 – The Physical Science Basis*, V. Masson-Delmotte, P. Zhai, A. Pirani, S. L. Connors, C. Péan, Y. Chen, L. Goldfarb, M. I. Gomis, J. B. R. Matthews, S. Berger, M. Huang, O. Yelekçi, R. Yu, B. Zhou, E. Lonnoy, T. K. Maycock, T. Waterfield, K. Leitzell, and N. Caud, eds., Cambridge University Press, 1055–1210.

Drijfhout, S., G. J. van Oldenborgh, and A. Cimatoribus, 2012: Is a Decline of AMOC Causing the Warming Hole above the North Atlantic in Observed and Modeled Warming Patterns? *Journal of Climate*, **25**, 8373–8379, doi:10.1175/jcli-d-12-00490.1.

Dyrrdal, A. V., T. Saloranta, T. Skaugen, and H. B. Stranden, 2012: Changes in snow depth in Norway during the period 1961–2010. *Hydrology Research*, **44**, 169–179, doi:10.2166/nh.2012.064.

ECMWF, 2023: ERA5: data documentation. WebPage.

URL `https://confluence.ecmwf.int/display/CKB/ERA5:+data+documentation`

Elliott, W. P. and R. K. Reed, 1973: Oceanic rainfall off the Pacific Northwest Coast. *Journal of Geophysical Research*, **78**, 941–948, doi:10.1029/jc078i006p00941.

— 1984: A Climatological Estimate of Precipitation for the World Ocean. *Journal of Climate and Applied Meteorology*, **23**, 434–439, doi:10.1175/1520-0450(1984)023<0434:aceopf>2.0.co;2.

Ellis, T. D., T. L'Ecuyer, J. M. Haynes, and G. L. Stephens, 2009: How often does it rain over the global oceans? the perspective from CloudSat. *Geophysical Research Letters*, **36**, doi:10.1029/2008gl036728.

Eyring, V., S. Bony, G. A. Meehl, C. A. Senior, B. Stevens, R. J. Stouffer, and K. E. Taylor, 2016: Overview of the Coupled Model Intercomparison Project Phase 6 (CMIP6) experimental design and organization. *Geoscientific Model Development*, **9**, 1937–1958, doi:10.5194/gmd-9-1937-2016.

Fan, J., R. Zhang, W.-K. Tao, and K. I. Mohr, 2008: Effects of aerosol optical properties on deep convective clouds and radiative forcing. *Journal of Geophysical Research*, **113**, doi:10.1029/2007jd009257.

Ferek, R. J., T. Garrett, P. V. Hobbs, S. Strader, D. Johnson, J. P. Taylor, K. Nielsen, A. S. Ackerman, Y. Kogan, Q. Liu, B. A. Albrecht, and D. Babb, 2000: Drizzle Suppression in Ship Tracks. *Journal of the Atmospheric Sciences*, **57**, 2707–2728, doi:10.1175/1520-0469(2000)057<2707:dsist>2.0.co;2.

Finney, D. L., R. M. Doherty, O. Wild, D. S. Stevenson, I. A. MacKenzie, and A. M. Blyth, 2018: A projected decrease in lightning under climate change. *Nature Climate Change*, **8**, 210–213, doi:10.1038/s41558-018-0072-6.

Fischer, E. M. and R. Knutti, 2016: Observed heavy precipitation increase confirms theory and early models. *Nature Climate Change*, **6**, 986–991, doi:10.1038/nclimate3110.

Foken, T. and R. Rülke, 2021: Visual Observations. *Spring Handbook of Atmospheric Measurements*, T. Foken, ed., Springer Nature Switzerland, 625–660.

Fowler, A. M. and K. J. Hennessy, 1995: Potential impacts of global warming on the frequency and magnitude of heavy precipitation. *Natural Hazards*, **11**, 283–303, doi:10.1007/bf00613411.

Freeman, E., S. D. Woodruff, S. J. Worley, S. J. Lubker, E. C. Kent, W. E. Angel, D. I. Berry, P. Brohan, R. Eastman, L. Gates, W. Gloeden, Z. Ji, J. Lawrimore, N. A. Rayner, G. Rosenhagen, and S. R. Smith, 2016: ICOADS release 3.0: a major update to the historical marine climate record. *International Journal of Climatology*, **37**, 2211–2232, doi:10.1002/joc.4775.

Fu, C. and L. Dan, 2014: Trends in the different grades of precipitation over South China during 1960–2010 and the possible link with anthropogenic aerosols. *Advances in Atmospheric Sciences*, **31**, 480–491, doi:10.1007/s00376-013-2102-7.

Fuchs, T., J. Rapp, F. Rubel, and B. Rudolf, 2001: Correction of synoptic precipitation observations due to systematic measuring errors with special regard to precipitation phases. *Physics and Chemistry of the Earth, Part B: Hydrology, Oceans and Atmosphere*, **26**, 689–693, doi:10.1016/s1464-1909(01)00070-3.

Garand, L., 1989: Two Automated Methods to Derive Probability of Precipitation Fields over Oceanic Areas from Satellite Imagery. *Journal of Applied Meteorology*, **28**, 913–924, doi:10.1175/1520-0450(1989)028<0913:tamtdp>2.0.co;2.

García-Herrera, R., D. Barriopedro, D. Gallego, J. Mellado-Cano, D. Wheeler, and C. Wilkinson, 2018: Understanding weather and climate of the last 300 years from ships' logbooks. *WIREs Climate Change*, **9**, doi:10.1002/wcc.544.

Ghate, V. P. and M. P. Cadeddu, 2019: Drizzle and Turbulence Below Closed Cellular Marine Stratocumulus Clouds. *Journal of Geophysical Research: Atmospheres*, **124**, 5724–5737, doi:10.1029/2018jd030141.

Goroch, A. K., T. Brown, and M. J. Vanderhill, 1984: Rain Rate Climatologies Over Marine Regions. Techical Report 84-04, Naval Environmental Prediction Research Facility.
URL `https://apps.dtic.mil/sti/pdfs/ADA144066.pdf`

Grigorieva, V. G., S. K. Gulev, and V. D. Sharmar, 2020: Validating Ocean Wind Wave Global Hindcast with Visual Observations from VOS. *Oceanology*, **60**, 9–19, doi:10.1134/s0001437020010130.

Grimm, N. B., F. S. Chapin, B. Bierwagen, P. Gonzalez, P. M. Groffman, Y. Luo, F. Melton, K. Nadelhoffer, A. Pairis, P. A. Raymond, J. Schimel, and C. E. Williamson, 2013: The impacts of climate change on ecosystem structure and function. *Frontiers in Ecology and the Environment*, **11**, 474–482, doi:10.1890/120282.

Groisman, P. Y. and D. R. Legates, 1995: Documenting and detecting long-term precipitation trends: Where we are and what should be done. *Climatic Change*, **31**, 601–622, doi:10.1007/bf01095163.

Gu, G. and R. F. Adler, 2012: Interdecadal variability/long-term changes in global precipitation patterns during the past three decades: global warming and/or pacific decadal variability? *Climate Dynamics*, **40**, 3009–3022, doi:10.1007/s00382-012-1443-8.

— 2023: Observed variability and trends in global precipitation during 1979–2020. *Climate Dynamics*, **61**, 131–150, doi:10.1007/s00382-022-06567-9.

Gulev, S., T. Jung, and E. Ruprecht, 2007: Estimation of the Impact of Sampling Errors in the VOS Observations on Air–Sea Fluxes. Part I: Uncertainties in Climate Means. *Journal of Climate*, **20**, 279–301, doi:10.1175/jcli4010.1.

Gulev, S. K., V. Grigorieva, K. Selemnov, and O. Zolina, 2003: Evaluation of Ocean Winds and Waves from Voluntary Observing Ship Data. *Advances in the Applications*

of Marine Climatology, Joint WMO/IOC Technical Commission for Oceanography and Marine Meteorology, 53–67.

URL `https://icoads.noaa.gov/jcomm_tr13.pdf`

Gutenstein, M., K. Fennig, M. Schröder, T. Trent, S. Bakan, J. B. Roberts, and F. R. Robertson, 2021: Intercomparison of freshwater fluxes over ocean and investigations into water budget closure. *Hydrology and Earth System Sciences*, **25**, 121–146, doi:10.5194/hess-25-121-2021.

Gutiérrez, J. M., R. G. Jones, G. T. Narisma, L. M. Alves, M. Amjad, I. V. Gorodetskaya, M. Grose, N. A. B. Klutse, S. Krakovska, J. Li, D. Martínez-Castro, L. O. Mearns, S. H. Mernild, T. Ngo-Duc, B. van den Hurk, and J.-H. Yoon, 2021: Atlas. *Climate Change 2021 – The Physical Science Basis*, V. Masson-Delmotte, P. Zhai, A. Pirani, S. L. Connors, C. Péan, Y. Chen, L. Goldfarb, M. I. Gomis, J. B. R. Matthews, S. Berger, M. Huang, O. Yelekçi, R. Yu, B. Zhou, E. Lonnoy, T. K. Maycock, T. Waterfield, K. Leitzell, and N. Caud, eds., Cambridge University Press, 1927–2058.

Hahn, C. J. and S. G. Warren, 1999: Extended Edited Synoptic Cloud Reports from Ships and Land Stations Over the Globe, 1952-1996. Technical report, Environmental Service Division.

Hahn, C. J., S. G. Warren, and J. London, 1992: The Use of COADS Ship Observations in Cloud Climatologies. *Proceedings of the International COADS Workshop*, H. F. Diaz, K. Wolter, and S. D. Woodruff, eds., NOAA Environmental Research Laboratories,

267–276.

URL https://www.icoads.noaa.gov/Boulder/Boulder.Hahn.pdf

Hanson, H. P., 1991: Marine stratocumulus climatologies. *International Journal of Climatology*, **11**, 147–164, doi:10.1002/joc.3370110204.

Harou, A. P., R. F. Lajoie, D. R. Kniveton, and M. R. Frogley, 2006: The influence of the Indian Ocean dipole mode on precipitation over the Seychelles. *International Journal of Climatology*, **26**, 45–54, doi:10.1002/joc.1239.

Hasse, L., M. Grossklaus, K. Uhlig, and P. Timm, 1998: A Ship Rain Gauge for Use in High Wind Speeds. *Journal of Atmospheric and Oceanic Technology*, **15**, 380–386, doi:10.1175/1520-0426(1998)015<0380:asrgfu>2.0.co;2.

Hersbach, H., B. Bell, P. Berrisford, S. Hirahara, A. Horányi, J. Muñoz-Sabater, J. Nicolas, C. Peubey, R. Radu, D. Schepers, A. Simmons, C. Soci, S. Abdalla, X. Abellan, G. Balsamo, P. Bechtold, G. Biavati, J. Bidlot, M. Bonavita, G. Chiara, P. Dahlgren, D. Dee, M. Diamantakis, R. Dragani, J. Flemming, R. Forbes, M. Fuentes, A. Geer, L. Haimberger, S. Healy, R. J. Hogan, E. Hólm, M. Janisková, S. Keeley, P. Laloyaux, P. Lopez, C. Lupu, G. Radnoti, P. Rosnay, I. Rozum, F. Vamborg, S. Villaume, and J.-N. Thépaut, 2020: The ERA5 global reanalysis. *Quarterly Journal of the Royal Meteorological Society*, **146**, 1999–2049, doi:10.1002/qj.3803.

Hoerling, M., J. Eischeid, and J. Perlwitz, 2010: Regional Precipitation Trends: Distinguishing Natural Variability from Anthropogenic Forcing. *Journal of Climate*, **23**, 2131–2145, doi:10.1175/2009jcli3420.1.

Houvenaghel, G. T., 1990: The First International Conference on Oceanography (Brussels, 1853). *Ocean Sciences: Their History and Relation to Man*, W. Lenz and M. Deacon, eds., Vlaams Instituut voor de Zee, Bundesamt für Seeschifffahrt und Hydrographie/Deutsches Hydrographisches Institut, number 22 in Ergänzungsheft Reihe B, 330–336.

URL `https://www.vliz.be/nl/imis?module=ref&refid=6170&basketaction=add`

Hu, Y., C. Zhou, and J. Liu, 2010: Observational evidence for poleward expansion of the Hadley circulation. *Advances in Atmospheric Sciences*, **28**, 33–44, doi:10.1007/s00376-010-0032-1.

Huang, B., P. W. Thorne, V. F. Banzon, T. Boyer, G. Chepurin, J. H. Lawrimore, M. J. Menne, T. M. Smith, R. S. Vose, and H.-M. Zhang, 2017: Extended Reconstructed Sea Surface Temperature, Version 5 (ERSSTv5): Upgrades, Validations, and Intercomparisons. *Journal of Climate*, **30**, 8179–8205, doi:10.1175/jcli-d-16-0836.1.

Huntington, T. G., 2006: Evidence for intensification of the global water cycle: Review and synthesis. *Journal of Hydrology*, **319**, 83–95, doi:10.1016/j.jhydrol.2005.07.003.

— 2010: Climate Warming-Induced Intensification of the Hydrologic Cycle. *Advances in Agronomy*, Elsevier, 1–53.

Iles, C. E., G. C. Hegerl, A. P. Schurer, and X. Zhang, 2013: The effect of volcanic eruptions on global precipitation. *Journal of Geophysical Research: Atmospheres*, **118**, 8770–8786, doi:10.1002/jgrd.50678.

Iversen, E. C., Ø. Hodnebrog, L. Seland Graff, B. E. Nygaard, and T. Iversen, 2023: Future Winter Precipitation Decreases Associated With the North Atlantic Warming Hole and Reduced Convection. *Journal of Geophysical Research: Atmospheres*, **128**, doi:10.1029/2022jd038374.

Jacobs, W. C., 1968: The Seasonal Apportionment of Precipitation over the Ocean. *Yearbook of the Association of Pacific Coast Geographers*, **30**, 63–78, doi:10.1353/pcg.1968.0003.

Jaeger, L., 1983: Monthly and Areal Patterns of Mean Global Precipitation. *Variations in the Global Water Budget*, Springer Netherlands, 129–140.

Jeong, J., M. K. Witte, and M. Smalley, 2023: Effects of Wind Shear and Aerosol Conditions on the Organization of Precipitating Marine Stratocumulus Clouds. *Journal of Geophysical Research: Atmospheres*, **128**, doi:10.1029/2023jd039081.

Jiang, P., Z. Yu, M. R. Gautam, and K. Acharya, 2016: The Spatiotemporal Characteristics of Extreme Precipitation Events in the Western United States. *Water Resources Management*, **30**, 4807–4821, doi:10.1007/s11269-016-1454-z.

Joint WMO-IOC Commission for Oceanography and Marine Meteorology, 2011: Proceedings of the Third International Workshop on Advances in the Use of Historical Marine Climate Data. Technical Report 59.
URL `https://library.wmo.int/doc_num.php?explnum_id=7448`

Joint WMO-IOC Commission for Oceanography and Marine Meteorology, 2021: International VOS Scheme. WebPage.

URL `http://sot.jcommops.org/vos/vos.html`

Jones, P. W., 1999: First- and Second-Order Conservative Remapping Schemes for Grids in Spherical Coordinates. *Monthly Weather Review*, **127**, 2204–2210, doi:10.1175/1520-0493(1999)127<2204:fasocr>2.0.co;2.

Joyce, R. J., J. E. Janowiak, P. A. Arkin, and P. Xie, 2004: CMORPH: A Method that Produces Global Precipitation Estimates from Passive Microwave and Infrared Data at High Spatial and Temporal Resolution. *Journal of Hydrometeorology*, **5**, 487–503, doi:10.1175/1525-7541(2004)005<0487:CAMTPG>2.0.CO;2.

Kaplan, A., M. A. Cane, Y. Kushnir, A. C. Clement, M. B. Blumenthal, and B. Rajagopalan, 1998: Analyses of global sea surface temperature 1856–1991. *Journal of Geophysical Research: Oceans*, **103**, 18567–18589, doi:10.1029/97jc01736.

Kaplan, J. O. and K. H.-K. Lau, 2021: The WGLC global gridded lightning climatology and time series. *Earth System Science Data*, **13**, 3219–3237, doi:10.5194/essd-13-3219-2021.

— 2022: World wide lightning location network (wwlln) global lightning climatology (wglc) and time series, 2022 update. *Earth System Science Data*, **14**, 5665–5670, doi:10.5194/essd-14-5665-2022.

Kennedy, J. J., N. A. Rayner, R. O. Smith, D. E. Parker, and M. Saunby, 2011: Reassessing biases and other uncertainties in sea surface temperature observations measured in situ since 1850: 1. measurement and sampling uncertainties. *Journal of Geophysical Research*, **116**, doi:10.1029/2010jd015218.

Kent, E. C., G. Ball, D. I. Berry, J. Fletcher, A. Hall, S. North, and S. D. Woodruff, 2010: The Voluntary Observing Ship (VOS) Scheme. *Proceedings of OceanObs'09: Sustained Ocean Observations and Information for Society*, European Space Agency, 21–25.

Kent, E. C. and D. I. Berry, 2005: Quantifying random measurement errors in Voluntary Observing Ships' meteorological observations. *International Journal of Climatology*, **25**, 843–856, doi:10.1002/joc.1167.

Kent, E. C., D. I. Berry, S. D. Woodruff, and P. K. Taylor, 2006: Voluntary Observing Ships: A Vital Marine Observing System in Decline. *CLIVAR Exchanges*, **11**, 20–21. URL `https://www.clivar.org/sites/default/files/documents/Exchanges38.pdf`

Kent, E. C., S. Fangohr, and D. I. Berry, 2012: A comparative assessment of monthly mean wind speed products over the global ocean. *International Journal of Climatology*, **33**, 2520–2541, doi:10.1002/joc.3606.

Kent, E. C., N. A. Rayner, D. I. Berry, R. Eastman, V. G. Grigorieva, B. Huang, J. J. Kennedy, S. R. Smith, and K. M. Willett, 2019: Observing Requirements for Long-Term Climate Records at the Ocean Surface. *Frontiers in Marine Science*, **6**, doi:10.3389/fmars.2019.00441.

Kent, E. C., N. A. Rayner, D. I. Berry, M. Saunby, B. I. Moat, J. J. Kennedy, and D. E. Parker, 2013: Global analysis of night marine air temperature and its uncertainty since 1880: The HadNMAT2 data set. *Journal of Geophysical Research: Atmospheres*, **118**, 1281–1298, doi:10.1002/jgrd.50152.

Kent, E. C. and P. K. Taylor, 1995: A Comparison of Sensible and Latent Heat Flux Estimates for the North Atlantic Ocean. *Journal of Physical Oceanography*, **25**, 1530–1549, doi:10.1175/1520-0485(1995)025<1530:acosal>2.0.co;2.

Kent, E. C., P. K. Taylor, B. S. Truscott, and J. S. Hopkins, 1993: The Accuracy of Voluntary Observing Ships' Meteorological Observations-Results of the VSOP-NA. *Journal of Atmospheric and Oceanic Technology*, **10**, 591–608, doi:10.1175/1520-0426(1993)010<0591:taovos>2.0.co;2.

Khan, S. and V. Maggioni, 2019: Assessment of Level-3 Gridded Global Precipitation Mission (GPM) Products Over Oceans. *Remote Sensing*, **11**, 255, doi:10.3390/rs11030255.

Kidd, C., J. Beauchamp, M. R. P. Sapiano, and N.-Y. Wang, 2022: Fundamental satellite precipitation data records. *Precipitation Science*, Elsevier, 177–199.

Kidd, C., A. Becker, G. J. Huffman, C. L. Muller, P. Joe, G. Skofronick-Jackson, and D. B. Kirschbaum, 2017a: So, How Much of the Earth's Surface Is Covered by Rain Gauges? *Bulletin of the American Meteorological Society*, **98**, 69–78, doi:10.1175/bams-d-14-00283.1.

Kidd, C. and V. Levizzani, 2011: Status of satellite precipitation retrievals. *Hydrology and Earth System Sciences*, **15**, 1109–1116, doi:10.5194/hess-15-1109-2011.

Kidd, C., J. Tan, P. Kirstetter, and W. A. Petersen, 2017b: Validation of the Version 05 Level 2 precipitation products from the GPM Core Observatory and constellation satellite sensors. *Quarterly Journal of the Royal Meteorological Society*, **144**, 313–328, doi:10.1002/qj.3175.

Kim, S., A. Sharma, C. Wasko, and R. Nathan, 2022: Linking Total Precipitable Water to Precipitation Extremes Globally. *Earth's Future*, **10**, doi:10.1029/2021ef002473.

Klein, S. A. and D. L. Hartmann, 1993: The Seasonal Cycle of Low Stratiform Clouds. *Journal of Climate*, **6**, 1587–1606, doi:10.1175/1520-0442(1993)006<1587:tscols>2.0.co;2.

Klepp, C., 2015: The oceanic shipboard precipitation measurement network for surface validation — OceanRAIN. *Atmospheric Research*, **163**, 74–90, doi:10.1016/j.atmosres.2014.12.014.

Klepp, C., S. Michel, A. Protat, J. Burdanowitz, N. Albern, M. Kähnert, A. Dahl, V. Louf, S. Bakan, and S. A. Buehler, 2018: OceanRAIN, a new in-situ shipboard global ocean surface-reference dataset of all water cycle components. *Scientific Data*, **5**, doi:10.1038/sdata.2018.122.

Krasting, J. P., A. J. Broccoli, K. W. Dixon, and J. R. Lanzante, 2013: Future Changes in Northern Hemisphere Snowfall. *Journal of Climate*, **26**, 7813–7828, doi:10.1175/jcli-d-12-00832.1.

Krishnan, R. and M. Sugi, 2003: Pacific decadal oscillation and variability of the Indian summer monsoon rainfall. *Climate Dynamics*, **21**, 233–242, doi:10.1007/s00382-003-0330-8.

Kummerow, C. D., D. L. Randel, M. Kulie, N.-Y. Wang, R. Ferraro, S. Joseph Munchak, and V. Petkovic, 2015: The Evolution of the Goddard Profiling Algorithm to a Fully Parametric Scheme. *Journal of Atmospheric and Oceanic Technology*, **32**, 2265–2280, doi:10.1175/jtech-d-15-0039.1.

Kunkel, K. E., D. A. Robinson, S. Champion, X. Yin, T. Estilow, and R. M. Frankson, 2016: Trends and Extremes in Northern Hemisphere Snow Characteristics. *Current Climate Change Reports*, **2**, 65–73, doi:10.1007/s40641-016-0036-8.

Landolt, S. D., J. S. Lave, D. Jacobson, A. Gaydos, S. DiVito, and D. Porter, 2019: The Impacts of Automation on Present Weather–Type Observing Capabilities across the Conterminous United States. *Journal of Applied Meteorology and Climatology*, **58**, 2699–2715, doi:10.1175/jamc-d-19-0170.1.

L'Ecuyer, T. S., W. Berg, J. Haynes, M. Lebsock, and T. Takemura, 2009: Global observations of aerosol impacts on precipitation occurrence in warm maritime clouds. *Journal of Geophysical Research*, **114**, doi:10.1029/2008jd011273.

Legates, D. R., 2014: Climate Models and Their Simulation of Precipitation. *Energy & Environment*, **25**, 1163–1175, doi:10.1260/0958-305x.25.6-7.1163.

Legates, D. R. and C. J. Willmott, 1990: Mean seasonal and spatial variability in gauge-corrected, global precipitation. *International Journal of Climatology*, **10**, 111–127, doi:10.1002/joc.3370100202.

Lelli, L., A. A. Kokhanovsky, V. V. Rozanov, M. Vountas, and J. P. Burrows, 2014: Linear trends in cloud top height from passive observations in the oxygen A-band. *Atmospheric Chemistry and Physics*, **14**, 5679–5692, doi:10.5194/acp-14-5679-2014.

Leung, G. R., S. M. Saleeby, G. A. Sokolowsky, S. W. Freeman, and S. C. van den Heever, 2023: Aerosol–cloud impacts on aerosol detrainment and rainout in shallow maritime tropical clouds. *Atmospheric Chemistry and Physics*, **23**, 5263–5278, doi:10.5194/acp-23-5263-2023.

Levizzani, V. and E. Cattani, 2019: Satellite Remote Sensing of Precipitation and the Terrestrial Water Cycle in a Changing Climate. *Remote Sensing*, **11**, 2301, doi:10.3390/rs11192301.

Li, L., M. S. Lozier, and F. Li, 2021: Century-long cooling trend in subpolar North Atlantic forced by atmosphere: an alternative explanation. *Climate Dynamics*, **58**, 2249–2267, doi:10.1007/s00382-021-06003-4.

Li, P., G. Wang, G. Fu, and C. Lu, 2016: On spatiotemporal characteristics of sea fog occurrence over the Northern Atlantic from 1909 to 2008. *Journal of Ocean University of China*, **15**, 958–966, doi:10.1007/s11802-016-3077-7.

Li, Z., F. Niu, J. Fan, Y. Liu, D. Rosenfeld, and Y. Ding, 2011: Long-term impacts of aerosols on the vertical development of clouds and precipitation. *Nature Geoscience*, **4**, 888–894, doi:10.1038/ngeo1313.

Li, Z., E. J. Thompson, A. Behrangi, H. Chen, and J. Yang, 2023: Performance of GPCP Daily Products Over Oceans: Evaluation Using Passive Aquatic Listeners. *Geophysical Research Letters*, **50**, doi:10.1029/2023gl104310.

Liu, C., E. Freeman, E. C. Kent, D. I. Berry, S. J. Worley, S. R. Smith, B. Huang, H. min Zhang, T. Cram, Z. Ji, M. Ouellet, I. Gaboury, F. Oliva, A. Andersson, W. E. Angel, A. R. Sallis, and A. Adeyeye, 2022: Blending TAC and BUFR Marine In Situ Data for ICOADS Near-Real-Time Release 3.0.2. *Journal of Atmospheric and Oceanic Technology*, **39**, 1943–1959, doi:10.1175/jtech-d-21-0182.1.

Liu, G., 2008: Deriving snow cloud characteristics from CloudSat observations. *Journal of Geophysical Research*, **113**, doi:10.1029/2007jd009766.

Liu, H., I. Koren, O. Altaratz, and M. D. Chekroun, 2023: Opposing trends of cloud coverage over land and ocean under global warming. *Atmospheric Chemistry and Physics*, **23**, 6559–6569, doi:10.5194/acp-23-6559-2023.

Liu, Z., 2016: Comparison of Integrated Multisatellite Retrievals for GPM (IMERG) and TRMM Multisatellite Precipitation Analysis (TMPA) Monthly Precipitation Products: Initial Results. *Journal of Hydrometeorology*, **17**, 777–790, doi:10.1175/jhm-d-15-0068.1.

Lohmann, U. and J. Feichter, 2005: Global indirect aerosol effects: a review. *Atmospheric Chemistry and Physics*, **5**, 715–737, doi:10.5194/acp-5-715-2005.

Lu, J., G. A. Vecchi, and T. Reichler, 2007a: Expansion of the Hadley cell under global warming. *Geophysical Research Letters*, **34**, doi:10.1029/2006gl028443.

Lu, M., W. C. Conant, H. H. Jonsson, V. Varutbangkul, R. C. Flagan, and J. H. Seinfeld, 2007b: The Marine Stratus/Stratocumulus Experiment (MASE): Aerosol-cloud relationships in marine stratocumulus. *Journal of Geophysical Research: Atmospheres*, **112**, doi:10.1029/2006jd007985.

L'Heureux, M. L., S. Lee, and B. Lyon, 2013: Recent multidecadal strengthening of the Walker circulation across the tropical Pacific. *Nature Climate Change*, **3**, 571–576, doi:10.1038/nclimate1840.

Mann, J. A. L., J. C. Chiu, R. J. Hogan, E. J. O'Connor, T. S. L'Ecuyer, T. H. M. Stein, and A. Jefferson, 2014: Aerosol impacts on drizzle properties in warm clouds from ARM Mobile Facility maritime and continental deployments. *Journal of Geophysical Research: Atmospheres*, **119**, 4136–4148, doi:10.1002/2013jd021339.

Mantua, N. J. and S. R. Hare, 2002: The Pacific Decadal Oscillation. *Journal of Oceanography*, **58**, 35–44, doi:10.1023/a:1015820616384.

Marchand, R., 2013: Trends in ISCCP, MISR, and MODIS cloud-top-height and optical-depth histograms. *Journal of Geophysical Research: Atmospheres*, **118**, 1941–1949, doi:10.1002/jgrd.50207.

Maroon, E. A., S. G. Yeager, G. Danabasoglu, and N. Rosenbloom, 2021: Was the 2015 North Atlantic subpolar cold anomaly predictable? *Journal of Climate*, 1–69, doi:10.1175/jcli-d-20-0750.1.

Martin, D. W. and W. D. Scherer, 1973: Review of Satellite Rainfall Estimation Methods. *Bulletin of the American Meteorological Society*, **54**, 661–675, doi:10.1175/1520-0477-54.7.661.

Marvel, K. and C. Bonfils, 2013: Identifying external influences on global precipitation. *Proceedings of the National Academy of Sciences*, **110**, 19301–19306, doi:10.1073/pnas.1314382110.

Maury, M. F., 1854: *Explanations and Sailing Directions to Accompany the Wind and Current Charts*, E. C. and J. Biddle, chapter Maritime Conference Held at Brussels for Devising an Uniform System of Meteorological Observations at Sea, August and September 1853. Sixth edition, 54–96.

McCoy, D. T., R. Eastman, D. L. Hartmann, and R. Wood, 2017: The Change in Low Cloud Cover in a Warmed Climate Inferred from AIRS, MODIS, and ERA-Interim. *Journal of Climate*, **30**, 3609–3620, doi:10.1175/jcli-d-15-0734.1.

Merenti-Välimäki, H.-L., J. Lönnqvist, and P. Laininen, 2001: Present weather: comparing human observations and one type of automated sensor. *Meteorological Applications*, **8**, 491–496, doi:10.1017/s1350482701004108.

Ming, Y., V. Ramaswamy, and G. Persad, 2010: Two opposing effects of absorbing aerosols on global-mean precipitation. *Geophysical Research Letters*, **37**, n/a–n/a, doi:10.1029/2010gl042895.

Minobe, S. and A. Maeda, 2005: A 1° monthly gridded sea-surface temperature dataset compiled from ICOADS from 1850 to 2002 and Northern Hemisphere frontal variability. *International Journal of Climatology*, **25**, 881–894, doi:10.1002/joc.1170.

Morrissey, M. L. and J. S. Greene, 2008: A theoretical framework for the sampling error variance for three-dimensional climate averages of ICOADS monthly ship data. *Theoretical and Applied Climatology*, **96**, 235–248, doi:10.1007/s00704-008-0027-3.

Mudryk, L., M. Santolaria-Otín, G. Krinner, M. Ménégoz, C. Derksen, C. Brutel-Vuilmet, M. Brady, and R. Essery, 2020: Historical Northern Hemisphere snow cover trends and projected changes in the CMIP6 multi-model ensemble. *The Cryosphere*, **14**, 2495–2514, doi:10.5194/tc-14-2495-2020.

Muhlbauer, A., I. L. McCoy, and R. Wood, 2014: Climatology of stratocumulus cloud morphologies: microphysical properties and radiative effects. *Atmospheric Chemistry and Physics*, **14**, 6695–6716, doi:10.5194/acp-14-6695-2014.

National Weather Service, 1971: *Weather Service Observing Handbook No. 1: Marine Surface Observations*.
URL https://www.google.com/books/edition/Weather_Service_Observing_Handbook/jDBRAAAAMAAJ?hl=en&gbpv=1

New, M., M. Todd, M. Hulme, and P. Jones, 2001: Precipitation measurements and trends in the twentieth century. *International Journal of Climatology*, **21**, 1889–1922, doi:10.1002/joc.680.

Norrant, C. and A. Douguédroit, 2005: Monthly and daily precipitation trends in the Mediterranean (1950–2000). *Theoretical and Applied Climatology*, **83**, 89–106, doi:10.1007/s00704-005-0163-y.

Office of the Federal Coordinator for Meteorological Services and Supporting Research, National Oceanic and Atmospheiric Administration, 2019: *Federal Meteorological Handbook No. 1: Surface Weather Observations and Reports*.
URL https://www.icams-portal.gov/resources/ofcm/fmh/FMH1/fmh1_2019.pdf

O'Gorman, P. A., 2015: Precipitation Extremes Under Climate Change. *Current Climate Change Reports*, **1**, 49–59, doi:10.1007/s40641-015-0009-3.

O'Gorman, P. A., 2014: Contrasting responses of mean and extreme snowfall to climate change. *Nature*, **512**, 416–418, doi:10.1038/nature13625.

Page, J., 1906: *Instructions to the Marine Meteorological Observers of the U.S. Weather Bureau*. United States Weather Bureau, first edition.
URL `http://hdl.handle.net/1834/5218`

Park, K. J., K. Yoshimura, H. Kim, and T. Oki, 2017: Chronological Development of Terrestrial Mean Precipitation. *Bulletin of the American Meteorological Society*, **98**, 2411–2428, doi:10.1175/bams-d-16-0005.1.

Parker, D. E., P. D. Jones, C. K. Folland, and A. Bevan, 1994: Interdecadal changes of surface temperature since the late nineteenth century. *Journal of Geophysical Research: Atmospheres*, **99**, 14373–14399, doi:10.1029/94jd00548.

Parkinson, C. L. and D. J. Cavalieri, 2012: Antarctic sea ice variability and trends, 1979–2010. *The Cryosphere*, **6**, 871–880, doi:10.5194/tc-6-871-2012.

Pendergrass, A. G. and D. L. Hartmann, 2014: Changes in the Distribution of Rain Frequency and Intensity in Response to Global Warming*. *Journal of Climate*, **27**, 8372–8383, doi:10.1175/jcli-d-14-00183.1.

Pendergrass, A. G., R. Knutti, F. Lehner, C. Deser, and B. M. Sanderson, 2017: Precipitation variability increases in a warmer climate. *Scientific Reports*, **7**, doi:10.1038/s41598-017-17966-y.

Petty, G. W., 1995: Frequencies and Characteristics of Global Oceanic Precipitation from Shipboard Present-Weather Reports. *Bulletin of the American Meteorological Society*, **76**, 1593–1616, doi:10.1175/1520-0477(1995)076<1593:facogo>2.0.co;2.

— 1997: An intercomparison of oceanic precipitation frequencies from 10 special sensor microwave/imager rain rate algorithms and shipboard present weather reports. *Journal of Geophysical Research: Atmospheres*, **102**, 1757–1777, doi:10.1029/96jd03000.

Petty, G. W. and H. K. Tran, 2023: Seventy-Year Trends in Ship-Reported Oceanic Precipitation Frequency. *Geophysical Research Letters*, **50**, doi:10.1029/2023gl104270.

Pradhan, R. K., Y. Markonis, M. R. V. Godoy, A. Villalba-Pradas, K. M. Andreadis, E. I. Nikolopoulos, S. M. Papalexiou, A. Rahim, F. J. Tapiador, and M. Hanel, 2022: Review of GPM IMERG performance: A global perspective. *Remote Sensing of Environment*, **268**, 112754, doi:10.1016/j.rse.2021.112754.

Prakash, S., M. R. R. Kumar, S. Mathew, and R. Venkatesan, 2017: How accurate are satellite estimates of precipitation over the north Indian Ocean? *Theoretical and Applied Climatology*, **134**, 467–475, doi:10.1007/s00704-017-2287-2.

Price, C. and D. Rind, 1994: Possible implications of global climate change on global lightning distributions and frequencies. *Journal of Geophysical Research: Atmospheres*, **99**, 10823–10831, doi:10.1029/94jd00019.

Qu, X., A. Hall, S. A. Klein, and A. M. DeAngelis, 2015: Positive tropical marine low-cloud cover feedback inferred from cloud-controlling factors. *Geophysical Research Letters*, **42**, 7767–7775, doi:10.1002/2015gl065627.

Radić, V. and R. Hock, 2013: Glaciers in the Earth's Hydrological Cycle: Assessments of Glacier Mass and Runoff Changes on Global and Regional Scales. *Surveys in Geophysics*, **35**, 813–837, doi:10.1007/s10712-013-9262-y.

Rasmussen, R. M., J. Vivekanandan, J. Cole, B. Myers, and C. Masters, 1999: The Estimation of Snowfall Rate Using Visibility. *Journal of Applied Meteorology*, **38**, 1542–1563, doi:10.1175/1520-0450(1999)038<1542:teosru>2.0.co;2.

Rast, M., J. Johannessen, and W. Mauser, 2014: Review of Understanding of Earth's Hydrological Cycle: Observations, Theory and Modelling. *Surveys in Geophysics*, **35**, 491–513, doi:10.1007/s10712-014-9279-x.

Reed, R. K., 1979: On the Relationship between the Amount and Frequency of Precipitation over the Ocean. *Journal of Applied Meteorology*, **18**, 692–696, doi:10.1175/1520-0450(1979)018<0692:otrbta>2.0.co;2.

— 1980: Reply. *Journal of Applied Meteorology*, **19**, 1133–1134, doi:10.1175/1520-0450(1980)019<1133:r>2.0.co;2.

Reed, R. K. and W. P. Elliott, 1973: Precipitation at ocean weather stations in the north Pacific. *Journal of Geophysical Research*, **78**, 7087–7091, doi:10.1029/jc078i030p07087.

— 1977: A Comparison of Oceanic Precipitation as Measured by Gage and Assessed from Weather Reports. *Journal of Applied Meteorology*, **16**, 983–986, doi:10.1175/1520-0450(1977)016<0983:acoopa>2.0.co;2.

— 1979: New precipitation maps for the North Atlantic and North Pacific oceans. *Journal of Geophysical Research*, **84**, 7839, doi:10.1029/jc084ic12p07839.

Reynolds, R. W. and T. M. Smith, 1994: Improved Global Sea Surface Temperature Analyses Using Optimum Interpolation. *Journal of Climate*, **7**, 929–948, doi:10.1175/1520-0442(1994)007<0929:igssta>2.0.co;2.

Rigby, M., 1965: The evolution of international cooperation in meteorology (1654–1965). *Bulletin of the American Meteorological Society*, **46**, 630–633, doi:10.1175/1520-0477-46.10.630.

Rizzi, J., I. B. Nilsen, J. H. Stagge, K. Gisnås, and L. M. Tallaksen, 2017: Five decades of warming: impacts on snow cover in Norway. *Hydrology Research*, **49**, 670–688, doi:10.2166/nh.2017.051.

Rodell, M., H. K. Beaudoing, T. S. L'Ecuyer, W. S. Olson, J. S. Famiglietti, P. R. Houser, R. Adler, M. G. Bosilovich, C. A. Clayson, D. Chambers, E. Clark, E. J. Fetzer, X. Gao, G. Gu, K. Hilburn, G. J. Huffman, D. P. Lettenmaier, W. T. Liu, F. R. Robertson, C. A. Schlosser, J. Sheffield, and E. F. Wood, 2015: The Observed State of the Water Cycle in the Early Twenty-First Century. *Journal of Climate*, **28**, 8289–8318, doi:10.1175/jcli-d-14-00555.1.

Rosenfeld, D., M. O. Andreae, A. Asmi, M. Chin, G. de Leeuw, D. P. Donovan, R. Kahn, S. Kinne, N. Kivekäs, M. Kulmala, W. Lau, K. S. Schmidt, T. Suni, T. Wagner, M. Wild, and J. Quaas, 2014: Global observations of aerosol-cloud-precipitation-climate interactions. *Reviews of Geophysics*, **52**, 750–808, doi:10.1002/2013rg000441.

Rosenfeld, D., U. Lohmann, G. B. Raga, C. D. O'Dowd, M. Kulmala, S. Fuzzi, A. Reissell, and M. O. Andreae, 2008: Flood or Drought: How Do Aerosols Affect Precipitation? *Science*, **321**, 1309–1313, doi:10.1126/science.1160606.

Saji, N. H., B. N. Goswami, P. N. Vinayachandran, and T. Yamagata, 1999: A dipole mode in the tropical Indian Ocean. *Nature*, **401**, 360–363, doi:10.1038/43854.

Sarojini, B. B., P. A. Stott, and E. Black, 2016: Detection and attribution of human influence on regional precipitation. *Nature Climate Change*, **6**, 669–675, doi:10.1038/nclimate2976.

Sarojini, B. B., P. A. Stott, E. Black, and D. Polson, 2012: Fingerprints of changes in annual and seasonal precipitation from CMIP5 models over land and ocean. *Geophysical Research Letters*, **39**, doi:10.1029/2012gl053373.

Scheff, J. and D. M. W. Frierson, 2012: Robust future precipitation declines in CMIP5 largely reflect the poleward expansion of model subtropical dry zones. *Geophysical Research Letters*, **39**, doi:10.1029/2012gl052910.

Schmidt, D. F. and K. M. Grise, 2017: The Response of Local Precipitation and Sea Level Pressure to Hadley Cell Expansion. *Geophysical Research Letters*, **44**, doi:10.1002/2017gl075380.

Seethala, C., J. R. Norris, and T. A. Myers, 2015: How Has Subtropical Stratocumulus and Associated Meteorology Changed since the 1980s? *Journal of Climate*, **28**, 8396–8410, doi:10.1175/jcli-d-15-0120.1.

Seidel, D. J., Q. Fu, W. J. Randel, and T. J. Reichler, 2007: Widening of the tropical belt in a changing climate. *Nature Geoscience*, **1**, 21–24, doi:10.1038/ngeo.2007.38.

Sharova, V. Y., 1990: Precipitation Maps for the World's Ocean Surface. *Mapping Sciences and Remote Sensing*, **27**, 280–294, doi:10.1080/07493878.1990.10641814.

Shi, S. and G. Liu, 2021: The latitudinal dependence in the trend of snow event to precipitation event ratio. *Scientific Reports*, **11**, doi:10.1038/s41598-021-97451-9.

Sims, E. M. and G. Liu, 2015: A Parameterization of the Probability of Snow–Rain Transition. *Journal of Hydrometeorology*, **16**, 1466–1477, doi:10.1175/jhm-d-14-0211.1.

Singh, M. S., Z. Kuang, E. D. Maloney, W. M. Hannah, and B. O. Wolding, 2017: Increasing potential for intense tropical and subtropical thunderstorms under global warming. *Proceedings of the National Academy of Sciences*, **114**, 11657–11662, doi:10.1073/pnas.1707603114.

Smith, S. R., G. Alory, A. Andersson, W. Asher, A. Baker, D. I. Berry, K. Drushka, D. Figurskey, E. Freeman, P. Holthus, T. Jickells, H. Kleta, E. C. Kent, N. Kolodziejczyk,

M. Kramp, Z. Loh, P. Poli, U. Schuster, E. Steventon, S. Swart, O. Tarasova, L. P. de la Villéon, and N. Vinogradova-Shiffer, 2019: Ship-Based Contributions to Global Ocean, Weather, and Climate Observing Systems. *Frontiers in Marine Science*, **6**, doi:10.3389/fmars.2019.00434.

Smith, S. R., E. Freeman, S. J. Lubker, S. D. Woodruff, S. J. Worley, A. Adeyeye, W. E. Angel, D. I. Berry, T. Cram, P. Brohan, Z. Ji, E. C. Kent, and C. Liu, 2016: The International Maritime Meteorological Archive (IMMA) Format. Technical report, International Comprehensive Ocean-Atmosphere Data Set.
URL `http://icoads.noaa.gov/e-doc/imma/R3.0-imma1.pdf`

Smith, T. M., 2013: Developing a Historical Precipitation Record. *Satellite-based Applications on Climate Change*, Springer Netherlands, 95–106.

Stephens, G. L., T. L'Ecuyer, R. Forbes, A. Gettelmen, J.-C. Golaz, A. Bodas-Salcedo, K. Suzuki, P. Gabriel, and J. Haynes, 2010: Dreary state of precipitation in global models. *Journal of Geophysical Research: Atmospheres*, **115**, doi:10.1029/2010jd014532.

Stephens, G. L., J. Li, M. Wild, C. A. Clayson, N. Loeb, S. Kato, T. L'Ecuyer, P. W. Stackhouse, M. Lebsock, and T. Andrews, 2012: An update on Earth's energy balance in light of the latest global observations. *Nature Geoscience*, **5**, 691–696, doi:10.1038/ngeo1580.

Stephens, G. L., D. G. Vane, R. J. Boain, G. G. Mace, K. Sassen, Z. Wang, A. J. Illingworth, E. J. O'connor, W. B. Rossow, S. L. Durden, S. D. Miller, R. T. Austin, A. Benedetti, and C. Mitrescu, 2002: The CloudSat Mission and the A-Train: A New

Dimension of Space-Based Observations of Clouds and Precipitation. *Bulletin of the American Meteorological Society*, **83**, 1771–1790, doi:10.1175/bams-83-12-1771.

Stevens, B., D. H. Lenschow, G. Vali, H. Gerber, A. Bandy, B. Blomquist, J.-L. Brenguier, C. S. Bretherton, F. Burnet, T. Campos, S. Chai, I. Faloona, D. Friesen, S. Haimov, K. Laursen, D. K. Lilly, S. M. Loehrer, S. P. Malinowski, B. Morley, M. D. Petters, D. C. Rogers, L. Russell, V. Savic-Jovcic, J. R. Snider, D. Straub, M. J. Szumowski, H. Takagi, D. C. Thornton, M. Tschudi, C. Twohy, M. Wetzel, and M. C. van Zanten, 2003: Supplement to Dynamics and Chemistry of Marine Stratocumulus—DYCOMS-II. *Bulletin of the American Meteorological Society*, **84**, 593–593, doi:10.1175/bams-84-5-stevens.

Sun, Q., C. Miao, Q. Duan, H. Ashouri, S. Sorooshian, and K.-L. Hsu, 2018: A Review of Global Precipitation Data Sets: Data Sources, Estimation, and Intercomparisons. *Reviews of Geophysics*, **56**, 79–107, doi:10.1002/2017rg000574.

Takahashi, H. G., 2020: Long-term trends in snowfall characteristics and extremes in Japan from 1961 to 2012. *International Journal of Climatology*, **41**, 2316–2329, doi:10.1002/joc.6960.

Tan, J., G. J. Huffman, D. T. Bolvin, and E. J. Nelkin, 2019: IMERG V06: Changes to the Morphing Algorithm. *Journal of Atmospheric and Oceanic Technology*, **36**, 2471–2482, doi:10.1175/jtech-d-19-0114.1.

Tan, J., W. A. Petersen, G. Kirchengast, D. C. Goodrich, and D. B. Wolff, 2018: Evaluation of Global Precipitation Measurement Rainfall Estimates against Three Dense

Gauge Networks. *Journal of Hydrometeorology*, **19**, 517–532, doi:10.1175/jhm-d-17-0174.1.

Tao, W.-K., J.-P. Chen, Z. Li, C. Wang, and C. Zhang, 2012: Impact of aerosols on convective clouds and precipitation. *Reviews of Geophysics*, **50**, doi:10.1029/2011rg000369.

Tapiador, F. J., A. Navarro, V. Levizzani, E. García-Ortega, G. J. Huffman, C. Kidd, P. A. Kucera, C. D. Kummerow, H. Masunaga, W. A. Petersen, R. Roca, J.-L. Sánchez, W.-K. Tao, and F. J. Turk, 2017: Global precipitation measurements for validating climate models. *Atmospheric Research*, **197**, 1–20, doi:10.1016/j.atmosres.2017.06.021.

Taszarek, M., J. T. Allen, M. Marchio, and H. E. Brooks, 2021: Global climatology and trends in convective environments from ERA5 and rawinsonde data. *npj Climate and Atmospheric Science*, **4**, doi:10.1038/s41612-021-00190-x.

Taylor, K. E., R. J. Stouffer, and G. A. Meehl, 2012: An Overview of CMIP5 and the Experiment Design. *Bulletin of the American Meteorological Society*, **93**, 485–498, doi:10.1175/bams-d-11-00094.1.

Teleti, P., E. Hawkins, and K. R. Wood, 2023: Digitizing weather observations from World War II US naval ship logbooks. *Geoscience Data Journal*, doi:10.1002/gdj3.222.

Terai, C. R., R. Wood, D. C. Leon, and P. Zuidema, 2012: Does precipitation susceptibility vary with increasing cloud thickness in marine stratocumulus? *Atmospheric Chemistry and Physics*, **12**, 4567–4583, doi:10.5194/acp-12-4567-2012.

Thornton, J. A., K. S. Virts, R. H. Holzworth, and T. P. Mitchell, 2017: Lightning enhancement over major oceanic shipping lanes. *Geophysical Research Letters*, **44**, 9102–9111, doi:10.1002/2017gl074982.

Titchner, H. A. and N. A. Rayner, 2014: The Met Office Hadley Centre sea ice and sea surface temperature data set, version 2: 1. Sea ice concentrations. *Journal of Geophysical Research: Atmospheres*, **119**, 2864–2889, doi:10.1002/2013jd020316.

Tramblay, Y. and S. Somot, 2018: Future evolution of extreme precipitation in the mediterranean. *Climatic Change*, **151**, 289–302, doi:10.1007/s10584-018-2300-5.

Trenberth, K. E., 2011: Changes in precipitation with climate change. *Climate Research*, **47**, 123–138, doi:10.3354/cr00953.

Trenberth, K. E. and D. J. Shea, 2005: Relationships between precipitation and surface temperature. *Geophysical Research Letters*, **32**, doi:10.1029/2005gl022760.

Trenberth, K. E. and Y. Zhang, 2018: How Often Does It Really Rain? *Bulletin of the American Meteorological Society*, **99**, 289–298, doi:10.1175/bams-d-17-0107.1.

Tsonis, A. A., 2002: The Problem of Extracting Precipitation Information in the Tropics from the UWM/COADS Data. *Journal of Applied Meteorology*, **41**, 1153–1162, doi:10.1175/1520-0450(2002)041<1153:tpoepi>2.0.co;2.

Tucker, G. B., 1961: Precipitation over the North Atlantic Ocean. *Quarterly Journal of the Royal Meteorological Society*, **87**, 147–158, doi:10.1002/qj.49708737204.

Ummenhofer, C. C., A. Biastoch, and C. W. Böning, 2017: Multidecadal Indian Ocean Variability Linked to the Pacific and Implications for Preconditioning Indian Ocean Dipole Events. *Journal of Climate*, **30**, 1739–1751, doi:10.1175/jcli-d-16-0200.1.

United States Weather Bureau, 1938: *Instructions to Marine Meteorological Observers.* Sixth edition.

URL `http://hdl.handle.net/1834/5238`

— 1950: *Manual of Marine Meteorological Observations.* Eighth edition.

URL `https://aquadocs.org/bitstream/handle/1834/5240/MarineMetObsInstr_CircularM_v8_1950.pdf?sequence=1&isAllowed=y`

— 1959: *Manual of Marine Meteorological Observations.* Tenth edition.

URL `https://aquadocs.org/bitstream/handle/1834/5243/MarineMetObsInstr_CircularM_v10_1959.pdf?sequence=1&isAllowed=y`

vanZanten, M. C., B. Stevens, G. Vali, and D. H. Lenschow, 2005: Observations of Drizzle in Nocturnal Marine Stratocumulus. *Journal of the Atmospheric Sciences*, **62**, 88–106, doi:10.1175/jas-3355.1.

Vettor, R. and C. G. Soares, 2014: Detection and Analysis of the Main Routes of Voluntary Observing Ships in the North Atlantic. *Journal of Navigation*, **68**, 397–410, doi:10.1017/s0373463314000757.

— 2021: On the Accuracy of Voluntary Observing Ship's Records. *Journal of Offshore Mechanics and Arctic Engineering*, **143**, doi:10.1115/1.4049828.

Wang, C., C. Deser, J.-Y. Yu, P. DiNezio, and A. Clement, 2016: El Niño and Southern Oscillation (ENSO): A Review. *Coral Reefs of the Eastern Tropical Pacific*, Springer Netherlands, 85–106.

Wang, H., J. G. Fyke, J. T. M. Lenaerts, J. M. Nusbaumer, H. Singh, D. Noone, P. J. Rasch, and R. Zhang, 2020: Influence of sea-ice anomalies on Antarctic precipitation using source attribution in the Community Earth System Model. *The Cryosphere*, **14**, 429–444, doi:10.5194/tc-14-429-2020.

Wang, H., Z. Shao, T. Gao, T. Zou, J. Liu, and H. Yuan, 2017: Extreme precipitation event over the Yellow Sea western coast: Is there a trend? *Quaternary International*, **441**, 1–17, doi:10.1016/j.quaint.2016.08.014.

Wang, S., J. Huang, Y. He, and Y. Guan, 2014: Combined effects of the Pacific Decadal Oscillation and El Niño-Southern Oscillation on Global Land Dry–Wet Changes. *Scientific Reports*, **4**, doi:10.1038/srep06651.

Wang, Y., Y. You, and M. Kulie, 2018: Global Virga Precipitation Distribution Derived From Three Spaceborne Radars and Its Contribution to the False Radiometer Precipitation Detection. *Geophysical Research Letters*, **45**, 4446–4455, doi:10.1029/2018gl077891.

Warren, S., R. Eastman, and C. J. Hahn, 2015: CLOUDS AND FOG — Climatology. *Encyclopedia of Atmospheric Sciences*, Elsevier, 161–169.

Warren, S. G., C. J. Hahn, J. London, R. M. Chervin, and R. L. Jenne, 1988: Global distribution of total cloud cover and cloud type amounts over the ocean. Technical report, United States Department of Energy.

Webster, P. J., 2004: The Elementary Hadley Circulation. *Advances in Global Change Research*, Springer Netherlands, 9–60.

Wei, W., Z. Yan, and Z. Li, 2021: Influence of Pacific Decadal Oscillation on global precipitation extremes. *Environmental Research Letters*, **16**, 044031, doi:10.1088/1748-9326/abed7c.

Wheeler, D. and C. Wilkinson, 2005: The Determination of Logbook Wind Force and Weather Terms: The English Case. *Climatic Change*, **73**, 57–77, doi:10.1007/s10584-005-6949-1.

Wilheit, T. T., A. T. C. Chang, M. S. V. Rao, E. B. Rodgers, and J. S. Theon, 1977: A Satellite Technique for Quantitatively Mapping Rainfall Rates over the Oceans. *Journal of Applied Meteorology nad Climatology*, **16**, 551–560, doi:10.1175/1520-0450(1977)016<0551:ASTFQM>2.0.CO;2.

Williams, E., A. Guha, R. Boldi, H. Christian, and D. Buechler, 2019: Global lightning activity and the hiatus in global warming. *Journal of Atmospheric and Solar-Terrestrial Physics*, **189**, 27–34, doi:10.1016/j.jastp.2019.03.011.

Willmott, C. J. and D. R. Legates, 1991: Rising estimates of terrestrial and global precipitation. *Climate Research*, **1**, 179–186.

URL `https://www.int-res.com/articles/cr/1/c001p179.pdf`

Wolter, K., 1997: Trimming Problems and Remedies in COADS. *Journal of Climate*, **10**, 1980–1997, doi:10.1175/1520-0442(1997)010<1980:tparic>2.0.co;2.

Wood, R. and C. S. Bretherton, 2006: On the Relationship between Stratiform Low Cloud Cover and Lower-Tropospheric Stability. *Journal of Climate*, **19**, 6425–6432, doi:10.1175/jcli3988.1.

Woodruff, S. D., H. F. Diaz, J. D. Elms, and S. J. Worley, 1998: COADS release 2 data and metadata enhancements for improvements of marine surface flux fields. *Physics and Chemistry of the Earth*, **23**, 517–526, doi:10.1016/s0079-1946(98)00064-0.

Woodruff, S. D., H. F. Diaz, E. C. Kent, R. W. Reynolds, and S. J. Worley, 2008: The Evolving SST Record from ICOADS. *Climate Variability and Extremes during the Past 100 Years*, Springer Netherlands, 65–83.

Woodruff, S. D., S. J. Lubker, K. WOlter, S. J. Worley, and J. D. Elms, 1993: Comprehensive Ocean-Atmosphere Data Set (COADS) Release 1a: 1980-92. *Earth System Monitor*, **4**, 1–8.

URL `https://www.nodc.noaa.gov/media/pdf/esm/ESM_SEP1993vol4no1.pdf`

Woodruff, S. D., R. J. Slutz, R. L. Jenne, and P. M. Steurer, 1987: A Comprehensive Ocean-Atmosphere Data Set. *Bulletin of the American Meteorological Society*, **68**, 1239–1250, doi:10.1175/1520-0477(1987)068<1239:acoads>2.0.co;2.

World Meteorological Organization, 1962: Precipitation Measurements at Sea. Technical Note 47, World Meteorological Organization.
URL `https://library.wmo.int/doc_num.php?explnum_id=1742`

— 2019: *Manual on Codes: International Codes, Volume I.1, Annex II to the WMO Technical Regulations, Part A – Alphanumeric Codes*. World Meteorological Organization.
URL `https://library.wmo.int/doc_num.php?explnum_id=10235`

— 2021: *Guide to Meteorological Instruments and Methods of Observation, Volume III – Observing Systems*, World Meteorological Organization, chapter Annex 4.B. Descriptions of Precipitation for Use by Ship-Borne Observers of Present Weather. 631–632.
URL `https://library.wmo.int/doc_num.php?explnum_id=11613`

Worley, S. J., 1992: Status of Other New Data Sets for COADS. *Proceedings of the International COADS Workshop, Boulder, Colorado, 13-15 January 1992*, H. F. Diaz, K. Wolter, and S. D. Woodruff, eds., NOAA Environmental Research Laboratories, 77–86.
URL `https://icoads.noaa.gov/Boulder/Boulder.Worley.pdf`

Wu, P., X. Dong, B. Xi, Y. Liu, M. Thieman, and P. Minnis, 2017: Effects of environment forcing on marine boundary layer cloud-drizzle processes. *Journal of Geophysical Research: Atmospheres*, **122**, 4463–4478, doi:10.1002/2016jd026326.

Xue, W., X. Sun, and X. Yang, 2022: Boreal Summer Negative Correlation Relationship Between Interannual SST and Precipitation Anomalies in the Tropical and Subtropical Western North Pacific. *Journal of Geophysical Research: Atmospheres*, **127**, doi:10.1029/2021jd035231.

Yamaguchi, T., G. Feingold, and J. Kazil, 2017: Stratocumulus to Cumulus Transition by Drizzle. *Journal of Advances in Modeling Earth Systems*, **9**, 2333–2349, doi:10.1002/2017ms001104.

Yang, F., E. P. Luke, P. Kollias, A. B. Kostinski, and A. M. Vogelmann, 2018: Scaling of Drizzle Virga Depth With Cloud Thickness for Marine Stratocumulus Clouds. *Geophysical Research Letters*, **45**, 3746–3753, doi:10.1029/2018gl077145.

Yang, J., P. Gong, R. Fu, M. Zhang, J. Chen, S. Liang, B. Xu, J. Shi, and R. Dickinson, 2013: The role of satellite remote sensing in climate change studies. *Nature Climate Change*, **3**, 875–883, doi:10.1038/nclimate1908.

You, Y., V. Petkovic, J. Tan, R. Kroodsma, W. Berg, C. Kidd, and C. Peters-Lidard, 2020: Evaluation of V05 Precipitation Estimates from GPM Constellation Radiometers Using KuPR as the Reference. *Journal of Hydrometeorology*, **21**, 705–728, doi:10.1175/jhm-d-19-0144.1.

Yu, L., S. A. Josey, F. M. Bingham, and T. Lee, 2020: Intensification of the global water cycle and evidence from ocean salinity: a synthesis review. *Annals of the New York Academy of Sciences*, **1472**, 76–94, doi:10.1111/nyas.14354.

Yuter, S. E. and W. S. Parker, 2001: Rainfall Measurement on Ship Revisited: The 1997 PACS TEPPS Cruise. *Journal of Applied Meteorology*, **40**, 1003–1018, doi:10.1175/1520-0450(2001)040<1003:rmosrt>2.0.co;2.

Zhao, C., X. Geng, and L. Qi, 2022: Atlantic Multidecadal Oscillation Modulates the Relation of ENSO With the Precipitation in the Central-Western Indian Ocean. *Frontiers in Earth Science*, **10**, doi:10.3389/feart.2022.866241.

Zhuang, J., R. Dussin, D. Huard, P. Bourgault, A. Banihirwe, S. Raynaud, B. Malevich, M. Schupfner, Filipe, S. Levang, A. Jüling, M. Almansi, RichardScottOZ, RondeauG, R. Stephan, T. J. Smith, J. Stachelek, M. Plough, Pierre, R. Bell, and X. Li, 2023: pangeo-data/xESMF: v0.7.1. Online.

URL https://zenodo.org/records/7800141

Zveryaev, I. I. and P. Chu, 2003: Recent climate changes in precipitable water in the global tropics as revealed in National Centers for Environmental Prediction/National Center for Atmospheric Research reanalysis. *Journal of Geophysical Research: Atmospheres*, **108**, doi:10.1029/2002jd002476.